Analysis of Non-Coherent Detectors for Opportunistic Spectrum Access in Broadband Wireless Networks

by

Vesh Raj Sharma Banjade

A thesis submitted in partial fulfillment of the requirements for the degree of

Doctor of Philosophy

in

Communications

Department of Electrical and Computer Engineering
University of Alberta

Abstract

The exponential growth in the number of wireless broadband service users demands an enormous increase in the available communication bandwidth, which inherently translates into an increased demand for the radio frequency spectrum. Opportunistically accessing the unused portions of the spectrum requires sensing the availability of unused bands. In this thesis, non-coherent detectors such as the energy detector and its more generalized version, the p-norm detector, which offer low-cost low-complexity spectrum sensing are considered and comprehensive techniques for performance analyses are developed.

To this end, a new approximate representation for the wireless fading channels is proposed and applied to facilitate accurate, asymptotic performance analysis for the energy detector across a variety of operating conditions including fading, antenna/cooperative diversity and interference. To address the analytical difficulty involved in spectrum sensing using the p-norm detector, several accurate analytical expressions are developed and utilized to comprehensively characterize the spectrum sensing performance in generalized fading channels and in fading channels with antenna diversity. To promote tractable spectrum sensing performance analysis for arbitrary sample sizes, five accurate approximations are introduced and investigated. In another comprehensive system setup, spectrum sensing performance of the p-norm detector under the cumulative effects of path-loss, fading, and a large number of randomly deployed interfering nodes is characterized by developing a comprehensive semi-analytical technique and extended to cooperative spectrum sensing.

Preface

Chapter 3 of the thesis has been published as V.R. Sharma Banjade, C. Tellambura, and H. Jiang, "Asymptotic Performance of Energy Detector in Fading and Diversity Reception," *IEEE Transactions on Communications*, vol. 63, no. 6, pp. 2031–2043, June 2015, and also in part as V.R. Sharma Banjade, C. Tellambura, and H. Jiang, "New Asymptotics for Performance of Energy Detector," *Proceedings of the IEEE Global Communications Conference (GLOBECOM)*, pp. 4020–4024, December 2014.

Chapter 4 of the thesis has been published as V.R. Sharma Banjade, C. Tellambura, and H. Jiang, "Performance of p-Norm Detector in AWGN, Fading, and Diversity Reception," *IEEE Transactions on Vehicular Technology*, vol. 63, no. 7, pp. 3209–3222, September 2014.

Chapter 5 of the thesis has been published as V.R. Sharma Banjade, C. Tellambura, and H. Jiang, "Approximations for Performance of Energy Detector and p-norm Detector," *IEEE Communications Letters*, vol. 19, no. 10, pp. 1678–1681, October 2015.

Chapter 6 of the thesis has been published as V.R. Sharma Banjade, C. Tellambura, and H. Jiang, "Spectrum Sensing Performance of p-norm Detector in Random Network Interference," *Proceedings of the IEEE International Conference on Communications (ICC)*, pp. 7474–7479, June 2015.

I have been the first co-author and major contributor of the above mentioned publications. My contributions in these works included literature survey, theoretical derivations, computer simulations, and preparation of the manuscript, under the joint supervision of my co-supervisors, Dr. Chintha Tellambura and Dr. Hai Jiang.

"Dedicated to my beloved mother, father, and brother..."

Acknowledgments

I would like to express my deepest and humblest sense of gratitude to my co-supervisors, Dr. Chintha Tellambura and Dr. Hai Jiang, for patiently letting me "learn through experience", during the course of my PhD study. I am greatly indebted to their continued support, effective guidance and timely feedback which have been pivotal in the progress of this thesis study. Their expert views, critical advise and directions have always served as stepping stones in my professional as well as personal growth.

My sincere gratitude goes to Dr. Yindi Jing for her time and interest to serve as one my PhD supervisory committee members. I am heartily grateful to my PhD final examination committee members: Dr. Ehab Elmallah, Dr. S. Ali Khajehoddin and Dr. Xiaodai Dong (external examiner, University of Victoria) for their time and interest to serve in the committee. I am obliged to Dr. Witold Krzymień and Dr. Mrinal K. Mandal for their valuable feedback during my PhD candidacy exam. I am greatly thankful to the departmental faculty and administrative staffs for their continued support throughout the period of my PhD study.

I would also like to thank my seniors: Gayan, Saman, Damith and Shuangshuang for sharing their experiences and for creating an extremely motivating atmosphere in the lab, and my lab-mates, Shashindra, Sachitha, Prasanna and Yun for their support.

I have to humbly thank two of my friends for more than ten years, Sandeep and Yamuna, for their untiring moral support, and for those joyful, everlasting experiences that we shared throughout my PhD study. I am also immensely grateful to a handful of my wonderful friends who were there in times of need.

Without any doubt, I am fully indebted to my beloved mother, father and brother, who have always been the constant source of inspiration, motivation and support throughout each and every path of my journey this far.

Table of Contents

1 Introduction **1**

1.1 Global Mobile Data Traffic Trends 1

1.2 Next Generation of Mobile Communications: 5G 2

1.3 Cognitive Radio for Dynamic Spectrum Access 7

1.3.1 Dynamic Spectrum Sharing Concept 9

1.3.2 Field Trials and Standardization activities on Dynamic Spectrum Access 10

1.4 Spectrum Sensing Techniques 11

1.5 Impact of Wireless Propagation on Spectrum Sensing 12

1.6 Motivation and Problem Statements 13

1.7 Outline of the Thesis 16

2 Background **18**

2.1 Characteristics of Wireless Channels 18

2.1.1 Multipath Fading 19

2.1.2 Shadowing 20

2.2 Spectrum Sensing as a binary hypothesis testing problem 21

2.3 Non-Coherent Detectors for Spectrum Sensing 21

2.3.1 The Energy Detector (ED) 21

2.3.2 The p-norm Detector 22

2.4 Detection Performance Metrics and Fading Channels 23

2.4.1 The Marcum-Q function 24

2.4.2 Classification of signals 24

2.4.2.1 Unknown deterministic signal model 25

2.4.2.2 Random signal model 26
2.5 Central-limit theorem (CLT) 27
2.5.1 Application to Spectrum Sensing 27
2.6 Classical Antenna Diversity Schemes for Spectrum Sensing 28
2.7 Cooperative Diversity in Spectrum Sensing 29

3 New Asymptotics for Performance of Energy Detector in Fading and Diversity Reception 31

3.1 Introduction and Motivation 32
3.2 Problem Statement 34
3.2.1 Performance of Energy Detector over Fading Channels 35
3.2.2 Existing Approximation for $f(\beta)$ 35
3.3 New Approximation for $f(\beta)$ 36
3.3.1 Proposed Approximation 37
3.3.2 Parameter determination using the exact PDF of β 37
3.3.3 Parameter determination using the exact MGF of β 39
3.4 Average Missed-Detection Probability 41
3.4.1 Accuracy of (3.16) 42
3.5 Fading channels without diversity 44
3.5.1 Nakagami-m fading 44
3.5.2 Nakagami-q (Hoyt) fading 45
3.6 Fading Channels with Antenna Diversity 46
3.6.1 MRC with L independent antennas 47
3.6.2 SC in Rayleigh fading 49
3.6.3 EGC and SC in Nakagami-m fading 50
3.7 Cooperative Detection with Multiple Relays 51
3.8 Detection in Interference 53
3.9 Average CAUC 55
3.10 Conclusion 58

4 Performance of p-norm Detector in AWGN, Fading and Diversity Reception 59

4.1 Introduction and Motivation 60
4.2 System Model 63

4.3 Derivation of P_d and P_f in AWGN 64
4.3.1 Closed-form MGF-based analysis for even-integer p 64
4.3.2 Series MGF-based analysis for arbitrary p 66
4.3.3 Generalized Laguerre polynomial series-based approximation 69
4.4 Analysis in Fading and Diversity Combining 72
4.4.1 The κ-μ Fading-No Diversity 74
4.4.2 The α-μ Fading-No Diversity 75
4.4.3 Analysis for Antenna Diversity 76
4.4.3.1 p-Law Combining (pLC) 76
4.4.3.2 p-Law Selection (pLS) 77
4.4.3.3 MRC 79
4.4.3.4 SC 80
4.4.4 Unified Expression for Average Detection Probability Over Fading and Diversity Cases 81
4.4.5 Computation of $\overline{P_{d,\text{fd}}}$ in (4.39) 82
4.5 Numerical results and discussions 83
4.5.1 Performance in AWGN (Fig. 4.4) 83
4.5.2 Effect of sample size N (Fig. 4.5) 84
4.5.3 Analysis in κ-μ fading (Fig. 4.6 and Fig. 4.7) 85
4.5.4 Analysis in α-μ fading (Fig. 4.8) 87
4.5.5 Analysis with diversity-combining (Fig. 4.9) 88
4.6 Conclusion 90

5 Approximations for Performance of Energy Detector and p-norm Detector 91
5.1 Introduction and Motivation 91
5.2 Problem Statement 93
5.3 New Approximations 93
5.3.1 Patnaik's approximation 93
5.3.2 Pearson's approximation 94
5.3.3 Three-parameter Gamma 95
5.3.4 Sankaran's third approximation 96
5.3.5 Moschopoulos' approximation 97

5.4 Numerical Results and Discussions 97
5.5 AUC of the p-norm Detector 99
5.5.1 Effect of noise variance uncertainty on AUC 101
5.6 Conclusion 103

6 Spectrum Sensing Performance of p-norm Detector in Random Network Interference 104

6.1 Introduction and Motivation 104
6.2 System Model 106
6.2.1 Network Model 106
6.2.2 Link Model 107
6.3 Conditional Performance of the p-norm detector 108
6.4 Average Detection Performance 110
6.5 Numerical Setup and Discussions 112
6.6 Cooperative Spectrum Sensing Performance 115
6.7 Conclusion 117

7 Conclusion and Future Work 118

7.1 Conclusion and contributions summary 118
7.2 Impact of the study 121
7.3 Future work 123

Bibliography 124

Appendix A Derivations for Chapter 3 138

A.1 Derivation of $\overline{P}_{md}^{\text{asy}}$ (3.16) 138
A.2 Derivation of (A-5) 140
A.3 Derivation of $\overline{A'}_{\text{asy}}$ (3.35) 141

Appendix B Gamma and CLT approximations for Chapter 4 142

B.1 Derivation of P_d and P_f for Gamma approximation 142
B.2 Derivation of P_d and P_f for CLT approximation 143

Appendix C Derivations for Chapter 5 144

C.1 Derivation of (5.11) 144

List of Symbols

Probability and Statistics

Let $\mathcal{X}$ be a random variable and $\mathcal{A}$ be a probabilistic event.

Notation	Definition
$f(\mathcal{X})$	probability density function of $\mathcal{X}$
$f(\mathcal{X}\|\mathcal{Y})$	PDF of $\mathcal{X}$ given $\mathcal{Y}$
$F(\mathcal{X})$	cumulative distribution function of $\mathcal{X}$
$\mathcal{M}_{\mathcal{X}}(\cdot)$	moment generating function of $\mathcal{X}$
$\mathbb{P}(\mathcal{A})$	probability of $\mathcal{A}$
$\mathbb{E}(\mathcal{X})$	mathematical expectation of $\mathcal{X}$
$\text{Var}[\mathcal{X}]$	variance of $\mathcal{X}$
$\mathcal{X} \sim \mathcal{N}(\mathbb{E}(\mathcal{X}), \text{Var}[\mathcal{X}])$	$\mathcal{X}$ is normal distributed with mean $\mathbb{E}(\mathcal{X})$ and variance $\text{Var}[\mathcal{X}]$
$\mathcal{X} \sim \mathcal{CN}(\mathbb{E}(\mathcal{X}), \text{Var}[\mathcal{X}])$	$\mathcal{X}$ is complex normal distributed with mean $\mathbb{E}(\mathcal{X})$ and variance $\text{Var}[\mathcal{X}]$
χ^2_n	central chi-square distributed with n degrees of freedom
$\chi^2_n(\epsilon)$	non-central chi-square distributed with n degrees of freedom and non-centrality parameter ϵ

Elementary and Special Functions

Notation	Definition
$\Gamma(\cdot)$	Gamma function
$\mathcal{G}(\cdot,\cdot)$	lower-incomplete Gamma function
$\Gamma(\cdot,\cdot)$	upper-incomplete Gamma function
$I_v(\cdot)$	v-th order modified Bessel function of the first kind
$K_v(\cdot)$	v-th order modified Bessel function of the second kind
$Q_N\cdot(\cdot,\cdot)$	N-th order generalized Marcum-Q function
$Q(\cdot)$	Gaussian-Q function
$u(\cdot)$	unit step function
$\ln(\cdot)$	natural logarithm
$(x)_y$	Pochhammer symbol
${}_1F_1(\cdot;\cdot;\cdot)$	confluent hypergeometric function of the first kind

${}_1\tilde{F}_1(\cdot;\cdot;\cdot)$	regularized confluent hypergeometric function of the first kind
${}_2F_1(\cdot,\cdot;\cdot;\cdot)$	Gauss hypergeometric function
${}_2\tilde{F}_1(\cdot,\cdot;\cdot;\cdot)$	regularized Gauss hypergeometric function
$U(\cdot;\cdot;\cdot)$	Confluent hypergeometric function of the second kind

Specific Symbols

Notation	**Definition**
N	number of samples
p	tunable parameter of the p-norm detector
γ	signal-to-noise ratio
H_0	hypothesis indicating the absence of primary user
H_1	hypothesis indicating the presence of primary user
P_d	probability of detection
P_f	probability of false alarm
h	channel gain from primary user to the detector
T	detector decision variable
λ	detection threshold
$\overline{P}_d$	average probability of detection
$\overline{P}_e$	average probability of error
$\text{Res}[g(z); z_0, n]$	residue of the function $g(z)$ at pole $z = z_0$ of order n

Miscellaneous Symbols

Notation	**Definition**
$\|x\|$	absolute value of x
$k!$	factorial of k
$\binom{n}{k}$	binomial coefficient n choose k
$(x)_n$	Pochhammer symbol
$O(h(x))$	In the notation $f(x) = g(x) + O(h(x))$, $O(h(x))$ indicates that $\|f(x) - g(x)\| \leq M\|h(x)\|$, where $M > 0$ is a constant
$\jmath$	the imaginary unit
$\mathcal{L}^{-1}[\cdot]$	the inverse Laplace transform
$u(x)$	unit-step function
$f^{(n)}(a)$	n-th derivative of the function $f(x)$ evaluated at $x = a$

List of Abbreviations

Acronyms	**Definition**
AE	absolute error
AWGN	additive white Gaussian noise
ADC	analog-to-digital converter
AUC	area under the ROC curve
BS	base station
CCDF	complementary cumulative distribution function
CDF	cumulative distribution function
CLT	central limit theorem
CSI	channel state information
CR	cognitive radio
CFAR	constant false alarm rate
CGA	cube of Gaussian approximation
DF	decode-and-forward
ED	energy detector
FCC	Federal Communications Commission
i.i.d.	independent and identically distributed
i.n.i.d.	independent and non-identically distributed
JPDF	joint probability density function
LOS	line-of-sight
LTE	Long Term Evolution
LTE-A	Long Term Evolution Advanced

MTC	machine-type-communication
MRC	maximal ratio combining
MIMO	multiple-input multiple-output
MGF	moment generating function
OFDM	orthogonal frequency division multiplexing
pLC	p-law combining
pLS	p-law selection combining
PU	primary user
PDF	probability density function
RAT	radio access technology
RF	radio frequency
ROC	receiver operating characteristics
SC	selection combining
SLC	square-law combining
SU	secondary user
SNR	signal-to-noise ratio
TDMA	time division multiple access
TMOSCFAR	trimmed-mean ordered-statistics CFAR
TVWS	TV white space
WRAN	Wireless Regional Area Network
WG	Working Group

List of Tables

4.1 The ϵ-table. 67
4.2 Number of terms needed in (4.12) for computation of P_d with and without (w.o.) using ϵ-algorithm. 69
4.3 Number of terms in (4.39) for computing $\overline{P_{d,\kappa\text{-}\mu}}$ with 4-decimal points accuracy ($\lambda = 7$). 82
4.4 Number of terms in (4.39) for computing $\overline{P_{d,\alpha-\mu}}$ with 4-decimal points accuracy. 82

7.1 Summary of Contributions for Chapters 3 - 6 120

List of Figures

1.1 Mobile data traffic forecast [1]. 1
1.2 MTC use cases for 5G with requirements [2] 4
1.3 Communication via spectrum holes across time and frequency. 8
1.4 Coexistence of CR networks with primary network in a licensed band. Spectrum sharing among two CR networks in unlicensed band is also depicted. 9
1.5 A typical wireless propagation environment. 13
1.6 Interference prone spectrum sensing 15

2.1 Basic structure of an ED. 22
2.2 The p-norm detector. 22
2.3 Cooperative spectrum sensing. 30

3.1 $f^{\text{app}}(\beta)$, $f^{\text{wg}}(\beta)$ and exact $f(\beta)$ for 4-branch SC in i.i.d. Rayleigh fading. . 38
3.2 Absolute error vs. SNR for a 5-branch SC in i.i.d. Rayleigh fading: Proposition 3 and [3]. 43
3.3 $\overline{P}_{md}$ vs. SNR in Nakagami-m fading channel for $N = 3$: exact, existing [3] and Proposition 3. 44
3.4 $\overline{P}_{md}$ vs. SNR in Nakagami-q channel with $q = 0.7$ for different N. 46
3.5 $\overline{P}_{md}$ vs. SNR for MRC in i.n.i.d. Rayleigh fading channels for different $\{N, L\}$. 48
3.6 $\overline{P}_{md}$ vs. SNR for SC in i.i.d. Rayleigh fading. 49
3.7 $\overline{P}_{md}$ vs. SNR for 2-branch EGC ($N = 5$) and 3-branch SC ($N = 2$) in Nakagami-2 fading. 51
3.8 $\overline{P}_{md}$ vs. SNR for multiple relays based detection ($N = 2$). 52
3.9 $\overline{P}_{md}$ vs. $\overline{\gamma}$ for $N = 2$ in presence of $N_I = 8$ interferers with powers $\{P_1, P_2, P_3, P_4, P_5, P_6, P_7, P_8\} = \{-5, -3, -1, 1, 3, 5, 7, 9\}$ dB, $N_0 = 0$ dB. 54
3.10 $\overline{A'}$ vs. SNR for SC in i.i.d. Rayleigh fading with $N = 2$. 56

4.1 Talbot's deformation of the Bromwich contour 65

4.2 The proposed pLC scheme 78
4.3 The proposed pLS scheme 78
4.4 Comparison of the derived Talbot solution (4.9), series solution (4.12) and the Laguerre approximation (4.18) against the existing Gamma (Appendix B.1) and CLT (Appendix B.2) approximations for AWGN. 84
4.5 Average detection probability ($\overline{P_d}$) vs. average SNR ($\overline{\gamma}$) for 3.5-norm detector in Rayleigh fading (using (4.39) with $\kappa \to 0$, $\mu = 1$) for various samples, compared to the CLT approximation and simulation. 85
4.6 Average detection probability ($\overline{P_{d,\kappa\text{-}\mu}}$) vs. average SNR ($\overline{\gamma}$) in a $\kappa = 1.5$, $\mu = 2.2$ fading channel for various p with $N = 6$. The AWGN plot is included for comparison. Discrete marks indicate simulation values. 86
4.7 ROC curves (in log-log scale) for a 3-norm detector with $N = 3$ for various κ-μ channels at SNR of 7 dB. The discrete marks indicate the simulation results. 87
4.8 ROC curves of a 2.7-norm detector for various α-μ channels at SNR $=$ 3 dB, $N = 5$. The ED ($p = 2$) plot is included for comparison. The discrete marks on the graphs indicate the simulation results. 88
4.9 Two sets of ROC curves at SNR -10 dB ($p = 2.5$, $N = 3$) and 0 dB ($p = 3$, $N = 4$) for various diversity-combining schemes in Nakagami-3 fading channels with $L = 3$. No-diversity curves are included for comparison. The discrete marks on the graphs indicate the simulation results. 89

5.1 ROC curves for various sample sizes for $P_f \leq 0.1$, $\gamma = 10$ dB. 98
5.2 Absolute error for P_d vs. γ for $P_f = 0.01$, $N = 5$. 99
5.3 AUC vs. SNR for different p and N. 100
5.4 AUC vs. p for different sample sizes and SNRs 101
5.5 AUC vs. p for various noise uncertainty levels x dB for $N = 10$ at $\gamma = -5$ dB. 102

6.1 Network Model. The total number of interferers K and the distances r_k, $\forall k \in \{1, 2, ...K\}$ are random. 107
6.2 ROC curves comparing (6.7) and simulation. The $p = 4$, $N = 100$ graph is plotted for SINR $= -10$ dB and $p = 2.5$, $N = 10$ is obtained with SINR $= 0$ dB. 110
6.3 ROC curves: semi-analytical (6.10) and (6.11) vs. simulations for 3-norm, $N = 20$ detector with $\beta = 0.0001$ $\alpha = 4$, $P_i = 10$ dB, $P_s = -10$ dB; and for 1.5-norm $N = 10$ detector with $\beta = 0.005$, $\alpha = 2.5$, $P_i = 5$ dB, $P_s = 0$ dB; $m = 2$, $\sigma_s = 4.66$ dB. 112

6.4 $\overline{P}_e$ vs. p for various P_s with $N = 20$, $\lambda = 10$, $\beta = 0.0001$, $\alpha = 4$, $P_i = 4\,\text{dB}$, $\sigma_s = 8.686\,\text{dB}$ and $m = 4.5$. 113
6.5 $\overline{P}_e$ vs. p for various interferer densities β with $N = 10$, $\lambda = 10$ $P_s = 5\,\text{dB}$, $P_i = 5\,\text{dB}$, $\alpha = 2$, $\sigma_s = 6.52\,\text{dB}$ and $m = 2.5$. 114
6.6 ROC curves for a 3-norm, $N = 10$ detector for various $\sigma_s\,\text{dB}$ with $\beta = 0.0001$, $\alpha = 2$, $P_i = 5\,\text{dB}$, $P_s = 0\,\text{dB}$ and $m = 2.5$. 115
6.7 $\overline{Q}_e$ vs. M with $C = 10$ for various β for a $N = 10$, 4.8-norm detector with $\lambda = 5.5$, $\alpha = 2$, $P_s = -5\,\text{dB}$, $\sigma_s = 8.69\,\text{dB}$, $P_i = 5\,\text{dB}$ and $m = 2.5$. 116

7.1 TMOSCFAR detector principle. 123

A.1 Possible poles of $g_i(z)$, $i = 1, 2$, in the z-plane. 139

Chapter 1

Introduction

1.1 Global Mobile Data Traffic Trends

The tremendous popularity of state-of-the-art mobile devices such as smart phones, tablets and ultra-books has catapulted the global multimedia data traffic from 1.5 exabytes per month in 2013 to a staggering 2.5 exabytes per month in 2014, a growth of 69% [1]. Moreover, according to the recent forecast by Cisco (Fig. 1.1), the mobile data traffic is expected to reach 24.3 exabytes per month by 2019 [1]. Furthermore, this study shows that in 2014, almost half a billion (497 million) mobile device connections were added. The usage of smartphones grew by 45%, and the mobile connected tablets increased by 1.6-fold. More-

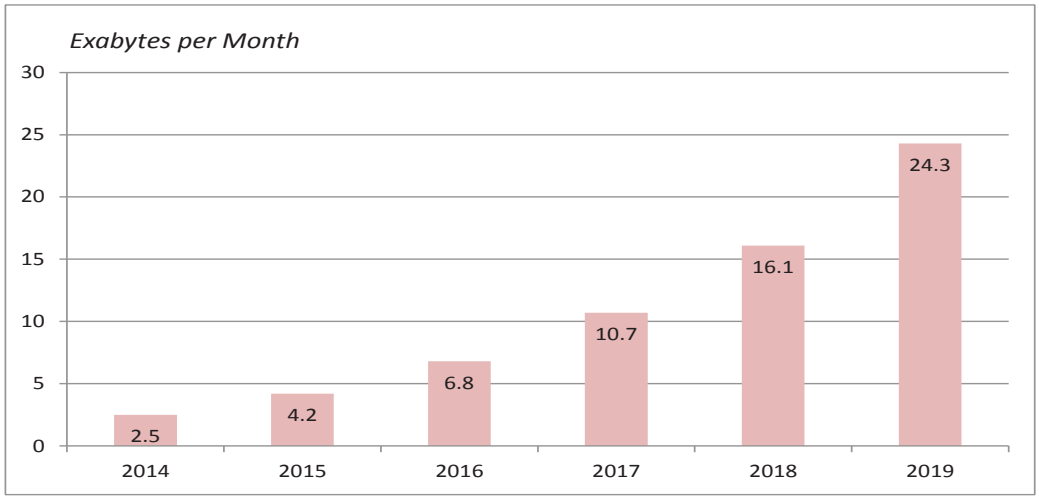

Fig. 1.1. Mobile data traffic forecast [1].

over, compared to 2014, the global mobile data traffic is expected to increase by almost 10-fold by 2019, thus reaching 24.3 exabytes per month, attributed to nearly 1.5 mobile devices per capita by that time. Such exponential growth in the mobile device usage exacerbates the inherent scarcity of the radio resources. Specifically, this near future trend will impose serious increase in demand for the fundamental spectral resource, the radio frequency (RF) spectrum which is becoming scarcer.

To alleviate this trend, in order to increase the efficient utilization of spectral resource and to meet the enormously increasing demand for mobile connectivity, several new technologies are being investigated by wireless communication researchers and engineers across leading industries and academia. Envisioning the massive number of interconnections, the next generation of mobile communications, the fifth generation, more popularly known as "5G", is the upcoming big wave in communications. Next, we briefly review the 5G wireless access requirements and the corresponding technical enablers.

1.2 Next Generation of Mobile Communications: 5G

By the year 2020, billions of devices are envisioned to be mutually interconnected to enable ubiquitous connectivity anytime, anywhere, and with any "thing". Such interconnections will give rise to an "Internet of Things" where everything from home appliances, surveillance cameras, sensors, vehicles, displays, actuators, smart meters, disaster response communication systems, and so forth, will be able to communicate with each other [4]. Thus, the future of wireless access will not only be about connectivity among mobile devices but also between any device which could benefit from network connectivity. All of such devices could benefit from wireless networking thus enabling much wider wireless service use cases with different requirements. Such futuristic era of next generation communications, 5G, is envisioned in 2020. While the state-of-the-art 4G cellular access (LTE/LTE-A), which has significantly improved the peak data rate, coverage and spectral efficiency compared to its predecessors (2G-3G), will continue to drive the development and evolution of next generation high data rate systems, disruptive changes in the system architecture and components on top of radical changes in the node architectural levels will be required to realize 5G deployments [5]. To this end, the major requirements and capabilities of 5G are discussed below.

Overall Requirements and Capabilities of 5G

1. *Massive Capacity*. The emergence of new usage scenarios in 5G includes deployment of billions of wireless sensors, actuators, smart meters, among others. While each of these devices will generate a small amount of traffic, the major challenge lies in terms of design of efficient signaling protocols to manage such massive number of interconnections.

2. *Very High Data Rates*. Depending upon the various scenarios, some of the 5G networks must provide high data rates everywhere. For example, data rates could exceed 10 Gbps in indoor and dense outdoor environments while it could be several hundred Mbps in urban and suburban environments. Data rates of at least 10 Mbps should be essential everywhere including areas with low population density.

3. *Ultra Low Latency, Very High Reliability and Availability*. For a 5G network targeted for critical applications, such as traffic safety, industrial control as well as for disaster communication systems, the network is envisioned to have an end-to-end latency of less than 1 ms, ultra high reliability in connectivity, and all-time availability.

4. *Very Low Cost and Energy Consumption*. To enable the existence of billions of wirelessly connected sensors, actuators, smart meters, and similar devices, such devices should be available at very low cost and with very long battery life (some up to 10 years).

Thus, these requirements and capabilities point towards a vastly diverse set of characteristics for 5G networks. It is clear that the requirements of 5G are not only about communications among humans but also among devices which may operate independently without any human intervention thus leading to machine-type-communication (MTC). Due to the wide range of different application scenarios, MTC devices are subdivided into two streams; massive MTC and mission critical MTC whose features are highlighted in Fig. 1.2.

The 5G massive MTC networks are targeted to serve billions of devices which generate sporadic data traffic, are cheap to deploy, and consume minimal battery. An example could be a large number of sensors deployed in a parking lot which record the number of vehicles and the duration of parking of each vehicle in a futuristic automated parking management

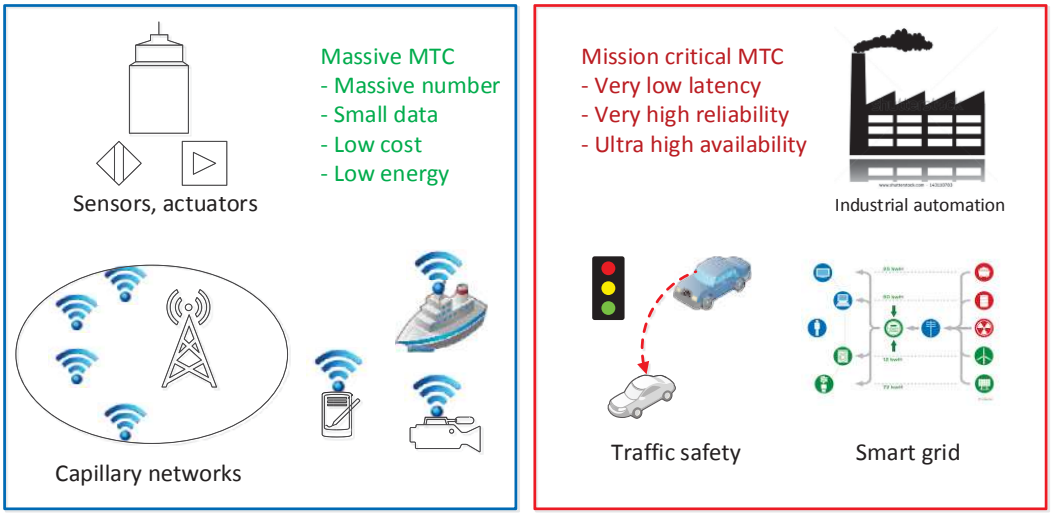

Fig. 1.2. MTC use cases for 5G with requirements [2]

system in a busy airport. For instance, these sensors may need to only periodically report their collected data to a central controller or gateway on a monthly basis for updating the firmware in an automated light control system or the billing system in the parking spots. On the other hand, the mission critical MTC networks must be designed to satisfy even more disruptive requirements such as ultra low-latency and ultra-high reliability in applications, for example, tactile surgery where the doctor needs to operate remotely on a patient using the tactile devices. Another example of ultra high availability could be related to an all-time available emergency control system in a very high-risk chemical plant to report the malfunctioning of any container or temperature fluctuations. Hence, in order to fulfill such diverse requirements and challenges, the 5G wireless access requires disruptive technological innovation. The major technical enablers for such innovation, which are envisioned for 5G wireless access, are briefly summarized next.

Technical Enablers for 5G

1. *Massive Beamforming*. Massive number of antenna elements, popularly known as massive multiple-input-multiple-output (MIMO) with advanced beamforming capabilities, enhance the data rates. Even though the massive MIMO concept has been incorporated into LTE-A, reaping its benefits in more challenging 5G usage scenarios is seen as a potential solution for vigorously increasing the data rates and efficiently managing interference. Deployment of massive MIMO in the mm-wave frequency

bands (30-50 GHz), where antenna dimensions become much more practical, is seen as a key technology enabler for 5G by major industry players [2], [6].

2. *Ultra-Lean Design*. For promoting energy-efficiency and reducing the overall interference levels, it is necessary to minimize the transmission of control signals. For example, reduced signaling for synchronization, channel estimation, and others is beneficial for reducing the control channel overhead [7].

3. *Design for Low Latency*. For some 5G usage scenarios like mission-critical MTC applications, low-latency is extremely important. It can be achieved by reduction of the transmission-time intervals achieved via high transmission rates, and also from availability of more transmission-bandwidth [7].

4. *Device-to-Device Communications (D2D)*. The D2D concept which has been introduced as an enhancement to LTE specifications could be an integral part of the 5G wireless access. Because the D2D communication model is based on the proximity of the users, the base stations and the core network have a minimal role to play (only in terms of signaling to setup the direct connections) in the exchange of data traffic among the devices [8]. This promotes the concept of low-latency wireless access, improves cellular coverage, and may also increase the area spectral efficiency through re-use of the same frequency spectrum as the macrocell or via use of the unlicensed spectrum [6], [7].

5. *Multiple Radio Access Technologies (RATs)*. Future devices in the 5G era need to operate across a variety of RATs ranging from the legacy 2G/3G devices, D2D communications based on, say, Wi-Fi Direct or LTE Direct, to mm-wave technologies which may require a completely new RAT. Thus, none of the existing RATs alone will be sufficient to satisfy all the requirements of the 5G era, and an integrated virtual radio network could emerge as the best solution to manage the radio resources across such diverse physical radio networks [6].

6. *Flexible use of the RF spectrum*. The premise of data rates in the orders of several Gbps for the mission critical MTC applications or the support for billions of devices for massive MTC applications would fundamentally demand much more RF spectrum than what is currently available. However, currently used RF bands are frag-

mented across different frequency ranges, which makes the availability of contiguous RF bands needed to support the gigabit data rates unrealistic. Moreover, the state-of-the-art cellular, satellite as well as broadcasting systems are already crowding the bands below 6 GHz because of better propagation characteristics of these bands thus rendering the large chunks of spectrum below 6 GHz unavailable. Due to this fact, the mm-wave bands (bands around 30-50 GHz) with the advancements in RF technology components are being considered for future cellular systems deployments [6]. These bands could be particularly suited for dense deployment of small-cells [9] for significantly boosting the spectral efficiency of the traditional cellular systems [10]. Moreover, the joint concept of exploiting small cells in high frequency bands along with massive MIMO with the ultimate goal of achieving an overall increase in system coverage and capacity are being considered.

Another means to collect RF spectrum for future wireless systems is via licensed shared access (LSA) concept by identifying the underutilized spectrum in non-cellular bands and cooperating with the incumbents in such bands for shared access of the bands. Moreover, such underutilized non-cellular spectrum could also be used by integrating with other cellular spectrum in a licensed manner with mutual agreement between different classes of licensees [6]. In a different paradigm of unlicensed shared access that is attracting interest is a concept called "LTE in unlicensed band (LTE-U)" where the LTE-U devices may operate over the Wi-Fi spectrum, that is, the 5 GHz band by exploiting the "listen-before-talk (LBT)" feature of the Wi-Fi devices which triggers the Wi-Fi devices to go into silent mode on detection of an LTE-U device in the given frequency slot(s) of interest. The Wi-Fi devices may then try to listen to some other frequency slot(s) (to identify whether they are occupied or vacant) for possible communication opportunities.

Fundamental Issue: RF Spectrum Scarcity

To fulfill the requirements of future 5G wireless access whether be it for the massive MTC or the mission critical MTC paradigms, one of the fundamental resources is the RF spectrum, which is the common spectral resource needed to deliver the capabilities of future wireless systems. Moreover, the usable RF spectrum is limited whereas accommodating the upcoming innovations in the wireless ecosystem would require additional radio bands

for successful deployment. An inherent question is how to make more radio spectrum available for enabling the future 5G services? We now proceed in search of the answer.

It is well-known that a fixed amount of electromagnetic spectrum is allocated separately for each wireless system. For example, in the United States, the frequency band $512 - 608$ MHz is specifically used only for broadcasting TV channels 21-36. The allocated spectrum band is further shared across a vast number of licensed users who utilize it as the primary licensees of the band. Such users are called the primary users (PUs) of that frequency band. Interestingly, a study by the Federal Communications Commission (FCC) showed that the electromagnetic spectrum allocated to the licensed users is vastly underutilized across time and space [11]. A study conducted in 2004-2005 for frequency bands below 3 GHz showed only 5.2% spectrum utilization in any location at a given time revealing that the licensed spectrum is sparsely utilized [12]. These findings indicate the two challenges: (i) the scarcity of the available RF spectrum, and (ii) its inefficient utilization. In addition, the rigid spectrum allocation policies of the government agencies globally have further exacerbated such inefficient spectrum utilization. In order to alleviate these problems, a revolutionary paradigm called *cognitive radio* (CR), originally introduced by Mitola in his PhD thesis [13], was brought into attention of the research community, much later by Haykin [14]. The landmark premises of CR are discussed next.

1.3 Cognitive Radio for Dynamic Spectrum Access

As the radio spectra allocated to the PUs are not always utilized in time and across space, chunks of frequency bands may become free at some point of time for a certain duration. As shown in Fig. 1.3, these unoccupied (unused) frequency bands are called spectrum holes [14] which offer opportunities for other devices to communicate over them whenever they become available. Whenever the higher priority PU returns to the band of interest, the unlicensed users must vacate the band. Such opportunistic unlicensed devices are termed as secondary users (SUs) of the spectrum. Inherently, an SU should be capable of performing the following tasks [14]:

1. Identification of the possible spectrum opportunities in its radio environment by detecting the spectrum holes. This process is called *spectrum sensing*.

2. Estimating the condition of the communication channel, that is, channel state infor-

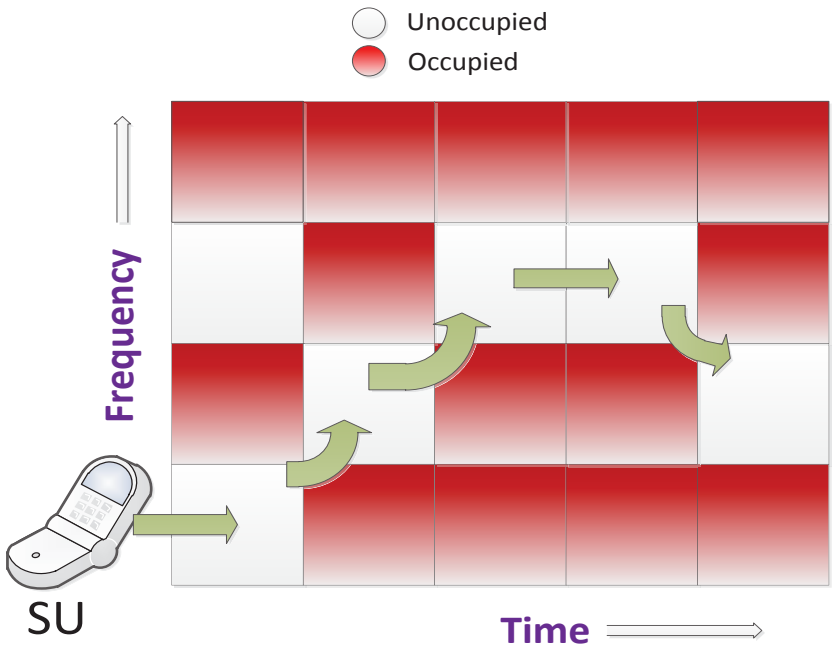

Fig. 1.3. Communication via spectrum holes across time and frequency.

mation (CSI) which is necessary for predicting the channel capacity.

3. Dynamic control of its transmission power for avoidance of any possible interference to PUs.

The need to fulfill these tasks led to the birth of an intelligent radio, the CR [13], [14]. Thus, a CR is vital in promoting the concept of *dynamic spectrum utilization* by enabling the sharing of the underutilized spectrum across a vast number of users. Broadly, the dynamic spectrum utilization paradigm may be classified as [15]:

(i) *Underlay spectrum sharing* in which the SUs communicate simultaneously with the PUs in the band of interest. In this technique, the transmit power of the SUs is strictly constrained so that they do not interfere with the PU transmissions.

(ii) *Interweave spectrum sharing* in which the SUs communicate opportunistically in the band of interest. This technique is the original motivation for CR and is based on utilizing the spectrum holes that temporally exist across time and space.

Thus, spectrum sensing is the fundamental task associated with the interweave spectrum sharing paradigm while it is not mandatory for the underlay technique. In the interweave

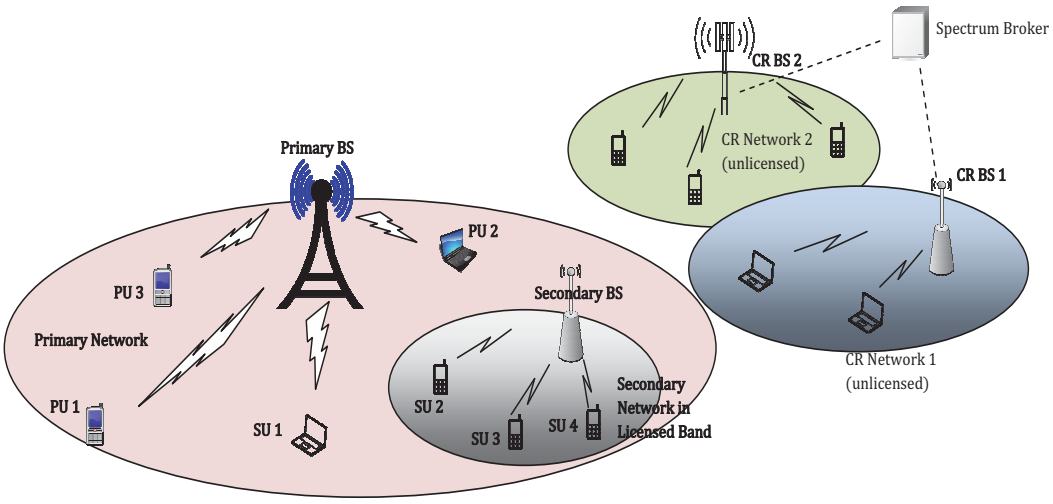

Fig. 1.4. Coexistence of CR networks with primary network in a licensed band. Spectrum sharing among two CR networks in unlicensed band is also depicted.

sharing strategy, the CR has to gather information from its radio environment and decide on the presence/absence of spectrum holes after rigorously analyzing the information. If a spectrum hole exists, it must be used by the CR long as the PU remains idle. Whenever the PU reappears, the CR should immediately vacate the channel so that it does not interfere with the PU (which is the higher-priority user of the licensed spectrum) and search for other opportunities. Thus, efficient spectrum sensing is important for establishing opportunistic communication links for use by the SUs.

An example CR network architecture supporting the dynamic spectrum management paradigm is presented in the next section.

1.3.1 Dynamic Spectrum Sharing Concept

Practically, the CR networks may not only be confined to operate in licensed spectrum. For example, the work in [16] endorses that the secondary (CR) networks can coexist with the PU network both in licensed as well as unlicensed bands. Such coexistence of primary and secondary networks in the licensed spectrum as well as that among two CR networks in an unlicensed band are depicted in Fig. 1.4. Spectrum holes existing in the licensed band must be detected and exploited by the SU network ensuring no interruption to the PUs' service. Moreover, in the licensed band operation, the SUs have to vacate the band on which they are operating immediately when the PUs are detected back in the band. Thus, the CR users

are inherently considered lower priority users. Contrary to this, operation in the unlicensed band relieves the CRs from such requirement. Similar to the operation in licensed band, any CR vying for an opportunity in an unlicensed band has to first detect the presence of other CRs in the band. Once an opportunity is detected successfully, the CR may communicate without the requirement to vacate the band as in licensed band operation. However, the CRs should keep sensing other portions of the spectrum to identify possible opportunities which may be needed for, say, handoff or to maintain the quality of service. To facilitate such processes (handoff, maintenance of quality of service), a spectrum broker may act as a resource manger among different CR networks [16]. Nevertheless, regardless of the licensed or unlicensed operation of the SUs, a highly reliable spectrum sensing mechanism is the fundamental requirement to initiate and maintain (via continued sensing of other opportunities) opportunistic communication via dynamic spectrum sharing.

1.3.2 Field Trials and Standardization activities on Dynamic Spectrum Access

Before moving on to the details of the spectrum sensing mechanism for enabling the concept of dynamic spectrum sharing, in this sub-section, we mention some of the interesting industrial trials and standardization activities in the potential deployment of the CR devices.

In order to evaluate the possible deployment of the CR devices in the TV white-space (TVWS) spectrum (between 54-790 MHz), the FCC field tested several prototype devices from leading companies such as Motorola, Philips and Adaptrum in 2008. The FCC test results showed the possibility of reliably detecting the TV signals in practical settings, given the spectrum sensing and geolocation databases are jointly consulted [17]. Another field trial included the first public white-space launch in Claudville, Virginia, in 2009 by Spectrum Bridge, Microsoft and Dell, which eventually led to the wider-scale deployment of one "Smart City" network in Wilmington, North Carolina, in 2010 [17].

Apart from the field trials, the industry has been committed to the standardization activities targeted for dynamic spectrum access using CR networks. Examples of such activities include the IEEE 802.22 standard working group (WG) on Wireless Regional Area Networks (WRAN) for rural areas supporting fixed CR devices exploiting TVWS, the Ecma 392 targeting indoor areas for streaming high speed video, the IEEE 802.11af standard enabling Wi-Fi like protocol over the TVWS and the IEEE 802.19 technical advisory group

(TAG) dealing with the co-existence issues among unlicensed wireless networks. [17]. Thus, all of these field trials and standardization activities clearly suggest that concept of dynamic spectrum access has a remarkable potential for enabling the 5G networks in the near future.

1.4 Spectrum Sensing Techniques

To identify any possible communication opportunities for the secondary users by ensuring that the operation of primary licensees is not disrupted, the foremost task is to reliably detect the presence or absence of spectrum holes in the specific frequency bands of interest. Several spectrum sensing algorithms exist for this purpose. Four of the well-known ones are briefly explained next.

1. *Matched Filter:* This detector is theoretically optimal for the specific case of known signals embedded in Gaussian noise in the sense that it maximizes the received signal-to-noise ratio (SNR). The matched filter receiver has an array of detectors coherently matched to the transmitted signals [18]. However, perfect knowledge of the transmitted signals and the channel response is required for such coherent detection, and the matched filter detector performance degrades significantly if no such information is available. Moreover, it needs a dedicated receiver matched to each class of PU signal and thus requires large implementation complexity.
2. *Energy Detector (ED):* The ED, also known as the radiometer [19], is a blind sensing technique which does not require any *a-priori* knowledge of the primary signal. It operates by measuring the energy of the received signal and comparing it against a pre-determined threshold to decide on the presence or absence of the PU signal. It is one of the most popular detectors due to very low-complexity and non-coherent nature. One inherent drawback is that its performance degrades at high levels of uncertainty in noise variance and interference [20].
3. *Cyclostationary Feature Detector:* In wireless systems, the transmit data often possess characteristics such as built-in periodicity in terms of statistics like mean and autocorrelation primarily induced due to modulation, coding and burst formatting schemes (for example, cyclic prefix in orthogonal frequency division multiplexing (OFDM) symbols, known pilot symbols, and others). This fact may be exploited to

identify the presence/absence of the transmitted signal [21]. In case the PU is present, the received data would possess some form of cyclostationarity, as opposed to the PU absence case where only the noise is present. Thus, detection of any cyclostationary features in the received signal indicates the presence of PU. Even though this method may be effective in identifying PU signal buried in noise and interference, high implementation complexity and need of *a-priori* PU signal information such as the modulation format are the tradeoffs.

4. *Covariance-based Detector:* In general, the statistical autocorrelation of the signals and noise are mutually independent. This knowledge may be utilized to differentiate between the presence or absence of the PU signal [22]. The work [22] showed that the presence (absence) of the PU signal would cause the off-diagonal elements of the covariance matrix of the received signal to be non-zero (zero). Thus, the covariance-based detector can be used even in absence of any *a-priori* knowledge of the PU signal, channel and noise variance. However, these features entail an additional cost and a relatively high computational complexity at the receiver.

It is important to note that the IEEE 802.22 WG does not impose any restrictions on the spectrum sensing technique to be used as long as a reliable detection performance is achieved [23]. However, the WG mostly targets at providing services to rural and remote areas and thus a detector with low-complexity as well as low-cost is an implicit requirement [12]. Hence, the popularity of the ED for such requirements is well motivated.

1.5 Impact of Wireless Propagation on Spectrum Sensing

Regardless of the spectrum sensing technique used, successful detection of the PU signal heavily relies upon the received PU signal strength which, in turn, depends upon the wireless propagation environment. In practical wireless communication environments as shown in Fig. 1.5, two inherent phenomena are multipath fading and shadowing, which degrade the quality of the received signals [24]. Multipath fading (small-scale fading), arises when the plane waves propagate from the source to the destination via multiple paths with different delays and amplitude variations due to stochastic nature of the wireless channel. In severe fading conditions, significant attenuation of the transmitted signal envelope diminishes the received SNR to a very low level such that the detection of the PU signal becomes difficult.

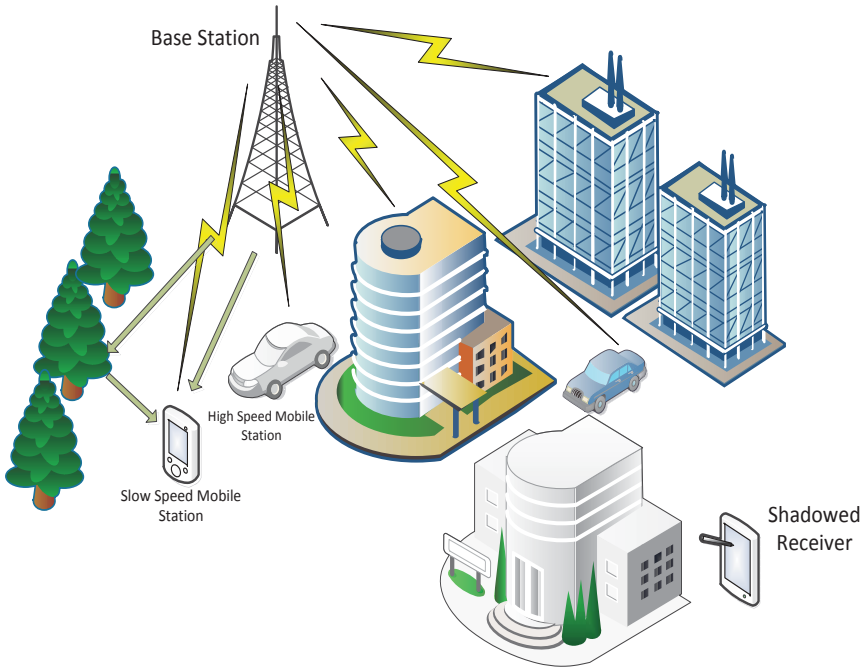

Fig. 1.5. A typical wireless propagation environment.

Another phenomenon called shadowing (large-scale fading), arises when large obstacles interrupt the transmitter-to-receiver path and a reliable signal reception at the destination is no longer guaranteed. This results in the hidden terminal problem [18], [21] in which the CR cannot detect the PU presence and thus starts to transmit thereby interfering with the PU transmission. Both of these phenomena severely impact the spectrum sensing reliability. The utilization of spatial degrees of freedom via antenna- and cooperative- diversity are known to be two of the potential solutions to these problems.

1.6 Motivation and Problem Statements

As low-hardware complexity and non-coherent operation are two of the most important features for low-cost, rapid spectrum sensing, this research focuses on the ED and its more generalized version, the recently introduced p-norm detector. As both of these detectors do not require any *a-priori* information of the PU signal, they can sense a wide range of spectrum across a variety of PUs deploying different modulation schemes, signal formats, and others. Moreover, their simple construction is attractive for practical hardware implementation resulting from agile operation and low-complexity. However, significant literary gaps remain in the existing works related to ED and the p-norm detector. These important open

problems, which are the focus of this study, are briefly summarized in problems **P1**-**P4** as follows.

P1: *Asymptotic performance of the ED:* The ED has received enormous attention from the spectrum sensing research community. Thus, its performance has been extensively analyzed in multipath fading, shadowing, with multiple antennas, in cooperative networks, and others. However, the existing analyses often involve complicated special functions, infinite series and/or residues and do not yield quick insights into the effect of fading/diversity combining on the ED performance. The primary cause of such drawbacks is the difficulty in averaging the generalized Marcum-Q function based expression for the detection probability over statistical distribution of the fading/diversity combining, primarily due to limited Marcum-Q integrals in the literature. The asymptotic analysis of ED performance could be a potential solution to the problem. However, a unified, accurate asymptotic analysis of the ED performance over practical SNR ranges has been lacking previously.

P2: *Accurate analysis of p-norm detector in fading and diversity:* The existing analyses of the p-norm detector, a more generalized version of the classical ED, have several limitations, either on the sample-size, operating SNR, or both. These limitations are because of the difficulty in deriving the exact statistical distribution of the p-norm detector decision variable, which consists of a sum of p-th powered random variables. Furthermore, an accurate, comprehensive performance analysis of the p-norm detector in generalized fading channels and with antenna diversity combining, which subsequently aids in the design and analysis of p-norm detector based spectrum sensing, is not available in the literature.

P3: *Finite sample approximations for performance of ED and p-norm detector*: The ED and p-norm detector performances are often analyzed by exploiting the central limit theorem (CLT) which yields simple approximate performance expressions in terms of the Gaussian-Q function. However, CLT based analyses are valid exclusively for large samples. To minimize the delay in spectrum sensing, the number of samples have to be chosen optimally (say, choosing the lowest number of samples that satisfies the performance constraints). This requires the expressions to work without any restrictions on the sample size. Although exact expressions which work for few

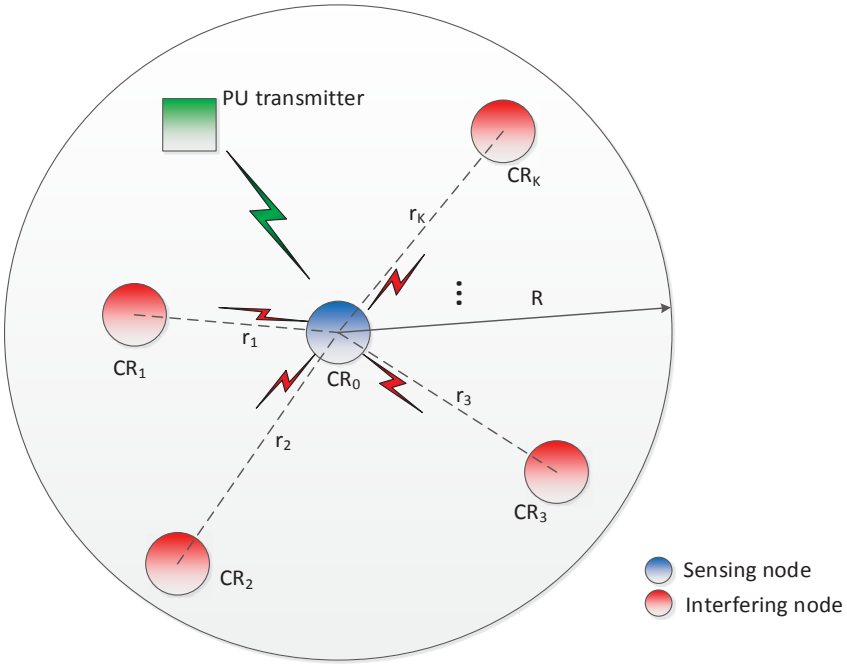

Fig. 1.6. Interference prone spectrum sensing

(finite) samples exist, they often involve a combination of complicated special functions, infinite series, and/or residues, which do not lend themselves to, say, parameter optimization problems, where either the detection threshold or the number of samples need to be chosen optimally to achieve the best sensing performance. Thus, a fundamental problem is to obtain simple approximate performance expressions for ED and p-norm detector, which are valid for arbitrary number of samples. However, only one such approximation, called the cube-of-Gaussian (CGA) approximation was available previously for the ED, which however, is not necessarily the only (or the best) one. Thus, it is desirable to have more approximation techniques for accurately characterizing the ED and p-norm detection performances.

P4: *The p-norm detector in random network interference:* Most of the ED based spectrum sensing analyses have neglected an underlying phenomenon in spectrum sensing, the presence of interfering transmissions in the vicinity of the sensing CR (see Fig. 1.6). However, the powers from undesired transmitters leak into space over relatively large distances thus interfering with the PU signal reception at the CR, especially in heterogeneous network settings where the interfering nodes may not be associated with the CR base station. Moreover, in such networks with densely deployed nodes (say, small cells), both the locations as well as number of interferers may vary randomly. The

analytical performance evaluation in such scenario is further complicated by three inherent phenomena in wireless propagation: path-loss, multipath fading and shadowing. As the ED performance degrades in interference, the p-norm detector may prove to be a potential solution to yield enhanced performance than the ED. However, a comprehensive framework for analyzing the possible performance gains offered by the p-norm detector compared to the traditional ED subject to the cumulative effects of path-loss, fading, and random network interference is lacking.

1.7 Outline of the Thesis

The rest of the thesis focuses on addressing the aforementioned problems **P1-P4** in spectrum sensing. Chapter 2 elaborates the relevant background needed for the topics covered in the thesis. The aforementioned problems **P1-P4** are treated through Chapters 3-6, respectively, by providing detailed background, novel analytical treatment, and numerical results. Brief summaries of each chapter are as follows.

- The problem **P1** is addressed in Chapter 3, where a new approximate probability density function (PDF) for statistically modeling the fading channel gain is proposed. By using it, accurate asymptotic performance of the ED is derived and unified across a wide array of practical scenarios including various fading channel models, antenna diversity combining schemes, cooperative spectrum sensing and co-channel interference. The proposed asymptotic framework is accurate across wide SNR ranges. The framework is further extended to demonstrate its usefulness in deriving a unified expression for the Complementary Area Under the receiver operating characteristic (ROC) Curves (CAUC), which was recently introduced in the literature as a single figure of merit to characterize the ED performance. Furthermore, for each of the system settings considered, the method of retrieving the sensing gain is presented, which reveals quick insights into the effect of operating conditions on the ED performance.

- In Chapter 4, the Problem **P2** is given a rigorous treatment. As the existing analyses are limited to ad hoc approximations and Rayleigh fading only, in this chapter, comprehensive and accurate p-norm detection performance analysis frameworks are proposed. Specifically, accurate computational methods, tight approximations and

series expansions are developed. Moreover, the treatment is extended for quantifying the p-norm detection performance in generalized fading channels. Furthermore, performance of the p-norm detector with antenna diversity is analyzed.

- For facilitating the finite sample performance of the ED and the p-norm detector to overcome the Problem **P3**, several accurate approximations for the classical ED problem are proposed in Chapter 5. The proposed approximations are accurate for any number of samples unlike the existing CLT approximation based on the large-sample assumption. Some of the proposed approximations also outperform the existing finite sample based CGA approximation. Moreover, one of these approximations is then further utilized to study the Area Under the ROC Curve (AUC) performance of the p-norm detector. Furthermore, the AUC performance is extended to characterize the effect of the underlying noise variance uncertainty on spectrum sensing.

- To overcome the issues outlined in Problem **P4**, a comprehensive semi-analytical technique is developed in Chapter 6 by modeling the cumulative effects of path-loss, fading and random network interference. This technique is utilized to study possible performance gains achieved by the p-norm detector (compared to the traditional ED) by deriving approximate, yet accurate expressions for the performance metrics of the p-norm detector. The framework is further extended to cooperative spectrum sensing involving multiple CRs. Possible performance gains compared to single CR based spectrum sensing are quantified.

Chapter 2

Background

This chapter reviews the background relevant to the rest of the thesis. The properties of the wireless propagation environment, which includes the effects of small-scale and large-scale fading, are elaborated. The formulation of the spectrum sensing problem and the widely popular ED along with its generalized cousin, the p-norm detector, are subsequently described. The inherent performance metrics for quantitatively characterizing the detection performance are discussed. The discussion is extended to account for the analysis in fading channels. The well-known CLT approximation is introduced before finally concluding the chapter with a summary of antenna diversity and cooperative diversity techniques for spectrum sensing.

2.1 Characteristics of Wireless Channels

Radio signals propagating from the transmitter to the receiver through the wireless medium are subject to various impediments resulting from the inherent characteristics of the propagation channels. These impediments arise due to existence of path-loss, large-scale (macroscopic) fading and small-scale (microscopic) fading between the transmitter and the receiver. Path-loss essentially is the attenuation of the transmit signals due to dissipation of the transmit power over large distances and thus depends upon the transmit frequency (wavelength), antenna height and the separation distance between the transmitter and receiver. The large-scale fading also known as shadowing occurs when the transmitter to receiver propagation path is affected by large obstacles such as buildings and hills, whose sizes are in the order of tens of wavelength thus leading to random variations of the re-

ceived power over distances which are tens of orders of wavelength. On the other hand, the small-scale fading termed as the multipath fading arises when multiple plane waves arrive at the receiver from various directions with different amplitudes, phases and delays thus constructively and destructively combining at the receiver. Such combination gives a much rapid fluctuation of the received signal envelope over shorter distances in the order of the wavelength. This phenomenon results in rapid random fluctuations in the received signal envelope which is termed as multipath fading.

To commonly characterize the time varying nature of the received signal envelope, various statistical models for characterizing the small- and large-scale fading exist. Next, a short review of these models is provided.

2.1.1 Multipath Fading

Three well-known channel models for representing the small-scale or multipath fading are Rayleigh, Rician and Nakagami-m fading which are briefly described below [25].

1. *Rayleigh fading*: When the received signal consists of a large number plane waves, the amplitude of the fading envelope $|h|$ is Rayleigh distributed with the PDF

$$f_{|h|}(x) = \frac{2x}{\Omega} e^{-\frac{x^2}{\Omega}}, \ x \geq 0, \tag{2.1}$$

   where $\Omega = \mathbb{E}[|h|^2]$ is the mean-squared envelope power with $\mathbb{E}[\cdot]$ denoting the expectation. Rayleigh fading is a reasonably suitable model for cases when no direct line-of-sight (LOS) between the transmitter and the receiver exists.

2. *Rician fading*: In the presence of a direct LOS in addition to the existence of several multipath components from the transmitter to the receiver, the fading envelope is better modeled by the Rician distribution. The PDF of $|h|$ for this distribution is given by

$$f_{|h|}(x) = \frac{x}{b_0} \exp\left\{-\frac{x^2+s^2}{2b_0}\right\} I_0\left(\frac{sx}{b_0}\right), \ x \geq 0, \tag{2.2}$$

   where s^2 is the specular power (non-centrality parameter), $2b_0$ is the scattered power and $I_0(\cdot)$ represents the zero-th order modified Bessel function of the first kind. The PDF (2.2) is also popularly expressed in terms of the Rice factor $K = s^2/(2b_0)$, defined as the ratio of the power of direct component to that of the scattered components. The special case $K = 0$ reduces to the Rayleigh fading case.

3. *Nakagami-m fading*: One of the most versatile fading channel models, the Nakagami-m distribution, fits empirical data and provides a better match than other models to some experimental data. For example, it accurately models land-mobile and indoor-mobile propagation environments [24]. For Nakagami-m fading, the PDF of $|h|$ is given by

$$f_{|h|}(x) = \frac{2m^m}{\Gamma(m)\Omega^m} x^{2m-1} \exp\left\{-\frac{mx^2}{\Omega}\right\}, \ x \geq 0, \tag{2.3}$$

where $\Gamma(x) = \int_0^\infty t^{x-1}e^{-t}dt$ is the Gamma function [26, eq. (6.1.1)] and $m \geq 0.5$ represents the severity of fading. Higher m means a less severe multipath effect. The Nakagami-m PDF reduces to the Rayleigh PDF for $m = 1$ and it can closely approximate the Rician PDF with $m = \frac{(1+K)^2}{1+2K}$.

2.1.2 Shadowing

The large-scale fading or shadowing causes the mean envelope $\Omega_{p,\text{dB}}$ to vary over large distances. This variation is traditionally modeled by the log-normal distribution as [25]

$$f_{\Omega_{p,\text{dB}}}(x) = \frac{1}{\sigma_{\Omega_{p,\text{dB}}}\sqrt{2\pi}} \exp\left\{-\frac{[10\log_{10}(x) - \mu_{\Omega_{p,\text{dB}}}]^2}{2\sigma^2_{\Omega_{p,\text{dB}}}}\right\}, \tag{2.4}$$

where $\mu_{\Omega_{p,\text{dB}}}$ and $\sigma_{\Omega_{p,\text{dB}}}$ are the mean and standard deviation of $\Omega_{p,\text{dB}} = 10\log_{10}(\Omega_p)$, respectively. However, an underlying difficulty with the log-normal distribution is that the performance analysis may not always be closed-form tractable. To overcome this difficulty, the shadowing part is often approximated by using the Gamma distribution which is frequently combined with the multipath fading model thus resulting in a composite fading distribution [27]. The squared envelope of the composite Gamma-shadowed Nakagami-m fading channel is popularly expressed by the K_G distribution as [28]

$$f_{|h|}(x) = \frac{4}{\Gamma(m)\Gamma(m_s)} \left(\frac{mm_s}{\Omega_s}\right)^{\frac{m+m_s}{2}} x^{m+m_s-1} \mathcal{K}_{m_s-m}\left(2x\sqrt{\frac{mm_s}{\Omega_s}}\right), x > 0, \tag{2.5}$$

where $\mathcal{K}_v(\cdot)$ is the v-th order modified Bessel function of second kind [26], the parameters $m_s = \frac{1}{e^{\sigma_s^2}-1}$, $\Omega_s = \mu_s\sqrt{\frac{m_s+1}{m_s}}$ are obtained by matching the mean and variance of the lognormal PDF with those of the Gamma PDF, respectively. It is interesting to note that recently, the composite fading distribution was also shown to be accurately representable in terms of the Mixture-Gamma (MG) distribution where the K_G distribution can be approximated by a weighted sum of Gamma random variables [29]. Such representation may be

more attractive for closed-form analysis.

2.2 Spectrum Sensing as a binary hypothesis testing problem

The task of detecting spectrum holes can be formulated as a composite binary hypothesis testing problem such that the received signal $y(t)$ at the detector at any time t can be represented as [30]

$$y(t) = \begin{cases} w(t) & : H_0, \\ h(t)\, S_p(t) + w(t) & : H_1, \end{cases} \tag{2.6}$$

where $S_p(t)$ is the signal transmitted by the PU, $w(t)$ is zero-mean additive white Gaussian noise (AWGN) at the receiver and $h(t)$ is the wireless fading channel coefficient. The PU signal is absent under hypothesis H_0 while hypothesis H_1 assumes its presence in the frequency band of interest. The fundamental task of the detector is to perform a discriminatory test and output a final decision in favor of one of the two hypotheses.

2.3 Non-Coherent Detectors for Spectrum Sensing

As emphasized in Section 1.4, non-coherent detectors such as the ED and its more general cousin, the p-norm detector are attractive because of their low-complexity attributed to non-requirement of PU signal information. This feature enables non-coherent detectors to be applicable across a variety of wireless systems deploying various modulation techniques, diversity combining schemes, and in disparity of wireless propagation conditions which largely affect the received signal at the detector. These scenarios may typically arise when CR networks aim to coexist with heterogeneous networks, where large variations in transmit powers, modulation schemes, differences in PHY and MAC specifications, among others, are prevalent [31].

2.3.1 The Energy Detector (ED)

The ED possesses a low implementation complexity as shown in Fig. 2.1. The received signal is passed through the pre-filter to obtain a band-limited noise power spectral density [19]. The filter output is then fed to a square-law device and subsequently integrated over a finite time interval to extract the decision variable T. An equivalent digital implementation of the ED essentially has an Analog-to-Digital Converter (ADC) at the filter output with a

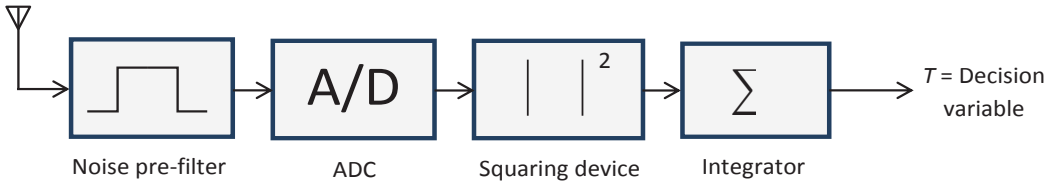

Fig. 2.1. Basic structure of an ED.

sufficiently high sampling rate followed by the squaring operation and a summing device to add the results over the observation interval such that the decision variable is given by [20]

$$T = \frac{1}{N}\sum_{i=1}^{N}\left(\frac{|y_i|}{\sigma_w}\right)^2 \underset{H_0}{\overset{H_1}{\gtrless}} \lambda, \tag{2.7}$$

where y_i is the digital signal sample at the output of the ADC, $\forall i \in \{1, 2, ..., N\}$, N is the sample size and σ_w^2 is the noise variance. The decision variable T is then compared against a pre-defined threshold λ to obtain a final decision on the hypothesis as shown in (2.7).

2.3.2 The p-norm Detector

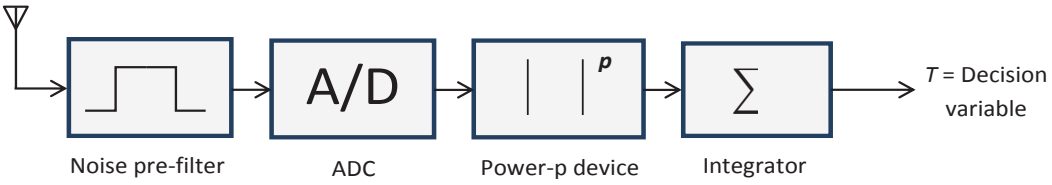

Fig. 2.2. The p-norm detector.

The ED, introduced to the research community in 1967 by the pioneering work by Urkowitz [19], has been very popular among researchers in its original form [30], [32]–[38]. However, to further improve the ED performance, a more general version of the ED with the squaring operation replaced by an arbitrary power $p > 0$ operation (see Fig. 2.2) is gathering significant attention. This generalized version of the ED is also termed as the improved ED [39] or the L_p-norm detector [40]. We refer to this detector as the p-norm detector throughout this thesis. The decision variable, T_p, of the p-norm detector has the following form

$$T_p = \frac{1}{N}\sum_{i=1}^{N}\left(\frac{|y_i|}{\sigma_w}\right)^p \underset{H_0}{\overset{H_1}{\gtrless}} \lambda, \tag{2.8}$$

where all the notations are consistent with (2.7). Clearly, the ED is a special case of it

with $p = 2$. This parameter p gives the detector a flexibility to tune itself according to various operating conditions to yield an improved performance compared to the traditional ED, especially at low SNRs [39] or in non-Gaussian noise [40].

2.4 Detection Performance Metrics and Fading Channels

The reliability of any detector is characterized in terms of two metrics called the probability of false alarm (P_f) and the probability of detection (P_d) which are defined as follows [41]:

1. *Probability of false alarm*: The probability that the detector falsely decides on H_1 when H_0 is true, given by $P_f = \mathbb{P}\left(T \geq \lambda | H_0\right)$ where $\mathbb{P}(\mathcal{X}|\mathcal{Y})$ denotes the probability of an event $\mathcal{X}$ conditioned on the event $\mathcal{Y}$. Naturally, for a reliable detection, a lower P_f is desirable.
2. *Probability of detection*: The probability that the detector correctly decides on H_1 when H_1 is true, i.e. $P_d = \mathbb{P}\left(T \geq \lambda | H_1\right)$. Thus, a higher P_d means a more reliable detector.

The fundamental requirement is to obtain analytical expressions for these metrics in order to gain useful insights on the detector's operating characteristics. Note that as only the detection probability (and not the false alarm probability) is affected by the SNR, γ, it can be denoted as $P_d(\gamma)$. Thus, only $P_d(\gamma)$ needs to be averaged over the fading statistics of γ for quantifying the average effect of fading/shadowing channels on the detection performance. Thus, in fading environments, the "average" performance over the fading distribution of the instantaneous SNR, γ, is important and thus, the average detection probability ($\overline{P}_d$) over the distribution of the received SNR is particularly of interest, which can be expressed as

$$\overline{P}_d = \mathbb{E}_\gamma[P_d(\gamma)], \tag{2.9}$$

where $\mathbb{E}_\gamma[\cdot]$ is the mathematical expectation with respect to the PDF of γ, which in turn, depends upon the underlying fading channel model under consideration.

In sub-section 2.4.2, the commonly adopted signal models in the ED literature, namely, the unknown deterministic signal model and the random signal model, are described. The corresponding expressions for the false alarm probability and the instantaneous detection probability of ED are also presented. However, before moving on to those details, we next briefly describe the Marcum-Q function which occurs in the representation of the in-

stantaneous detection probability $P_d(\gamma)$ in case of the unknown deterministic signal model (details in sub-section 2.4.2.1)

2.4.1 The Marcum-Q function

One of the most frequently arising functions in differentially coherent, partially coherent and non-coherent communication systems is the N-th order generalized Marcum-Q function, which is defined as [42]

$$Q_N(a,b) = \int_b^\infty \frac{x^N}{a^{N-1}} e^{-\frac{x^2+a^2}{2}} I_{N-1}(ax)dx \tag{2.10}$$

where a and b are non-negative real numbers and $I_M(\cdot)$ is the M-th order modified Bessel function of the first kind [26]. The Marcum-Q function often arises in practical cases, for example, the complementary cumulative distribution function (CCDF) of the non-central chi-square random variable occurring in signal detection problems; bit error probability expression for binary and quaternary modulation schemes, and others [42].

Due to the complicated nature of the canonical form (2.10) an alternative representation of the Marcum-Q function in terms of the contour integral is sometimes used [43]

$$Q_N(a,b) = \frac{1}{2\pi j} \oint_\Delta \frac{e^{\frac{a^2}{2}(\frac{1}{z}-1)+\frac{b^2}{2}(z-1)}}{z^N(1-z)} dz \tag{2.11}$$

where Δ is a circular contour of radius r and $\jmath$ denotes the imaginary unit. Since the singularities of the integrand are at $z = 0$ and $z = 1$, by Cauchy's theorem [44], any r, $0 < r < 1$, can be chosen. The form (2.11) has been shown to be useful for evaluating the average probability of detection under many practical cases of interest in fading and diversity combining [34], [36].

2.4.2 Classification of signals

According to the classical literature on signal detection theory, the signal to be detected can be classified as one of the three basic types: (i) completely known - deterministic; (ii) known except for a set of unknown parameters; (iii) completely random and thus specified by using probability distribution [45]. Among these, the models (ii) and (iii) are more practical ones in the communication theory problems and thus are interest of this thesis.

These two models along with their respective expressions for the probability are discussed in the following two sections.

2.4.2.1 Unknown deterministic signal model

Due to uncertain propagation characteristics of the mobile radio environment, it is common to assume the parameters of the signal received at the detector to be unknown although the signal generated at the PU transmitter is deterministic, that is, takes on the values determined by the exploited signaling waveform (for example, "one" or "zero" in case of a binary phase shift keying (BPSK) modulation). Thus, in the performance analysis of ED, one of the most widely used PU signal models is to assume the PU signal as unknown deterministic (non-random). The underlying notion for this model is that almost no information about the PU signal form is known such that no assumptions about it can be made [19]. For example, no assumptions on the amplitude, phase, time of arrival or frequency of the PU signal can be made at the CR receiver [45]. Hence, in these situations, it is common to treat the PU signal as deterministic (non-random) so that for the case when PU signal is present, the input to the detector would be a Gaussian signal (due to AWGN) with non-zero mean.

To this end, the SNR can be defined as

$$\gamma = \frac{|h|^2 E_s}{\sigma_w^2},$$

E_s being the signal energy. Following the developments of the well-known work [30] for the unknown deterministic signal model, the ED decision variable T under hypothesis H_0 is central chi-square distributed with $2N$ degrees of freedom. Similarly, T conditioned on γ under hypothesis H_1 is non-central chi-square distributed with $2N$ degrees of freedom and non-centrality parameter 2γ. Then, the detection probability and the false alarm probability can be expressed as [30]

$$\begin{aligned} P_d(\gamma) &= Q_N(\sqrt{2\gamma}, \sqrt{\lambda}), \\ P_f &= \frac{\Gamma(N, \lambda/2)}{\Gamma(N)}, \end{aligned} \tag{2.12}$$

respectively, where $Q_N(\cdot,\cdot)$ is the N-th order generalized Marcum-Q function [24]. The notation $\Gamma(a,x) \triangleq \int_x^\infty t^{a-1}e^{-t}dt$ is the upper incomplete Gamma function [26]. Even-

tually, as the interest is in evaluation of the average detection probability (2.9), it can be expressed as the following well-known integral [30]

$$\overline{P}_d = \int_0^\infty P_d(\gamma)\, f(\gamma) d\gamma = \int_0^\infty Q_N(\sqrt{2\gamma}, \sqrt{\lambda})\, f(\gamma) d\gamma, \tag{2.13}$$

where $f(\gamma)$ is the PDF of γ, which depends upon the fading environment. Hence, the fundamental problem is to obtain a solution for the integral (2.13), whose rigor is largely dependent upon the form of $f(\gamma)$.

2.4.2.2 Random signal model

In communications, certain cases may arise when the origin of the PU signals possess complex structure, for example, signals generated using spread spectrum modulation and encryption techniques, or when the PU signal is composed of a large number of independent but identical components such as: (i) large number of sub-carriers in an OFDM based system or (ii) in frequency-shift keying (FSK) signals having complex time-structure (continuous). In such cases, the resulting waveforms can be best modeled by a completely random distribution. To this end, one of the most popular PU signal models in the signal detection theory literature is that of the random Gaussian signal model [27], [45].

In this model, the PU signal $S_P(t)$ is treated as a complex Gaussian random variable with mean zero and variance σ_s^2 such that the received signals under hypotheses H_0 and H_1 are complex Gaussian with mean zero, variance σ_w^2 and $\sigma_w^2(1+\gamma)$ where the SNR is defined as

$$\gamma = \frac{|h|^2 \sigma_s^2}{\sigma_w^2}$$

(abusing the notation γ). Then, the false alarm probability in this case is same as in (2.12) while the detection probability is given by

$$P_d(\gamma) = \frac{\Gamma\big(N, \frac{\lambda}{2(1+\gamma)}\big)}{\Gamma(N)}. \tag{2.14}$$

Similar to the unknown deterministic model, subsequent use of (2.9) yields the desired average detection probability for this signal model as

$$\overline{P}_d = \int_0^\infty \frac{\Gamma\big(N, \frac{\lambda}{2(1+\gamma)}\big)}{\Gamma(N)}\, f(\gamma) d\gamma, \tag{2.15}$$

whose solution ease is largely determined by the form of $f(\gamma)$.

2.5 Central-limit theorem (CLT)

In probability theory, the CLT provides one of the most widely used approximations for the distribution of the arithmetic mean of a sufficiently large number of occurrences of independent random variables with given mean and variance. According to the Lindeberg-Lévy's CLT theorem, if $X_1, X_2, ..., X_N$ are independent and identically distributed (i.i.d.) random variables with mean $\mu < \infty$ and variance $\sigma^2 < \infty$, then the normalized average $Z_N = \frac{S_N - m_N}{s_N}$, where $S_N = \sum_{k=1}^{N} X_k$, $m_N = \mathbb{E}[S_N]$ and $s_N^2 = \text{Var}[S_N]$, converges in distribution to the standard normal random variable as $N \to \infty$ [46]. That is,

$$\lim_{N\to\infty} \left(Z_N \triangleq \sum_{k=1}^{N} \frac{X_k - \mu}{\sqrt{N}\sigma} \right) \xrightarrow{\mathcal{D}} \mathcal{N}(0,1). \tag{2.16}$$

Although other variations (by Lyapunov, Linderberg-Feller) of the CLT for independent but non-identical random variables exist in the literature, the CLT (2.16) suffices the purpose for this thesis study.

2.5.1 Application to Spectrum Sensing

In order to characterize and design sensing systems for the potential spectrum holes over fading channels, the evaluation of (2.9) often becomes a critical limiting factor, mainly because closed-form solutions for $\overline{P}_d$ which requires solution of integrals (2.13) or (2.15) are often lacking. The problem becomes often tedious because of the form of $f(\gamma)$ which is further attributed to the operating conditions (fading, shadowing, interference, diversity, and others) under consideration. Closed-form solutions for $\overline{P}_d$ are desirable mainly because of their ease of applicability in parameter optimization problems. Thus, in order to impart ease of analysis in further applications, a popular approximation, which yields a simpler functional form (than the generalized Marcum-Q or the incomplete Gamma function), is based on the CLT. According to CLT approximation, given a large number of samples are available ($N \gg 1$), the ED decision variable T can be approximated by a Gaussian distributed random variable under both hypotheses as $T|H_0 \sim \mathcal{N}(m_0, \sigma_0^2)$ and $T|H_1 \sim \mathcal{N}(m_1, \sigma_1^2)$. Then, detection probability, P_d^{clt}, and the false alarm probability, P_f^{clt} for the

CLT approximation can be easily expressed as

$$P_d^{\text{clt}} \approx Q\left(\frac{\lambda - m_1}{\sigma_1}\right), \\ P_f^{\text{clt}} \approx Q\left(\frac{\lambda - m_0}{\sigma_0}\right), \tag{2.17}$$

where $Q(\cdot)$ is the Gaussian-Q function. The approximate forms (2.17), although being valid only for the large samples, have been widely used in analyzing problems related to sensing-throughput tradeoff [47], low SNR parameter optimization [37], optimal multiband joint sensing [48], and others.

2.6 Classical Antenna Diversity Schemes for Spectrum Sensing

Antenna diversity techniques are known to improve the signal reception by exploiting the advantage of the spatial dimension at the receiver. Receiving multiple replica of the fading signal via different antenna branches and combining them improves the overall received SNR [24]. This technique has been known to combat the effect of multipath fading since different diversity branches may not concurrently go into deep fading and the branches with better SNR quality can compensate even if the signals in other branches are in deep fade. The ED performance has been shown to significantly improve through the use of multiple antennas [33], [34], [49], [50].

The signal received at the multiple antennas may be combined in different ways. Four classical diversity combining schemes are briefly summarized below:

1. *Maximal Ratio Combining (MRC):* A coherent combining scheme which requires CSI thus requiring estimation of both amplitude and phase of the fading branches. Signals received at each branch are weighted by their respective channel coefficients before combining [24]. This scheme is optimal in performance (in absence of interference), the requirement of complete CSI being a tradeoff in terms of cost and complexity.

2. *Equal Gain Combining (EGC):* The EGC scheme, unlike MRC, does not require the amplitudes of the fading channels but only their phases thus reducing the estimation complexity [24]. This scheme is particularly useful for symbols with equal energy (such as symbols from phase shift keying constellation).

3. *Selection Combining (SC):* A reduced complexity scheme which processes a single branch with the largest SNR and thus does not require processing of the signals coming from each branch [24]. This scheme requires continuous monitoring of signals from each branch.

4. *Square Law Combining (SLC):* A non-coherent combining scheme in which the received signal at each branch is squared before combining [33]. This scheme is particularly useful for non-coherent operation without any CSI.

2.7 Cooperative Diversity in Spectrum Sensing

To overcome the hidden terminal problem, one solution is to exploit a collaborative network of CRs for the detection of the presence/absence of the PU. In such a collaborative network, each CR independently senses the spectrum and reports its observation to the SU entity called the fusion center (FC) (for example, a central coordinator such as the secondary base station [16]). As shown in Fig. 2.3, the FC is shadowed from the PU transmission. However, the other CRs ($\mathrm{CR}_1, \mathrm{CR}_2, ..., \mathrm{CR}_K$), which are not shadowed from the PU can listen to the PU transmission and thus can forward their observations/decisions to the FC which combines the individual observations/decisions to yield the final decision on the presence/absence of the PU. Several analytical and simulation studies with different protocols have underlined the benefits of cooperative spectrum sensing in improving the detection reliability [51]–[54].

At the FC, the possible schemes to combine the observations received from several CRs can be broadly categorized into two: data fusion and decision fusion, as described next [36].

1. *Data Fusion:* In this fusion scheme, the cooperative nodes simply receive and forward their observations without making any decision on the presence/absence of the PU. One example of such scheme is the amplify-and-forward scheme where the cooperative node scales the received signal and forwards the resulting one to the FC [55]. This is a form of soft-combination of the individual CR observations. In this case, the bandwidth of each CR-to-FC channel should be equal to the corresponding PU-to-CR channel bandwidth for reporting the observation from the CR to the FC.

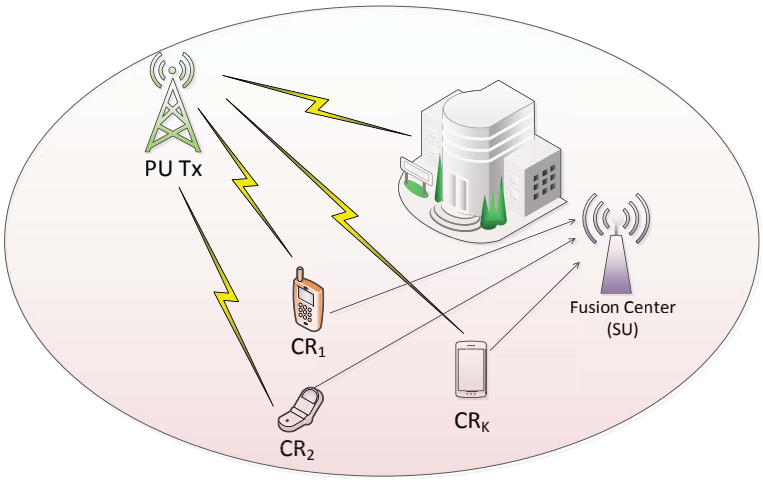

Fig. 2.3. Cooperative spectrum sensing.

2. *Decision Fusion:* In the decision fusion scheme, the cooperative nodes independently decide on the presence/absence of the PU signal based on their observation and forward the resulting decisions to the FC. Thus, this scheme is a hard-combination of the individual CR observations. Since only the binary decisions based on the received signals are forwarded by the CRs to the FC, this scheme requires a lower CR-to-FC channel bandwidth than that required for the data fusion scheme. Examples of decision fusion rules are the OR and AND rules [21]. In case of the OR rule, the FC decides on the presence of the PU if any one of the CRs have decided on its presence whereas in case of the AND rule, the PU decides on the presence of the PU only if all the CRs have their decisions in favor of its presence.

Chapter 3

New Asymptotics for Performance of Energy Detector in Fading and Diversity Reception

Missed-detection probability expressions for ED often involve infinite series and do not provide quick insights into the effects of operating conditions. To overcome these limitations, in this chapter [1] we develop novel asymptotic analyses by proposing an approximate PDF of a random variable β, which, in general, can characterize fading channels in diverse operating conditions. The coefficients of the proposed approximate PDF of β are obtained by matching the coefficients of the approximate PDF's series expansion (or coefficients of the approximate PDF's moment generating function (MGF)) with those of the exact PDF (or MGF) of β. By using the proposed approximation, a unified closed-form asymptotic missed-detection probability is derived. Its usefulness is then demonstrated for fading channels without and with antenna diversity, for cooperative detection, and in co-channel interference. For each case, the sensing gain, which reveals the effect of the operating conditions on the spectrum sensing performance, is determined explicitly. Furthermore, the asymptotic Complementary Area Under the receiver operating characteristic Curve, an alternative performance metric, is derived, and found to reveal the sensing gain. Numerical results verify the accuracy of our derived asymptotic expressions over a wider SNR range compared to the existing asymptotic solution, which is accurate only for high SNRs.

[1] Chapter 3 has been published in the *IEEE Transactions on Communications* as [56] and also in part in the *Proceedings of IEEE Global Communications Conference* as [57].

3.1 Introduction and Motivation

The ED performance is fundamentally measured by the false alarm probability, P_f, and the detection probability, P_d, or, equivalently, the missed-detection probability $P_{md} = 1 - P_d$. However, in fading channels, the average P_{md} (P_d) denoted by $\overline{P}_{md}$ ($\overline{P}_d$) is the critical measure. The process of determining $\overline{P}_{md}$ ($\overline{P}_d$) involves two steps. First, $P_{md}(\gamma)$ ($P_d(\gamma)$) for a fixed channel realization is given in terms of the generalized Marcum-Q function (see (3.2) in Section 3.2), which depends on the random (instantaneous) SNR γ. By definition, γ can be expressed as $\gamma = \overline{\gamma}\beta$, where $\overline{\gamma}$ is the average SNR (referred to as "SNR" henceforth),[2] and β is a non-negative random variable, which in turn depends on the operating conditions (including the fading channel, antenna diversity, co-operative diversity, interference, and others). For example, in case of fading, β can represent the squared channel amplitude as $\beta = |h|^2$. Thus, β being random, is characterized by a PDF $f(\beta)$. In the second step, $P_{md}(\gamma)$ ($P_d(\gamma)$) is integrated over $f(\beta)$ to obtain the average detection performance (see details in Section 3.2).

This process has been extensively used for accurately characterizing the ED performance in a wide variety of operating conditions [30], [32]–[34], [58], [59]. Although these results are exact (without any approximations), they have some limitations. For example,

(i) The multiple-antenna based results in [30] and [33] are restricted to the Rayleigh fading model only, due mainly to the intractability of Marcum-Q integrals, in general.

(ii) The results for Nakagami-m and Rician fading derived by utilizing contour-integral representation of the generalized Marcum-Q function consist of complicated higher-order derivatives of composite functions [34].

(iii) The unified expressions presented in [58] and [59] involve infinite series, which require truncation (to finite terms). However, tight bounds on the truncation error are often analytically intractable, and hence, trial-and-error methods are needed to determine the truncation point for the desired level of precision.

(iv) None of the derived expressions provide quick insights into the impact of the operating conditions, but require numerical analysis to reveal such insights.

[2]For brevity, in the remainder of this chapter, the term "SNR" without "instantaneous" means the "average SNR".

These limitations, however, can be mitigated by using asymptotic techniques. Before discussing their advantages, we will briefly elaborate on the meaning of the term "asymptotic." For example, $1/x$ is an asymptotic of $1/(x+1)$ because $\lim_{x\to\infty} \frac{x}{x+1} = 1$. More specifically, if $x \to 0^+$ (x tends to 0 from above), then the notation $h(x) = g(x) + O(x^{r+1})$, where $g(x) = \sum_{j=0}^{r} a_j x^j$, implies that the difference $|h(x) - g(x)|$ is smaller than $C|x^{r+1}|$ for a constant C as $x \to 0^+$. Then, $g(x)$ is called an asymptotic (approximation) of $h(x)$ with an error term $O(x^{r+1})$ as $x \to 0^+$. Similarly, for $x \to \infty$, a series of x^{-j} forms an asymptotic expansion. Thus, for an ED, if $\overline{P}_{md}^{\text{exact}}$ is the exact missed-detection probability, and $\overline{P}_{md}^{\text{asy}}$ is an approximation at high SNR ($\overline{\gamma} \gg 1$), assume

$$\overline{P}_{md}^{\text{exact}} = \overline{P}_{md}^{\text{asy}} + O\left(\frac{1}{\overline{\gamma}^M}\right),$$

where M is a non-negative integer. Then, $\overline{P}_{md}^{\text{asy}}$ is called an asymptotic (approximation) of $\overline{P}_{md}^{\text{exact}}$ with error term $O(1/\overline{\gamma}^M)$. Moreover, since the error term decays as $1/\overline{\gamma}^M$, for sufficiently large $\overline{\gamma}$, the accuracy of $\overline{P}_{md}^{\text{asy}}$ is good enough for all practical engineering applications. Hence, to derive such $\overline{P}_{md}^{\text{asy}}$, we first note that as the SNR becomes large ($\overline{\gamma} \gg 1$), detection errors occur only if the channel fades deeply. Since a deep fading is equivalent to $\beta \to 0^+$, a suitable polynomial representation of $f(\beta)$ near $\beta = 0$ can be used to derive the average asymptotic missed-detection probability $\overline{P}_{md}^{\text{asy}}$.

Despite having such advantages, the existing asymptotic analysis of ED is limited only to [3]. This work utilizes the simple, approximate analysis presented in the seminal work by Wang and Giannakis [60] to derive the asymptotic $\overline{P}_{md}$, which is accurate for the high SNR regime ($\overline{\gamma} \gg 1$). The results of [3] are important for determining the "sensing gain," which is the magnitude of the slope of the log-log plot of $\overline{P}_{md}$ vs. $\overline{\gamma}$ at high SNR. More importantly, the sensing gain provides quick insights into how fading impacts the ED, and thus is a useful performance indicator.

However, the asymptotic analysis [3] is inherently limited to the high SNR regime (say, $\overline{\gamma} \geq 20$ dB). In practice, the operating SNR can be well below 20 dB, in, for example, the IEEE 802.16 local and metropolitan area networks [61]. Thus, the analysis in [3] is not sufficient for characterizing the ED performance over a wider SNR range (optimistically, $0 \leq \overline{\gamma}\,\text{dB} < \infty$). Moreover, a unified expression for $\overline{P}_{md}$, which would be applicable to a multitude of wireless communication scenarios thus providing an effective platform

for designing practical spectrum sensing systems, is needed. However, such a platform is lacking. To address these requirements, we propose a new simple approximation for the PDF of β as $\beta \to 0^+$ and derive the corresponding asymptotic $\overline{P}_{md}$. The attractive features of the results derived by using our proposed analysis are the following:

1. Unified expressions for multipath fading channels without and with antenna diversity, with multiple cooperative relays, with interferers, and in other operating conditions;
2. Explicit sensing gain expressions;
3. Closed-form expressions without infinite-series sums or higher order derivatives; and
4. High accuracy over wider SNR ranges.

These features are achieved by our proposed approximation $f^{\text{app}}(\beta)$ (3.6), whose parameters can be obtained from the operating conditions by matching $f^{\text{app}}(\beta)$ to the exact $f(\beta)$ or by matching the MGF of β obtained by using $f^{\text{app}}(\beta)$ to that obtained by using the exact $f(\beta)$ (see details in Section 3.3). Besides these benefits, performance metrics other than $\overline{P}_{md}$ can also be analyzed. For example, we derive a unified asymptotic expression for the average CAUC, which serves as a single figure of merit for characterizing the ED performance [37].

The rest of this chapter is organized as follows. The problem is stated in Section 3.2. The new approximation for the exact PDF is proposed in Section 3.3. The unified asymptotic $\overline{P}_{md}$ is derived in Section 3.4. Analyses for fading channels without diversity, with antenna diversity, with cooperative diversity, and in interference are presented in Section 3.5, Section 3.6, Section 3.7 and Section 3.8, respectively. The asymptotic expression for the average CAUC is derived in Section 3.9. Concluding remarks are made in Section 3.10.

3.2 Problem Statement

For the unknown deterministic signal model, from Chapter 2, the false alarm probability and the miss-detection probability are

$$P_f = \frac{\Gamma(N, \lambda/2)}{\Gamma(N)}, \tag{3.1}$$

$$P_{md}(\gamma) = 1 - Q_N(\sqrt{2\gamma}, \sqrt{\lambda}), \tag{3.2}$$

respectively, where, the instantaneous SNR is expressed as $\gamma = \overline{\gamma}\beta$, with β being the random variable depending upon the operating conditions ($\overline{\gamma}$ being the average SNR). Reiterating, the false alarm probability (3.1) is independent of β while the missed-detection probability (3.2) depends upon β (as $\gamma = \overline{\gamma}\beta$) and needs to be averaged over $f(\beta)$ for evaluating the overall (average) performance, as shown next.

3.2.1 Performance of Energy Detector over Fading Channels

The average probability of missed-detection, $\overline{P}_{md}$, is the expectation of (3.2) over $f(\beta)$ which can be expressed as

$$\overline{P}_{md} = \mathbb{E}_{\beta}[P_{md}(\gamma)] = 1 - \int_0^{\infty} Q_N(\sqrt{2\overline{\gamma}\beta}, \sqrt{\lambda}) f(\beta) d\beta, \tag{3.3}$$

where $\mathbb{E}_{\beta}[\cdot]$ denotes the expectation with respect to β. Thus, the main challenge in (3.3) is averaging the generalized Marcum-Q function over $f(\beta)$. Since closed-form solutions for integrals involving the generalized Marcum-Q function are limited [62], it is important to find an approximate form of $f(\beta)$ that facilitates the evaluation of (3.3) without leading to tedious analytical expressions involving complicated special functions and/or infinite series.

3.2.2 Existing Approximation for $f(\beta)$

As stated in Section 3.1, the idea is to approximate the exact $f(\beta)$ by using its polynomial representation near $\beta = 0$. The underlying concept is that of the local approximations via polynomials where a function's behavior may be captured by using polynomial representation of the function. This concept is supported by the fact that many practical functions of interest locally behave like the polynomials at most of the points in their domain, that is, the functions can be thought of as "locally polynomial" [63], [64]. Then, the problem would be to find the coefficients of the polynomials.

To this end, the Taylor's theorem is one of the most suited concepts for approximating an analytic function $g(x)$ about a point $x = a$ as

$$g(x) = \sum_{n=0}^{\infty} \frac{g^{(n)}(a)}{n!} (x - a)^n$$

where $g^{(n)}(a)$ denotes the n-th derivative of $g(x)$ evaluated at $x = a$. Following this con-

cept of using local approximations via polynomials, the work [3] utilizes the approximate $f(\beta)$ proposed by Wang and Giannakis [60], to derive the asymptotic $\overline{P}_{md}$. Suppose the exact PDF $f(\beta)$ can be expanded as a Taylor's series as $\beta \to 0^+$ (Maclaurin's series) in the form

$$f(\beta) = \sum_{i=0}^{\infty} a_i \beta^{t+i}, \tag{3.4}$$

where a_i for $i = 0, 1, 2, ...$ are coefficients in the expansion, and $t \geq 0$ represents the order of smoothness of $f(\beta)$ at $\beta = 0$. The main idea of [60] is to approximate $f(\beta)$ by the monomial [60]

$$f^{\text{wg}}(\beta) = a_o \beta^t + O(\beta^{t+1}). \tag{3.5}$$

Here, the superscript 'wg' indicates 'Wang and Giannakis'. Note that the expansion (3.4) holds for all practical fading models like Rayleigh, Nakagami-q, Nakagami-n and Nakagami-m [60]. Also, if antenna diversity is employed, the PDF of the combined β depends upon the number of antennas and the underlying fading model. The representation (3.4) has been shown to hold for different combining schemes such as MRC, SC, EGC as well.

By utilizing $f^{\text{wg}}(\beta)$, the authors in [3] derive an asymptotic $\overline{P}_{md}$ and show that for large SNRs ($\overline{\gamma} \gg 1$), the sensing gain is equal to $t+1$. However, their $\overline{P}_{md}$ is accurate only in the high SNR regime (say, $\overline{\gamma} \geq 20\,\text{dB}$). Intuitively, this result suggests that an approximation for $f(\beta)$ other than $f^{\text{wg}}(\beta)$ is needed that can yield a closed-form $\overline{P}_{md}$ which is accurate over a wider range of SNRs (say, $0 \leq \overline{\gamma}\,\text{dB} < \infty$). Furthermore, the derived $\overline{P}_{md}$ at high SNR should also reveal the sensing gain. With these goals in mind, we propose a new approximation for the exact $f(\beta)$ in the following section.

3.3 New Approximation for $f(\beta)$

The existing approximation (3.5) utilizes a single term in (3.4) and is accurate only for high SNRs. The reason is that $f^{\text{wg}}(\beta)$ is accurate for $\beta \to 0^+$ only. When $\beta \to \infty$, $a_0\beta^t$ grows unbounded. So, $f^{\text{wg}}(\beta)$ is only a localized approximation for $f(\beta)$. One way to achieve a better accuracy over wider SNR ranges may be to utilize more number of terms in (3.4). However, simply considering more number of terms in (3.4) may still lead to a diverging behavior of the approximate $f(\beta)$ at $\beta \to \infty$ (as shown in Fig. 3.1 later) which may further lead to the average (over $0 \leq \beta < \infty$) P_{md} to exceed 1 for small SNRs (as explained in

Section 3.3.2). Thus, in addition to improving the accuracy, it is also necessary to ensure that the approximate $f(\beta)$ does not diverge as $\beta \to \infty$. Additionally, the approximate $f(\beta)$ should facilitate a closed-form evaluation of (3.3).

3.3.1 Proposed Approximation

To this end, since an exponential function of the form $e^{-\beta}$ would converge to zero as $\beta \to \infty$, we consider a new representation of $f(\beta)$ by combining (3.5) with a dual exponential sum to propose an approximation $f^{\text{app}}(\beta)$ of the form

$$f^{\text{app}}(\beta) = a\beta^t(e^{-\theta_1\beta} + e^{-\theta_2\beta}), \text{ as } \beta \to 0^+, \tag{3.6}$$

where $a > 0$, t is a non-negative integer, $\theta_1 \geq 0$, and $\theta_2 \geq 0$ are the parameters that can be chosen to match the operating conditions (fading, antenna diversity, cooperative diversity, etc.). Interestingly, the Maclaurin's series expansion of (3.6) satisfies (3.4) (details in Section 3.3.2). Note that $f^{\text{wg}}(\beta)$ is a special case of our $f^{\text{app}}(\beta)$ when $\theta_1 = \theta_2 = 0$. Also, $f^{\text{app}}(\beta)$ is equivalent to [65, eq. (3)] for the case $\theta_1 = \theta_2 = \theta$. Thus, $f^{\text{app}}(\beta)$ is more general than either $f^{\text{wg}}(\beta)$ or [65, eq. (3)]. Moreover, $f^{\text{app}}(\beta)$, just like $f^{\text{wg}}(\beta)$, is not a proper PDF; that is, the area under $f^{\text{app}}(\beta)$ is not necessarily 1. Next, the parameters of $f^{\text{app}}(\beta)$ are derived from two methods based on the availability of the exact PDF or MGF of β.

3.3.2 Parameter determination using the exact PDF of β

In some cases of interest, when the exact $f(\beta)$ is known analytically and satisfies the Maclaurin's series (3.4), the parameters of $f^{\text{app}}(\beta)$ can be readily obtained as stated in Proposition 1.

Proposition 1. *Given a_0, a_1 and a_2 from (3.4), the parameters of $f^{app}(\beta)$ can be expressed as*

$$a = \frac{a_0}{2} \tag{3.7}$$

$$(\theta_1, \theta_2) = \left(\frac{b_1 + \sqrt{2b_2 - b_1^2}}{2}, \frac{b_1 - \sqrt{2b_2 - b_1^2}}{2}\right), \tag{3.8}$$

with $b_1 = -2a_1/a_0$ and $b_2 = 4a_2/a_0$.

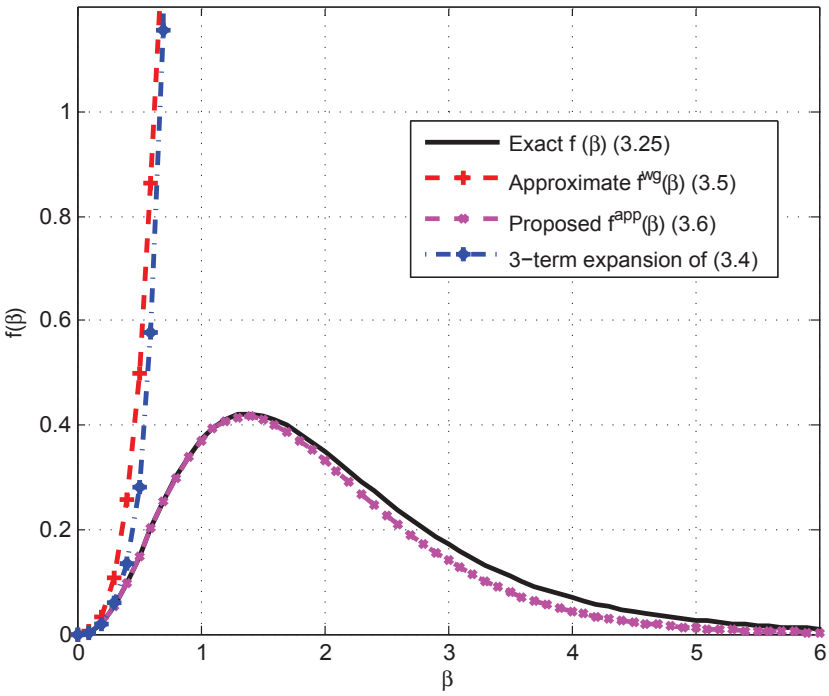

Fig. 3.1. $f^{\text{app}}(\beta)$, $f^{\text{wg}}(\beta)$ and exact $f(\beta)$ for 4-branch SC in i.i.d. Rayleigh fading.

Proof. By Maclaurin's series expanding (3.6) and grouping the resulting terms in ascending powers of β, we get

$$f^{\text{app}}(\beta) = 2a\beta^t - (\theta_1 + \theta_2)a\beta^{t+1} + \frac{(\theta_1^2 + \theta_2^2)}{2}a\beta^{t+2} + O(\beta^{t+3}). \tag{3.9}$$

Then, by matching the coefficients of the first three terms in (3.4) with the corresponding coefficients in (3.9), the parameter a in (3.6) is immediately given by (3.7) while the other two parameters, θ_1 and θ_2, satisfy the simultaneous equations

$$\theta_1 + \theta_2 = -\frac{2a_1}{a_0} \triangleq b_1 \text{ and } \theta_1^2 + \theta_2^2 = \frac{4a_2}{a_0} \triangleq b_2, \tag{3.10}$$

which can be easily solved to yield (3.8). □

To quickly gain insights into the benefits of Proposition 1, we compare $f^{\text{app}}(\beta)$ and $f^{\text{wg}}(\beta)$ for SC in i.i.d. Rayleigh fading with $L = 4$ antennas (Fig. 3.1). Here, the exact $f(\beta)$ is given by (3.25), and by using Proposition 1, the parameters of $f^{\text{app}}(\beta)$ are derived in Section 3.6.2. Fig. 3.1 reveals that $f^{\text{wg}}(\beta)$ widely diverges from the exact $f(\beta)$ as β gets large. Thus, $f^{\text{wg}}(\beta)$ works only for $\beta \to 0^+$, which implies the deep fade condition. That

is, $f^{\text{wg}}(\beta)$ requires the operating SNR to be large ($\overline{\gamma} \gg 1$) in order to yield low detection errors. Another interesting observation in Fig. 3.1 is that the 3-term based expansion of (3.4), which has been plotted for comparison, clearly shows the diverging behavior similar to $f^{\text{wg}}(\beta)$ as $\beta \to \infty$. This observation thus indicates that simply increasing the number of terms in (3.4) may still lead to a diverging behavior of the approximate $f(\beta)$ as $\beta \to \infty$. To this end, these results inherently suggest that when $f^{\text{wg}}(\beta)$ is used in (3.3) for averaging the missed-detection probability, the resulting probability can even exceed 1 for small SNRs ($\overline{\gamma} \to 0^+$). This finding indicates the breakdown of the asymptotic approach of [3] (demonstrated later in Section 3.4 through Section 3.9). In contrast, Fig. 3.1 shows that our proposed $f^{\text{app}}(\beta)$ follows the exact $f(\beta)$ more closely (without-diverging) over $0 \leq \beta < \infty$. Thus, we can expect the resulting $\overline{P}_{md}^{\text{asy}}$ expression to not break down even as $\overline{\gamma} \to 0^+$. These advantages of $f^{\text{app}}(\beta)$ have two causes:

(i) $f^{\text{app}}(\beta)$ matches the first three terms of the series expanded exact $f(\beta)$ (3.4) while $f^{\text{wg}}(\beta)$ utilizes only the first term of (3.4). Thus, $f^{\text{app}}(\beta)$ uses more information from the exact $f(\beta)$, and this feature leads to highly accurate asymptotic results (see Section 3.4.1).

(ii) $f^{\text{app}}(\beta)$ does not grow unbounded as $\beta \to \infty$ because of the factor $(e^{-\theta_1 \beta} + e^{-\theta_2 \beta})$, a sum of two exponentials. This characteristic extends the valid SNR range of the resulting $\overline{P}_{md}^{\text{asy}}$, thus maintaining reasonable accuracy even as $\overline{\gamma} \to 0^+$.

These advantages are numerically verified with some practical examples presented in Sections 3.5-3.9. Next, an alternative method to obtain the parameters of $f^{\text{app}}(\beta)$ based on the MGF of β is presented.

3.3.3 Parameter determination using the exact MGF of β

To use Proposition 1, one needs the exact analytical $f(\beta)$. However, as β depends on the fading model, antenna diversity combining schemes and other factors, the exact $f(\beta)$ may be be intractable in some cases. On the other hand, for say, multiple antenna systems, the exact MGF of β may be readily obtainable (for example, when β is given by a sum of independent random variables, its MGF is the product of MGFs of those random variables). Thus, in such cases, the MGF is easier to obtain than the corresponding PDF. So, whenever the exact MGF of β is directly available, the parameters of $f^{\text{app}}(\beta)$ can be derived as

follows.

Proposition 2. *If the exact MGF of β, $\mathcal{M}_\beta(s)$, $s > 0$ is expandable in the series-form*

$$\mathcal{M}_\beta(s) = \frac{X_0}{s^\alpha} + \frac{X_1}{s^{\alpha+1}} + \frac{X_2}{s^{\alpha+2}} + O\left(\frac{1}{s^{\alpha+3}}\right), \tag{3.11}$$

then as $s \to \infty$, the parameters t and a of $f^{app}(\beta)$ are given by

$$t = \alpha - 1, \;\; a = \frac{X_0}{2\Gamma(\alpha)}, \tag{3.12}$$

with the parameters θ_1 and θ_2 satisfying

$$\begin{aligned} \theta_1 + \theta_2 &= -\frac{2X_1}{X_0\alpha} \triangleq b_1, \\ \theta_1^2 + \theta_2^2 &= \frac{4X_2}{X_0\alpha(\alpha+1)} \triangleq b_2. \end{aligned} \tag{3.13}$$

Then, substitution of b_1 and b_2 from (3.13) into (3.8) immediately yields θ_1 and θ_2.

Proof. According to the initial value theorem for (one-sided) Laplace transforms, if $F(s) = \int_0^\infty f(t)e^{-st}dt$ is the (one-sided) Laplace transform of $f(t)$, then [66]

$$\lim_{t\to 0} f(t) = \lim_{s\to\infty} sF(s).$$

Thus, as suggested by this theorem, the behavior of $f(\beta)$ at $\beta \to 0^+$ depends on its MGF at $s \to \infty$ [60]. Thus, the idea is to match the exact MGF of β with the MGF obtained by using $f^{\text{app}}(\beta)$ as $s \to \infty$, provided the MGFs exist. The MGF corresponding to $f^{\text{app}}(\beta)$, denoted by $\mathcal{M}_\beta^{\text{app}}(s)$, can be obtained as

$$\begin{aligned} \mathcal{M}_\beta^{\text{app}}(s) &= a\int_0^\infty e^{-s\beta}\beta^t(e^{-\theta_1\beta} + e^{-\theta_2\beta})d\beta \\ &= a\Gamma(t+1)\left[\frac{1}{(s+\theta_1)^{t+1}} + \frac{1}{(s+\theta_2)^{t+1}}\right] \end{aligned} \tag{3.14}$$

where the definition of Gamma function $\Gamma(\cdot)$ is used. Expanding (3.14) in a series-form as

$s \to \infty$, and re-arranging the terms, we get

$$\mathcal{M}_{\beta}^{\text{app}}(s) = \frac{2a\Gamma(t+1)}{s^{t+1}} - \frac{a(t+1)\Gamma(t+1)(\theta_1+\theta_2)}{s^{t+2}} + \frac{a(t+1)(t+2)\Gamma(t+1)(\theta_1^2+\theta_2^2)}{2s^{t+3}} + O\left(\frac{1}{s^{t+4}}\right). \tag{3.15}$$

Thus, matching (3.11) and (3.15) yields the parameters (3.12) and the two simultaneous equations in (3.13), which have the same form as (3.10) with the solution given by (3.8). □

Having shown how the parameters of $f^{\text{app}}(\beta)$ are retrieved, we next derive the corresponding asymptotic missed-detection probability, $\overline{P}_{md}^{\text{asy}}$.

3.4 Average Missed-Detection Probability

To derive $\overline{P}_{md}^{\text{asy}}$, we need to substitute $f^{\text{app}}(\beta)$ into (3.3) and evaluate the resulting integral. However, direct evaluation of this integral would yield an infinite series expression [34, eq. (5)]. To eliminate this problem, we use the MGF $\mathcal{M}_{\beta}^{\text{app}}(s)$ (3.14) along with the contour integral representation of the generalized Marcum-Q function [67], [68] to derive $\overline{P}_{md}^{\text{asy}}$. Although such an approach has been utilized by [34], the results are given in terms of higher-order derivatives. In contrast, we derive a simpler closed-form $\overline{P}_{md}^{\text{asy}}$ expression which does not contain infinite series sums and/or higher-order derivatives. Furthermore, the derived $\overline{P}_{md}^{\text{asy}}$ unifies the analysis for fading channel models without diversity (Section 3.5), with antenna diversity (Section 3.6), with cooperative diversity (Section 3.7), and in interference (Section 3.8). Moreover, the excellent numerical match of our derived $\overline{P}_{md}^{\text{asy}}$ with the exact results is reported in the corresponding sections. Next, we give one of our principal results in Proposition 3 below.

Proposition 3. *Based on the proposed approximation $f^{app}(\beta)$, the average missed-detection probability $\overline{P}_{md}^{asy}$ can be expressed as* (3.16)*,*

$$\overline{P}_{md}^{asy} = \begin{cases} 1 - a\Gamma(t+1)e^{-\lambda/2}\sum_{i=1}^{2}\frac{1}{(\theta_i+\widetilde{\gamma})^{t+1}}\left[\Psi(i)+\Phi(i)\right] & \text{for } N > t+1 \\ 1 - a\Gamma(t+1)e^{-\lambda/2}\sum_{i=1}^{2}\frac{1}{(\theta_i+\widetilde{\gamma})^{t+1}}\Psi(i) & \text{for } N \leq t+1, \end{cases} \tag{3.16}$$

with $\Psi(i)$ and $\Phi(i)$ given by

$$\begin{aligned}\Psi(i) &= \frac{e^{\lambda\eta_i/2}}{t!}\sum_{k=0}^{t}\Bigg[\binom{t}{k}\frac{(-1)^k\prod_{j=1}^{k}(N-t+j-2)}{\eta_i^{N-t-1+k}} \\ &\qquad\times\sum_{\nu=0}^{t-k}\frac{(\lambda/2)^{t-k-\nu}}{(1-\eta_i)^{\nu+1}}\frac{(t-k)!}{(t-k-\nu)!}\Bigg], \\ \Phi(i) &= \frac{(-1)^{-(t+1)}}{(N-t-2)!}\sum_{k=0}^{N-t-2}\Bigg[\binom{N-t-2}{k}\frac{\prod_{j=1}^{k}(t+j)}{\eta_i^{t+k+1}} \\ &\qquad\times\sum_{\nu=0}^{N-t-k-2}\frac{(\lambda/2)^{N-t-k-2-\nu}(N-t-k-2)!}{(N-t-k-2-\nu)!}\Bigg]\end{aligned} \tag{3.17}$$

with $\eta_i = \overline{\gamma}/(\theta_i + \overline{\gamma})$, $i = 1, 2$.

Proof. The proof is given in Appendix A.1. □

At a sufficiently high SNR ($\overline{\gamma} \gg 1$), $\overline{P}_{md}^{\text{asy}}$ (3.16) reduces to the form $\overline{P}_{md}^{\text{asy}} \approx 1 - g(N,t,\lambda)\overline{\gamma}^{-(t+1)}$, where $g(N,t,\lambda)$ is a function independent of $\overline{\gamma}$. Clearly, the sensing gain, which is equal to the magnitude of the slope of the log-log plot of $\overline{P}_{md}^{\text{asy}}$ vs. $\overline{\gamma}$ at high SNR, is given by magnitude of the exponent of $\overline{\gamma}$ occurring in $\overline{P}_{md}^{\text{asy}}$, which is equal to $(t+1)$. This observation is consistent with the sensing gain given by [3]. Hence, our derived asymptotic explicitly reveals the sensing gain.

3.4.1 Accuracy of (3.16)

The accuracy of the derived $\overline{P}_{md}^{\text{asy}}$ (3.16) and $\overline{P}_{md}^{\text{wg}}$ (asymptotic $\overline{P}_{md}$ of [3]) is depicted in terms of the log-log plots of the absolute error (AE) vs. $\overline{\gamma}$ in Fig. 3.2 for a 5-branch SC in i.i.d. Rayleigh fading channels. The exact PDF $f(\beta)$ (3.25) and the corresponding parameters of $f^{\text{app}}(\beta)$ are given in Section 3.6.2. The absolute errors for $\overline{P}_{md}^{\text{asy}}$ and $\overline{P}_{md}^{\text{wg}}$ are defined as the difference $|\overline{P}_{md}^{\text{asy}} - \overline{P}_{md}^{\text{exact}}|$ and $|\overline{P}_{md}^{\text{wg}} - \overline{P}_{md}^{\text{exact}}|$, respectively, where $\overline{P}_{md}^{\text{exact}}$ is computed from [30, eq. (30)]. At high SNR (say, $\overline{\gamma} \geq 14\,\text{dB}$), the rate of decrease of the absolute error of $\overline{P}_{md}^{\text{asy}}$ (slope $= -6$) is greater by an order of magnitude than that of $\overline{P}_{md}^{\text{wg}}$ (slope $= -5$). As well, the absolute error of $\overline{P}_{md}^{\text{asy}}$ is 10^{-5} or less for $\overline{\gamma} \geq 12.5\,\text{dB}$ while $\overline{P}_{md}^{\text{wg}}$ attains the same accuracy only for $\overline{\gamma} \geq 19\,\text{dB}$. Therefore, the SNR gain of $\overline{P}_{md}^{\text{asy}}$ in attaining an absolute error of 10^{-5} is at least $6.5\,\text{dB}$ relative to $\overline{P}_{md}^{\text{wg}}$. Furthermore, for SNRs as low as $0\,\text{dB}$, $|\overline{P}_{md}^{\text{asy}} - \overline{P}_{md}^{\text{exact}}|$ is still very small (≤ 0.1), while $|\overline{P}_{md}^{\text{wg}} - \overline{P}_{md}^{\text{exact}}|$ is

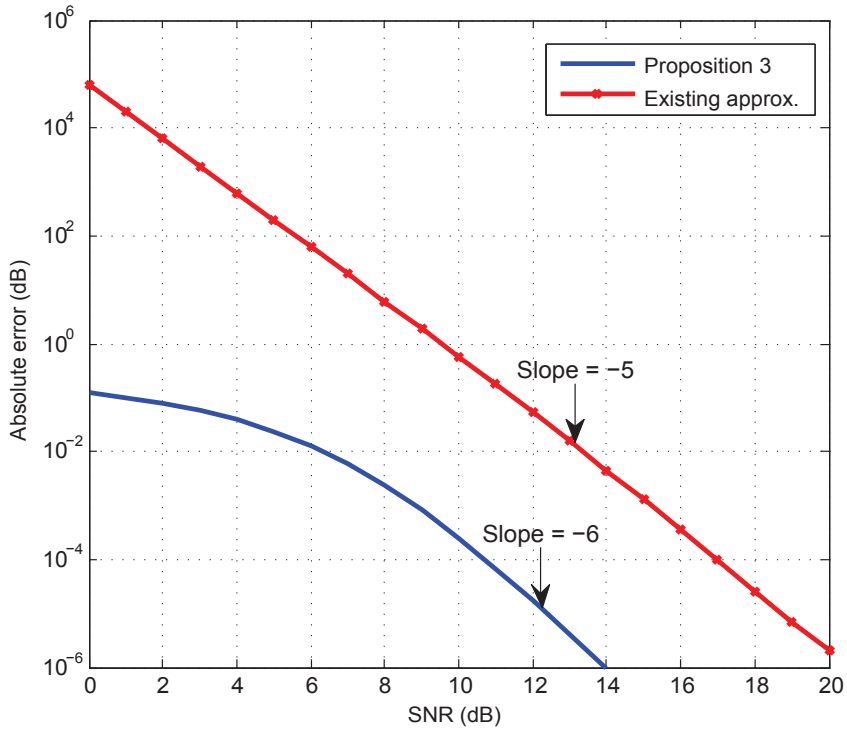

Fig. 3.2. Absolute error vs. SNR for a 5-branch SC in i.i.d. Rayleigh fading: Proposition 3 and [3].

far more than 1 (the breakdown mentioned in Section 3.3.2). Thus, $\overline{P}_{md}^{\text{asy}}$ is more accurate than $\overline{P}_{md}^{\text{wg}}$ throughout the practical SNR range. This result can be attributed to our finding that $f^{\text{app}}(\beta)$ can indeed approximate the exact PDF more accurately for any $\beta > 0$, unlike $f^{\text{wg}}(\beta)$, which is accurate for mainly $\beta \to 0^+$ (as discussed previously in the context of Fig. 3.1 in Section 3.3.2).

Now that the accuracy of the derived $\overline{P}_{md}^{\text{asy}}$ has been numerically verified, next we will assess the ED performance for various cases without and with antenna diversity reception, with cooperative detection, and in interference. We will first apply Proposition 1 or Proposition 2 (whichever most readily applies) to determine the parameters of $f^{\text{app}}(\beta)$ and then use Proposition 3 to compute $\overline{P}_{md}^{\text{asy}}$. To evaluate the performance, we consider log-log plots of $\overline{P}_{md}$ vs. $\overline{\gamma}$. The magnitude of the slopes of these plots at large SNR (say, $\overline{\gamma} \geq 20$ dB) yields the sensing gain. As well, since low false alarm probability is needed (for example, $P_f \leq 0.1$ for IEEE 802.22 CR networks [23]), we fix $P_f = 0.01$. The detection threshold λ is then determined by solving (3.1) for the given P_f and used for evaluating $\overline{P}_{md}$.

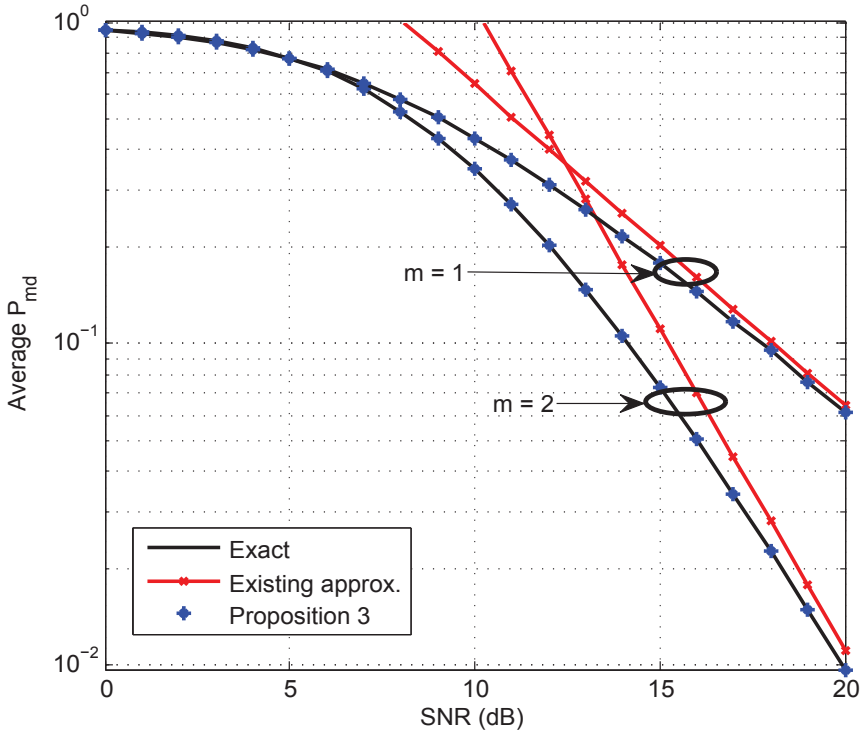

Fig. 3.3. $\overline{P}_{md}$ vs. SNR in Nakagami-m fading channel for $N = 3$: exact, existing [3] and Proposition 3.

3.5 Fading channels without diversity

3.5.1 Nakagami-m fading

For the Nakagami-m fading model, the exact $f(\beta)$ can be expressed as

$$f(\beta) = \frac{m^m}{\Gamma(m)}\beta^{m-1}e^{-m\beta},\ \beta > 0, \tag{3.18}$$

By comparing (3.18) with (3.6), it is clear that $f^{\text{app}}(\beta)$ exactly represents (3.18) when $a = m^m/[2\Gamma(m)]$, $t = m - 1$ and $\theta_1 = \theta_2 = m$. Nevertheless, we will extract these parameters by using our Proposition 1 for verification.

Thus, performing the Maclaurin's series expansion of (3.18), we get

$$f(\beta) = \frac{m^m}{\Gamma(m)}\beta^{m-1} - \frac{m^{m+1}}{\Gamma(m)}\beta^m + \frac{m^{m+2}}{2\Gamma(m)}\beta^{m+1} + O(\beta^{m+2}). \tag{3.19}$$

Then, comparing (3.19) with (3.9) and use of Proposition 1 leads to $t = m - 1$, $a = m^m/[2\Gamma(m)]$, $b_1 = 2m$ and $b_2 = 2m^2$. The substitution of b_1 and b_2 into (3.8) then gives

$\theta_1 = \theta_2 = m$, as expected. This result validates our Proposition 1.

Now that the parameters of $f^{\text{app}}(\beta)$ have been extracted, the use of Proposition 3 gives the desired expression for $\overline{P}_{md}^{\text{asy}}$. In Fig. 3.3, our derived $\overline{P}_{md}^{\text{asy}}$ (3.16) is compared against the exact $\overline{P}_{md}$ computed from [34, eq. (5)] and against the asymptotic $\overline{P}_{md}$ of [3]. As discussed in Section 3.3.2, the asymptotic $\overline{P}_{md}$ of [3] breaks down below a certain SNR. For instance, at $\overline{\gamma} \leq 8\,\text{dB}$ for $m = 1$, the asymptotic $\overline{P}_{md}$ of [3] exceeds 1. In contrast, our derived $\overline{P}_{md}^{\text{asy}}$ does not suffer from such a drawback. In fact, $\overline{P}_{md}^{\text{asy}}$ is virtually identical to the exact values computed from [34, eq. (5)] over the entire SNR range ($0 \leq \overline{\gamma}\,\text{dB} \leq 20$), whereas the asymptotic $\overline{P}_{md}$ of [3] approaches the exact values only for $\overline{\gamma} \geq 19\,\text{dB}$. Also, the exact $\overline{P}_{md}$ computed from [34, eq. (5)] contains an infinite series, which requires series-truncation. Moreover, the number of terms in such series has to be experimentally determined for a given precision requirement for each set of parameters and must be updated whenever the parameters change. In contrast, our derived solution (3.16) does not require such computations. Finally, the magnitude of the slopes of the curves corresponding to $m = 1$ and $m = 2$ at high SNR (say, $\overline{\gamma} \geq 19$) are observed to be 1 and 2, respectively, thus verifying that the sensing gain is equal to $m(= t + 1)$.

3.5.2 Nakagami-q (Hoyt) fading

This fading is observed on satellite links suffering from strong ionospheric scintillation and spans from one-sided Gaussian ($q = 0$) to Rayleigh fading ($q = 1$) [24]. For the Nakagami-q fading channel, the exact $f(\beta)$ is of the form

$$f(\beta) = \frac{1+q^2}{2q} e^{-\frac{(1+q)^2}{4q^2}\beta} I_0\left(\frac{1-q^4}{4q^2}\beta\right), \tag{3.20}$$

where $I_0(\cdot)$ is the zero-th order modified Bessel function of the first kind. By Maclaurin's series expanding (3.20), grouping the terms in ascending powers of β, and comparing the result with (3.4), we find that $t = 0$ and

$$\begin{aligned} a_0 &= \frac{1+q^2}{2q},\ a_1 = -\frac{(1+q^2)}{2q}\left(\frac{q^4+2q^2+1}{4q^2}\right), \\ a_2 &= \frac{(1+q^2)}{2q}\left(\frac{3q^8+8q^6+10q^4+8q^2+3}{64q^4}\right). \end{aligned} \tag{3.21}$$

Then, Proposition 1 readily yields a, θ_1 and θ_2, and Proposition 3 furnishes $\overline{P}_{md}^{\text{asy}}$.

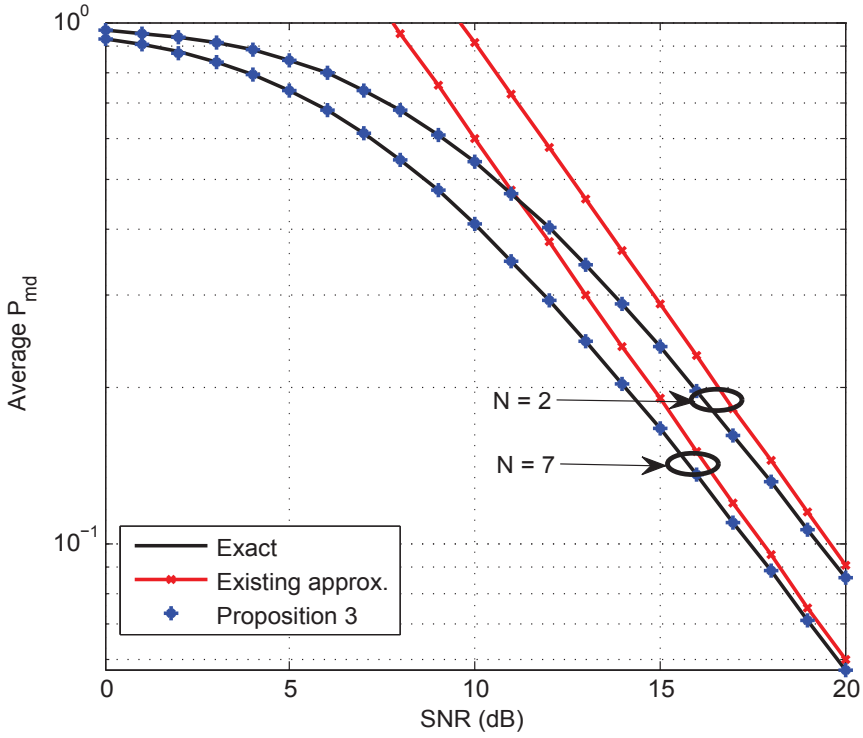

Fig. 3.4. $\overline{P}_{md}$ vs. SNR in Nakagami-q channel with $q = 0.7$ for different N.

The comparative results for Nakagami-q fading are depicted in Fig. 3.4. Clearly, our derived $\overline{P}_{md}^{\text{asy}}$ is virtually exact (it has 7-digit precision) over the entire SNR range ($0 \leq \overline{\gamma}\,\text{dB} \leq 20$) while the asymptotic $\overline{P}_{md}$ of [3] is accurate for $\overline{\gamma} \geq 19\,\text{dB}$ only. Also, the magnitude of the slopes of the graphs at high SNR ($\overline{\gamma} \geq 19\,\text{dB}$) are observed to be 1 (which equals the sensing gain $t + 1$).

3.6 Fading Channels with Antenna Diversity

Until now, only the single-antenna reception has been treated. Next, $L(\geq 1)$ antennas with mutually independent fading are considered. The parameters of $f^{\text{app}}(\beta)$ for MRC, EGC, and SC are derived. The MRC and SC are coherent combining schemes which require CSI at the ED. Although the CSI availability requirement contradicts the premise of ED (requiring no *a priori* information), these combining schemes are important for establishing the ED performance limits, a benchmark relative to which the performance of the alternative diversity combiners can be measured. Thus, the ED performance with antenna diversity combining assuming perfect CSI availability has been investigated extensively in the litera-

ture [30], [33], [34], [58], [59]. Moreover, as highlighted by [34] (and the reference therein), for CR networks, the CSI may be available at the CRs over control/broadcast channels (for example, by using low-rate pilot signal exchanges as shown in [69]). Nevertheless, since the purpose of this section is to demonstrate the applicability of our proposed analysis to antenna diversity combining, we proceed with the CSI availability notion for MRC and SC. On the other hand, EGC operates without any CSI.

3.6.1 MRC with L independent antennas

The optimal combining scheme in the absence of interference is the MRC which thus establishes an upper-bound performance for antenna diversity combining [24]. The MRC receiver combines all the diversity branches after weighting each branch with the complex conjugate of the corresponding fading channel coefficient to yield $y_{\text{mrc}}(t) = \sum_{l=1}^{L} h_l^* y_l(t)$, where $y_l(t)$ is the received signal at the l-th branch, and h_l^* is the complex conjugate of the l-th fading channel coefficient. The overall channel gain can then be expressed as $\beta = \sum_{l=1}^{L} \beta_l$, where $\beta_1, \beta_2, ..., \beta_L$ are statistically independent fading channel gains. Regardless of the fading channel model under consideration, if the MGF of each β_l as $s \to \infty$ can be expressed in the form [3]

$$\mathcal{M}_{\beta_l}(s) = \frac{c_l}{s^{\mu_l}} + \frac{d_l}{s^{\mu_l+1}} + \frac{e_l}{s^{\mu_l+2}} + O\left(\frac{1}{s^{\mu_l+3}}\right), \tag{3.22}$$

then, the MGF of β as $s \to \infty$ can be expressed as

$$\mathcal{M}_{\beta}(s) = \prod_{l=1}^{L}\left[\frac{c_l}{s^{\mu_l}} + \frac{d_l}{s^{\mu_l+1}} + \frac{e_l}{s^{\mu_l+2}} + O\left(\frac{1}{s^{\mu_l+3}}\right)\right],$$

which after some algebraic manipulations, can be expressed as (3.23)

$$\begin{aligned}\mathcal{M}_{\beta}(s) = & \frac{\prod_{l=1}^{L} c_l}{s^{\sum_l \mu_l}} + \frac{\sum_{j=1}^{L} d_l \prod_{l=1, l\neq j}^{L} c_l}{s^{\sum_{l=1}^{L} \mu_l+1}} \\ & + \frac{\sum_{j=1}^{L} e_j \prod_{l=1, l\neq j}^{L} c_l + \sum_{j=1}^{L-1} d_j \left(\sum_{k=j+1}^{L} d_k \prod_{l=1, l\neq k, l\neq j}^{L} c_l\right)}{s^{\sum_{l=1}^{L} \mu_l+2}} \\ & + O\left(\frac{1}{s^{\sum_{l=1}^{L} \mu_l+3}}\right).\end{aligned} \tag{3.23}$$

[3] For the cases of practical interest (for example, multi-branch reception in Rayleigh fading, Nakagami-m fading), the MGF of each branch can be written in the form (3.22). This is demonstrated with an example, shortly.

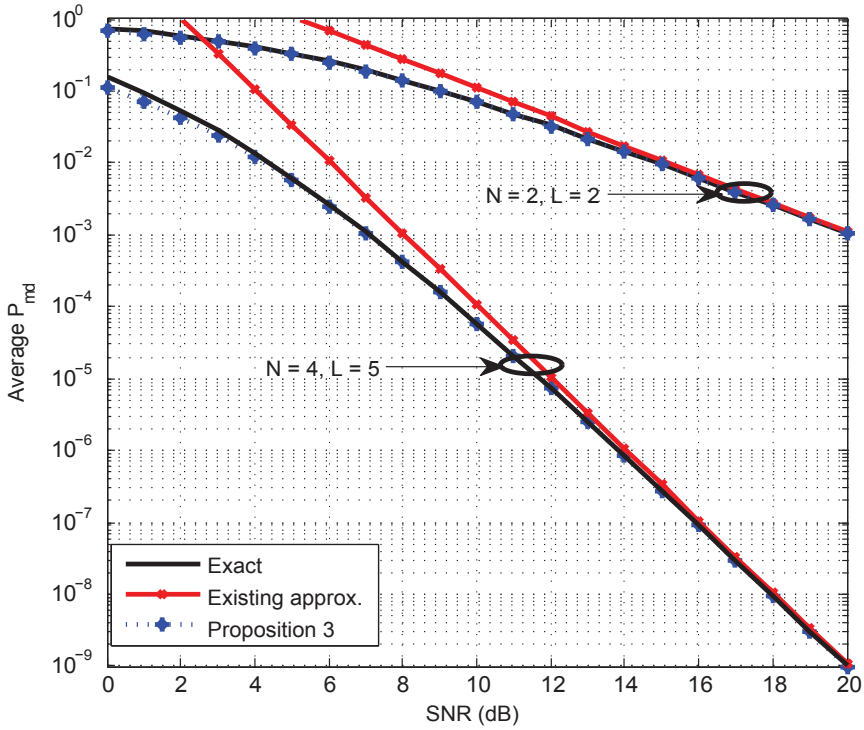

Fig. 3.5. $\overline{P}_{md}$ vs. SNR for MRC in i.n.i.d. Rayleigh fading channels for different $\{N, L\}$.

Then, comparing (3.23) with (3.11) yields

$$\begin{aligned} &\alpha = \sum_{l=1}^{L} \mu_l; \;\; X_0 = \prod_{l=1}^{L} c_l; \;\; X_1 = \sum_{j=1}^{L} d_l \prod_{l=1, l\neq j}^{L} c_l, \\ &X_2 = \sum_{j=1}^{L} e_j \prod_{l=1, l\neq j}^{L} c_l + \sum_{j=1}^{L-1} d_j \Bigg(\sum_{k=j+1}^{L} d_k \prod_{l=1, l\neq k, l\neq j}^{L} c_l \Bigg). \end{aligned} \tag{3.24}$$

Thus, Proposition 2 readily gives the desired parameters t, a, θ_1 and θ_2, and Proposition 3 yields the corresponding $\overline{P}_{md}^{\text{asy}}$.

To demonstrate the usefulness of (3.23), let us consider an example when the channel gains of the branches are independent and non-identically distributed (i.n.i.d.) Rayleigh random variables such that $f_{\beta_l}(x) = 1/l \cdot e^{-x/l}$. Then, the MGF for each β_l is $\mathcal{M}_{\beta_l}(s) = 1/(1 + ls)$. Performing the series expansion of $\mathcal{M}_{\beta_l}(s)$ as $s \to \infty$ and comparing the result with (3.22), we get $\mu_l = 1$, $c_l = 1/l$, $d_l = 1/l^2$ and $e_l = 1/l^3$. Substituting these coefficients in (3.24) immediately yields α, X_0, X_1, and X_2. Then, the use of Proposition 2 followed by Proposition 3 gives $\overline{P}_{md}^{\text{asy}}$.

The high accuracy of our derived $\overline{P}_{md}^{\text{asy}}$ (3.16) over $0 \leq \overline{\gamma} \leq 20$ dB is visible in Fig. 3.5

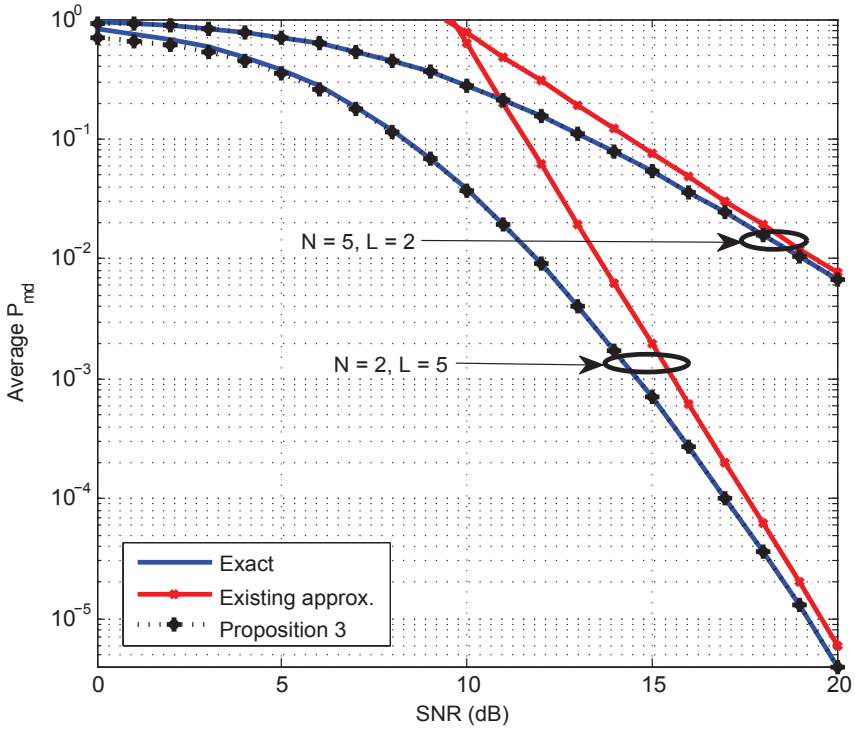

Fig. 3.6. $\overline{P}_{md}$ vs. SNR for SC in i.i.d. Rayleigh fading.

while the asymptotic $\overline{P}_{md}$ of [3] is accurate only for say, $\overline{\gamma} > 14\,\text{dB}$. Also, the magnitude of the slopes of the graphs observed at $\overline{\gamma} \geq 14\,\text{dB}$ are 2 and 5, respectively, for $L = 2$ and $L = 5$. These results are equal to the corresponding sensing gains (thus verifying $t + 1 = L$).

3.6.2 SC in Rayleigh fading

For an L-branch SC in i.i.d. Rayleigh fading, the PDF of β is given by

$$f(\beta) = Le^{-\beta}(1 - e^{-\beta})^{L-1}, \ \beta \geq 0. \tag{3.25}$$

The Maclaurin's series expansion of (3.25) followed by some algebraic manipulations and comparison of the resulting expression with (3.4) yields $t = L - 1$, $a_i = \frac{\mathcal{D}(L-1+i)}{(L-1+i)!}$ for $i = 0, 1, 2$, and $\mathcal{D}(\cdot)$ is defined as

$$\mathcal{D}(n) = L \sum_{k=0}^{L-1} \binom{L-1}{k} (-1)^{k+n} (k+1)^n. \tag{3.26}$$

Then, the use of Proposition 1 provides a, θ_1 and θ_2, and Proposition 3 subsequently yields $\overline{P}_{md}^{\text{asy}}$. The graphs in Fig. 3.6 yet again depict the remarkable accuracy of our $\overline{P}_{md}^{\text{asy}}$ (3.16) compared against the asymptotic $\overline{P}_{md}$ of [3] and the exact $\overline{P}_{md}$ obtained from [30, eq. (30)]. The observed sensing gain from all the graphs at high SNR ($\overline{\gamma} \geq 15\,\text{dB}$) is clearly equal to L (consistent with $t+1=L$).

3.6.3 EGC and SC in Nakagami-m fading

For a 2-branch EGC in Nakagami-m fading, the exact $f(\beta)$ can be obtained from [34, eq. (32)] to be

$$f(\beta) = \frac{2^{2-2m}\sqrt{\pi}\Gamma(2m)m^{2m}}{\Gamma^2(m)\Gamma(2m+\frac{1}{2})}\beta^{2m-1}e^{-2m\beta}{}_1F_1\left(2m; 2m+\frac{1}{2}; m\beta\right), \tag{3.27}$$

where ${}_1F_1(\cdot;\cdot;\cdot)$ is the confluent hypergeometric function [70]. Maclaurin's series expansion of (3.27) followed by comparison with (3.4) yields the parameters $t = 2m-1$, $a_0 = [2^{2-2m}\sqrt{\pi}\Gamma(2m)m^{2m}]/[\Gamma^2(m)\Gamma(2m+1/2)]$, $a_1 = -[2m(2m+1)a_0]/[4m+1]$, $a_2 = [2m^2(4m^2+6m+3)a_0]/[(4m+1)(4m+3)]$. Then, use of Proposition 1 and Proposition 3 subsequently yields the desired $\overline{P}_{md}^{\text{asy}}$. Note that we consider the 2-branch EGC case here because the PDFs of SNR for the $L(>2)$-branch EGC in Nakagami-m fading do not have a closed-form and rather contain one or more infinite series (see [34, eq. (40)], [34, eq. (45)]) for which the number of terms needed for obtaining a desired precision (accuracy) is unknown. Thus, the parameters of $f^{\text{app}}(\beta)$ for such cases will be in terms of infinite series, and the number of terms needed for precise truncation of the infinite series is unknown.

Next, we consider 3-branch SC in Nakagami-m fading. Using [34, eq. (50)] with $L=3$, we can write the exact PDF of β to be

$$f(\beta) = \frac{3m^m}{\Gamma^3(m)}\beta^{m-1}e^{-m\beta}[\mathcal{G}(m, m\beta)]^2, \tag{3.28}$$

where $\mathcal{G}(a,z) = \int_0^z x^{a-1}e^{-x}dx$ is the lower incomplete Gamma function [26]. Maclaurin's series expansion of $f(\beta)$ gives $t = 3m-1$, $a_0 = [3m^{3m-2}]/[\Gamma^3(m)]$, $a_1 = -[3m^{3m-1}(2m+1)]/[(m+1)\Gamma^3(m)]$ and $a_2 = [3m^{3m}(9m^3+24m^2+15m+2)]/[2\Gamma^3(m)(m+1)^2(m+2)]$. Then, the use of Proposition 1 followed by Proposition 3 subsequently gives $\overline{P}_{md}^{\text{asy}}$. It is worth noting that SC cases with $L \geq 4$ can be treated similarly because the exact $f(\beta)$ (obtained using [34, eq. (50)]) can still be Maclaurin's series expanded in the form (3.9),

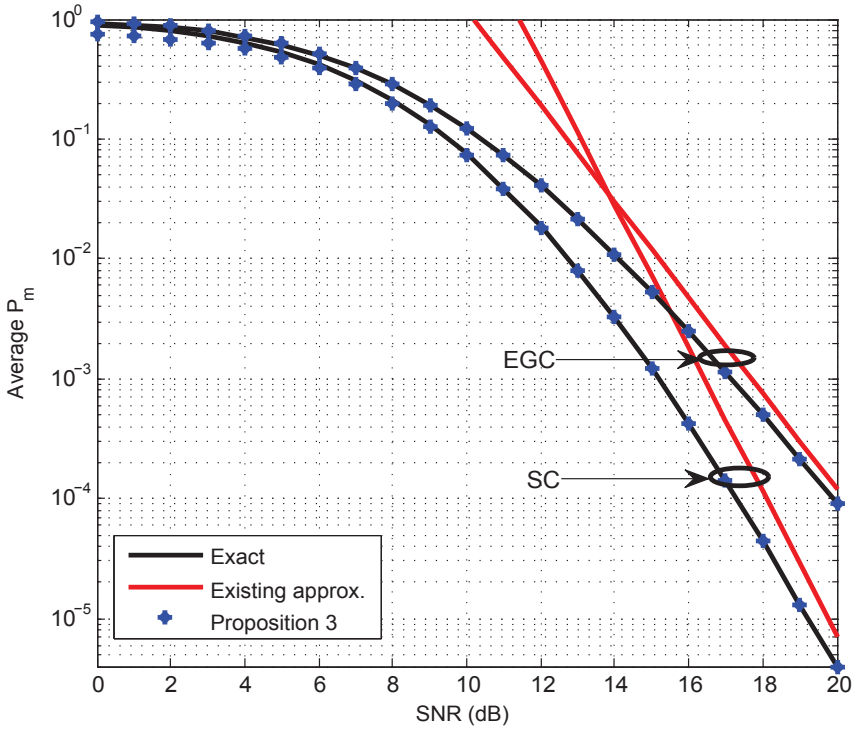

Fig. 3.7. $\overline{P}_{md}$ vs. SNR for 2-branch EGC ($N = 5$) and 3-branch SC ($N = 2$) in Nakagami-2 fading.

however, at the expense of additional algebraic manipulations. Nevertheless, those cases are not treated any further for brevity.

The comparative results for the 2-branch EGC and 3-branch SC in Nakagami-2 fading are depicted in Fig. 3.7 where the benefit of our $\overline{P}_{md}^{\text{asy}}$ (3.16) over the asymptotic $\overline{P}_{md}$ of [3] is clear. The exact $\overline{P}_{md}$ for EGC and SC are obtained by using [34, eq. (38)] and [34, eq. (59)], respectively, which are infinite series expressions involving the hypergeometric functions and thus the sensing gains from such expressions are not explicit. Unlike the use of these equations, application of Proposition 1 clearly suggests a sensing gain of $2m$ ($= 4$) for EGC and $3m$ ($= 6$) for SC, respectively (given by slopes of the graphs at, say, $\overline{\gamma} \geq 19\,\text{dB}$).

3.7 Cooperative Detection with Multiple Relays

In the previous section, the performance of an ED equipped with co-located multiple antennas has been characterized for several antenna diversity combining schemes. Although the benefits of co-located multiple antennas are widely accepted, deploying them may be

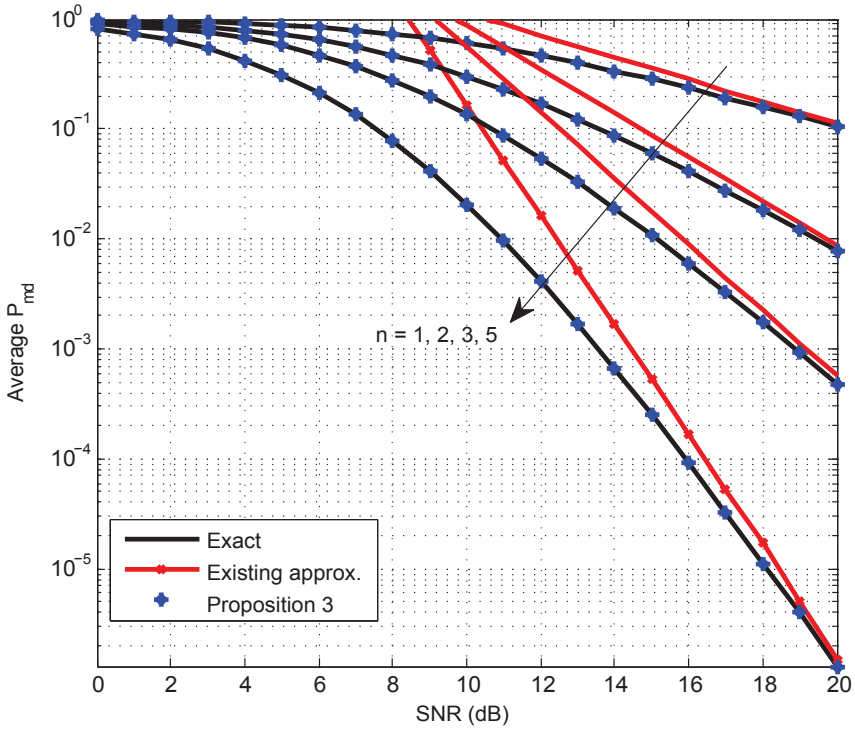

Fig. 3.8. $\overline{P}_{md}$ vs. SNR for multiple relays based detection ($N = 2$).

impractical in situations where size, cost, or hardware pose limitations. Examples include low-cost handsets (where size is a limitation) and low-power, small-size nodes in a wireless sensor network [71]. In these scenarios, the cooperative diversity by using multiple CRs for sensing the presence/absence of the PU is more beneficial. We thus consider a cooperative data fusion based spectrum sensing network where a number ($n \geq 1$) of relays amplify-and-forward their received signals to the FC, which then makes the final decision on the presence/absence of the PU based on these n observations. Furthermore, the FC may have access to CSI of the channels from the PU to the relays and from relays to the FC. This may be possible via channel estimation at the relays through the use of low-rate pilot signals [69] and control channel signaling [72].

The total instantaneous SNR γ of such a network can be upper-bounded by γ_{up} as $\gamma \leq \gamma_{\text{up}} = \sum_{i=1}^{n} \gamma_i^{\min}$, where $\gamma_i^{\min} = \min\{\gamma_{pr_i}, \gamma_{r_i d}\}$; γ_{pr_i} and $\gamma_{r_i d}$ are the instantaneous SNRs of the links from the transmitter to the i-th relay r_i and from r_i to the FC, respectively [36].[4] Assume the channels from each relay to the FC are statistically independent Rayleigh

[4]Since use of the exact MGF of γ to obtain a closed-form $\overline{P}_{md}$ is analytically intractable [36], we use γ_{up} instead, which can lead to a closed-form upper bound for $\overline{P}_{md}$.

fading. The MGF of γ_{up}, $\mathcal{M}_{\gamma_{\text{up}}}(s)$, is given by [36, eq. (10)]

$$\mathcal{M}_{\gamma_{\text{up}}}(s) = \prod_{i=1}^{n} \frac{\overline{\gamma}_{pr_i} + \overline{\gamma}_{r_i d}}{\overline{\gamma}_{pr_i}\overline{\gamma}_{r_i d}} \cdot \frac{1}{\left(s + \frac{\overline{\gamma}_{pr_i} + \overline{\gamma}_{r_i d}}{\overline{\gamma}_{pr_i}\overline{\gamma}_{r_i d}}\right)}, \tag{3.29}$$

where $\overline{\gamma}_{pr_i}$ and $\overline{\gamma}_{r_i d}$ are the average SNRs of the respective links. In general, the series expansion of the MGF (3.29) at $s \to \infty$ would result in MGF of the form (3.23), which was derived for the MRC with L independent antennas. Without loss of generality and for the sake of brevity, we omit similar details, and rather provide an example where the link SNRs are identical, i.e., $\overline{\gamma}_{pr_i} = \overline{\gamma}_{r_i d} = \overline{\gamma}$. This set-up allows (3.29) to be expressed in the form

$$\mathcal{M}_{\gamma_{\text{up}}}(s) = \frac{(2/\overline{\gamma})^n}{s^n[1 + 2/(\overline{\gamma}s)]^n}.$$

We define $\gamma_{\text{up}} = \overline{\gamma}\beta_{\text{up}}$. Then, by using the transformation of the random variables, the MGF of β_{up} can be obtained from that of γ_{up} as $\mathcal{M}_{\beta_{\text{up}}}(s) = \mathcal{M}_{\gamma_{\text{up}}}(s/\overline{\gamma})$. Performing a series expansion of the resulting expression for $\mathcal{M}_{\beta_{\text{up}}}(s)$ at $s \to \infty$ gives

$$\mathcal{M}_{\beta_{\text{up}}}(s) = \frac{2^n}{s^n} - \frac{n2^{n+1}}{s^{n+1}} + \frac{n(n+1)2^{n+1}}{s^{n+2}} + O\left(\frac{1}{s^{n+3}}\right).$$

Then, applying Proposition 2, we get $\alpha = n$, $X_0 = 2^n$, $X_1 = -n2^{n+1}$ and $X_2 = n(n+1)2^{n+1}$. These findings readily yield the parameters t, a, θ_1 and θ_2. Thus, Proposition 3 can be applied to obtain $\overline{P}_{md}^{\text{asy}}$. The results comparing the exact $\overline{P}_{md}$ (based on γ_{up}) obtained from [36, eq. (11)], the asymptotic $\overline{P}_{md}$ of [3], and our derived $\overline{P}_{md}^{\text{asy}}$ (3.16) are depicted in Fig. 3.8. Clearly, these results indicate the benefit of our derived $\overline{P}_{md}^{\text{asy}}$ over the asymptotic $\overline{P}_{md}$ of [3]. Also, the magnitude of the slopes of the graphs at high SNR ($\geq$ 19 dB) are found to be same as the number of cooperating relays n, which is equal to the sensing gain ($t + 1 = n$).

3.8 Detection in Interference

In the previous sections, as in existing works on ED performance analysis [3], [30], [32]–[34], [36], [58], [59], the presence of interfering transmissions has been disregarded. In emerging broadband technologies (such as LTE-Advanced), small cells (pico- and femto-cells) are commonly deployed by overlaying them over the traditional macrocells of cellular

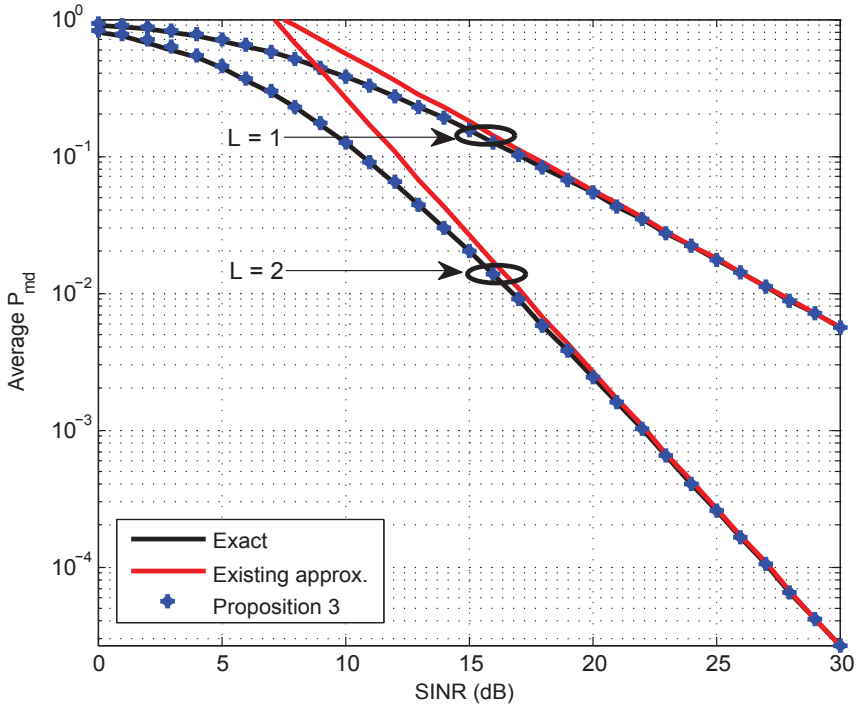

Fig. 3.9. $\overline{P}_{md}$ vs. $\overline{\gamma}$ for $N = 2$ in presence of $N_I = 8$ interferers with powers $\{P_1, P_2, P_3, P_4, P_5, P_6, P_7, P_8\} = \{-5, -3, -1, 1, 3, 5, 7, 9\}$ dB, $N_0 = 0$ dB.

networks, thus extending the wireless coverage and capacity [10]. This set-up results in a heterogeneous network consisting of a large number of wireless nodes such that the reception (at the destination) of undesired transmissions (that have leaked in space over relatively large distances) occurs inevitably [73]. Thus, all the heterogeneous nodes sharing the same spectrum suffer from interference. In such situations, an ED equipped node will receive interfering transmissions, which will deteriorate its sensing performance [74].

Thus, in the presence of interference, the received signal (at the ED) is composed of the faded version of the PU, numerous interfering signals from other users, and AWGN. In this situation, rather than SNR, the signal-to-interference-plus-noise ratio (SINR) has to be taken into account, which is defined (with abuse of the notation γ) as

$$\gamma = \frac{h_0 P_0}{\sum_{i=1}^{N_I} h_i P_i + N_0}, \tag{3.30}$$

where N_0 is noise variance, h_0 and P_0 are the desired transmitter-to-receiver channel gain and the average power of the desired signal, respectively, while h_i and $P_i, \forall i \in \{1, 2, ..., N_I\}$, are the channel gain and average power of the i-th interfering link, respectively, with N_I

being the total number of interferers. We assume all the channels undergo Rayleigh fading. Furthermore, the detector is equipped with $L \geq 1$ antennas, whose signals are combined by using MRC. Hence, SINR can still be expressed as $\gamma = \overline{\gamma}\beta$, where $\overline{\gamma} = P_0/(I_{\text{total}} + N_0)$ is the average SINR with $I_{\text{total}} = \sum_{i=1}^{N_I} P_i$ and $\beta = h_0(I_{\text{total}} + N_0)/[\sum_{i=1}^{N_I} P_i h_i + N_0]$. This set-up leads to the following PDF of β [75]

$$f(\beta) = \frac{\beta^{L-1}}{(L-1)!} \sum_{i=1}^{N_I} \frac{\mathcal{A}_i e^{\mathcal{C}_i} \mathcal{B}_i^L}{(1+\mathcal{B}_i\beta)^{L+1}} \Gamma\big[L+1, \mathcal{C}_i\big(1+\mathcal{B}_i\beta\big)\big], \tag{3.31}$$

where $\mathcal{A}_i = \prod_{k=1,k\neq i}^{N_I} P_i/(P_i - P_k)$, $\mathcal{B}_i = P_i/[I_{\text{total}} + N_0]$, and $\mathcal{C}_i = N_0/P_i$. With the abuse of notations, we use β and $\overline{\gamma}$ here for presentation simplicity and for notational consistency. Then, the Maclaurin's series expansion of (3.31) yields $t = L - 1$,

$$\begin{aligned}
a_0 &= \sum_{i=1}^{N_I} \mathcal{A}_i \mathcal{B}_i^L e^{\mathcal{C}_i} \Gamma(L+1, \mathcal{C}_i), \\
a_1 &= -\sum_{i=1}^{N_I} \mathcal{A}_i \mathcal{B}_i^{L+1} [\mathcal{C}_i^{L+1} + e^{\mathcal{C}_i}(L+1)\Gamma(L+1, \mathcal{C}_i)], \\
a_2 &= \sum_{i=1}^{N_I} \frac{1}{2} \mathcal{A}_i \mathcal{B}_i^{L+2} \big[e^{\mathcal{C}_i}(L^2+3L+2)\Gamma(L+1, \mathcal{C}_i) \\
&\quad + \mathcal{C}_i^{L+1}\big\{2 + 2L - e^{\mathcal{C}_i}\Gamma(L+1)\,{}_1\tilde{F}_1(L+1; L; -\mathcal{C}_i)\big\}\big],
\end{aligned} \tag{3.32}$$

where ${}_1\tilde{F}_1(\cdot;\cdot;\cdot)$ is the regularized confluent hypergeometric function of the confluent hypergeometric function ${}_1F_1(\cdot;\cdot;\cdot)$ [76]. Thus, Proposition 1, and subsequently, Proposition 3 can be used to obtain the desired parameters and $\overline{P}_{md}^{\text{asy}}$, respectively.

A numerical example for this case is depicted in Fig. 3.9, which indicates significantly better accuracy of our derived $\overline{P}_{md}^{\text{asy}}$ over $0 \leq \overline{\gamma}\,\text{dB} \leq 30$, in contrast to the asymptotic $\overline{P}_{md}$ of [3], which is accurate only for say, $\overline{\gamma} \geq 18\,\text{dB}$. Furthermore, the sensing gains are equal to the number of antennas L (the magnitude of the slopes of the graphs at $\overline{\gamma} \geq 20\,\text{dB}$ are equal to 1 and 2 for $L = 1$ and $L = 2$, respectively).

3.9 Average CAUC

Thus far, we have considered the problem of averaging the generalized Marcum-Q function over $f^{\text{app}}(\beta)$ (Proposition 3). However, we emphasize that the application of $f^{\text{app}}(\beta)$ goes

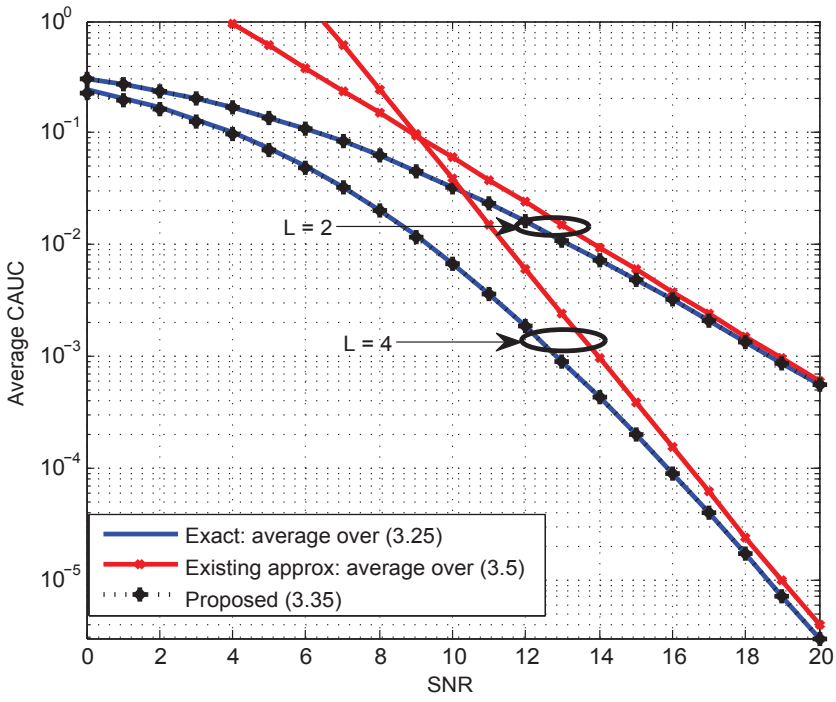

Fig. 3.10. $\overline{A'}$ vs. SNR for SC in i.i.d. Rayleigh fading with $N = 2$.

beyond Proposition 3. In general, its wider applications could include analyses of the outage probability, bit error rates, average capacity, and symbol error rates, which are critical performance metrics of practical digital wireless systems. However, since our scope is limited to the ED, we concentrate on the one more application for ED, the analysis of CAUC performance.

Although the ROC curves graphically represent the ED performance, a single figure of merit for concisely representing the ED's overall sensing capability is desirable. For this purpose, the area under the ROC curve (AUC), which varies between $1/2$ and 1, was recently proposed [37]. If the AUC is $1/2$, then the decision is as reliable as that of a coin toss, meaning $P_{md} = 0.5$. Thus, a larger AUC implies a better detector. However, neither the ROC curves nor the AUC graphs explicitly reveal the order of improvement in sensing performance with increasing SNR. This shortcoming led to the introduction of yet another single figure of merit, CAUC, which reveals the order of improvement in sensing performance with increasing SNR, explicitly. The instantaneous CAUC for ED is given by [38]

$$A'(\gamma) = \sum_{k=0}^{N-1} \frac{1}{2^k k!} \gamma^k e^{-\frac{\gamma}{2}} - \sum_{k=1-u}^{N-1} \frac{\Gamma(N+k)}{2^{N+k}\Gamma(N)} e^{-\gamma} {}_1\tilde{F}_1\left(N+k; k+1; \frac{\gamma}{2}\right). \quad (3.33)$$

Intuitively, a lower CAUC implies a better sensing capability.

We are interested in evaluating the average asymptotic CAUC, denoted by $\overline{A'}_{\text{asy}}$, which can be obtained by integrating $A'(\gamma)|_{\gamma=\overline{\gamma}\beta}$ over $f^{\text{app}}(\beta)$ as

$$\overline{A'}_{\text{asy}} = \int_0^\infty A'(\overline{\gamma}\beta) f^{\text{app}}(\beta) d\beta, \quad (3.34)$$

which can be derived to be

$$\begin{aligned} \overline{A'}_{\text{asy}} = a \sum_{k=0}^{N-1} \frac{\overline{\gamma}^k}{2^k k!} \Gamma(t+k+1) \sum_{i=1}^{2} \frac{1}{(\theta_i + \overline{\gamma}/2)^{t+k+1}} \\ - a \sum_{k=1-N}^{N-1} \frac{\Gamma(N+k)\Gamma(t+1)}{2^{N+k}\Gamma(N)} \\ \cdot \left[\sum_{i=1}^{2} \frac{1}{(\theta_i + \overline{\gamma})^{t+1}} {}_2\tilde{F}_1\left(t+1, N+k; k+1; \frac{\overline{\gamma}}{2(\theta_i + \overline{\gamma})}\right) \right] \end{aligned} \quad (3.35)$$

(see Appendix A.3 for derivation details), where ${}_2\tilde{F}_1(\cdot,\cdot;\cdot;\cdot)$ is the regularized confluent hypergeometric function of the confluent hypergeometric function ${}_2F_1(\cdot,\cdot;\cdot;\cdot)$ [77]. At large SNRs ($\overline{\gamma} \gg 1$), (3.35) reduces to the form $\overline{A'}_{\text{asy}} \approx g_{\text{auc}}(N,t)\overline{\gamma}^{-(t+1)}$, where $g_{\text{auc}}(N,t)$ is a term independent of $\overline{\gamma}$. Thus, magnitude of the exponent of $\overline{\gamma}$ occurring in $\overline{A'}_{\text{asy}}$ at large SNRs is equal to $(t+1)$, which in fact is the sensing gain obtained from our derived asymptotic missed-detection probability $\overline{P}_{md}^{\text{asy}}$ (3.16) at high SNR. The same exponent is equivalently defined as the "detection diversity gain order" in [38]. Hence, the sensing gain is also given by the magnitude of the slope of the log-log plot of $\overline{A'}_{\text{asy}}$ vs. $\overline{\gamma}$ at high SNR.

A numerical example for the average CAUC (denoted by $\overline{A'}$) for SC in i.i.d. Rayleigh fading (for which the parameters of $f^{\text{app}}(\beta)$ were derived in Section 3.6.2) is shown in Fig. 3.10 where our derived asymptotic CAUC $\overline{A'}_{\text{asy}}$ (3.35) is compared against the approximate and exact CAUCs computed by using the approximation $f^{\text{wg}}(\beta)$ (3.5) and the exact $f(\beta)$ (3.25), respectively. Interestingly, our $\overline{A'}_{\text{asy}}$ is virtually identical to the exact values over the entire SNR range ($0 \leq \overline{\gamma}\,\text{dB} \leq 20$), while $\overline{A'}$ computed by using $f^{\text{wg}}(\beta)$ is accurate for only $\overline{\gamma} \geq 19\,\text{dB}$. Furthermore, the sensing gains obtained from the graphs at high SNR ($\overline{\gamma} \geq 19\,\text{dB}$) are 2 and 4 for $L = 2$ and $L = 4$, respectively (thus verifying

$t+1=L$). Thus, the proposed $f^{\text{app}}(\beta)$ serves as a unified approximation for the exact PDF of β, which can also be applied for deriving the average performance metrics from the instantaneous ones involving functions other than the generalized Marcum-Q function.

3.10 Conclusion

In this chapter, a new approximation $f^{\text{app}}(\beta)$ with parameters matching the operating conditions (the fading channel, antenna diversity, cooperative diversity, and others) is proposed. These parameters are obtained using the exact PDF or MGF of β. By utilizing the MGF corresponding to $f^{\text{app}}(\beta)$ along with the contour integral representation of the generalized Marcum-Q function, the unified asymptotic missed-detection probability $\overline{P}_{md}^{\text{asy}}$ of the ED is derived in closed-form. The derived $\overline{P}_{md}^{\text{asy}}$ is then specialized to single-antenna systems, antenna diversity, multiple-relay-based cooperative detection, and to interference environments. Our $\overline{P}_{md}^{\text{asy}}$ is found to be highly accurate (achieving upto 7-digit precision for some cases), and valid over a wider SNR range than that derived by using the approximation in [3]. Thus, compared with [3], although our approximation requires only a simple additional step for extracting more information, this step improves both the accuracy and valid SNR range of the asymptotic analysis. Moreover, the derived $\overline{P}_{md}^{\text{asy}}$ also explicitly reveals the sensing gain. To show another application of our proposed $f^{\text{app}}(\beta)$, we also derive the asymptotic CAUC, the result being highly accurate, and additionally revealing the sensing gain. Thus, we have developed a unified comprehensive analytical framework to characterize the ED performance in different practical communication scenarios. This framework may subsequently help in designing robust detectors in state-of-the-art and future wireless communication networks.

In this work, we consider $f^{\text{app}}(\beta)$ for analyzing ED performance only. However, the application of our proposed $f^{\text{app}}(\beta)$ to analyze other crucial metrics , may be of interest to wireless communication researchers and engineers. For example, metrics such as the symbol error rate, outage probability, and others could be considered for characterizing wireless systems deploying space-time coding and modulations, MIMO, antenna/relay selection schemes, and numerous other techniques [78]–[88]. Thus, this work opens up interesting and diverse future research opportunities.

Chapter 4

Performance of p-norm Detector in AWGN, Fading and Diversity Reception

Recent results have indicated that the ED does not necessarily achieve the best sensing performance, especially in terms of maximizing the detection probability or minimizing the probability of decision making at all SNRs. This has led to the evolution of the p-norm detector, a more generalized version of the ED, where $p = 2$ represents the ED case. However, the existing p-norm detector performance analyses impose restrictions on either the number of samples and/or the operating SNR, mainly for analytical tractability. Moreover, the results are limited to Rayleigh fading channels only. In this chapter [1], we address these issues by proposing several accurate analytical solutions to derive the performance metrics. Then, the p-norm detection performance is characterized in two of the most generalized fading channel models, the κ-μ and the α-μ. Furthermore, two new non-coherent combining schemes; p-law combining (pLC) and p-law selection (pLS) are proposed and found to perform better (as good) than the coherent SC scheme at relatively high-SNR (low-SNR). Numerical results are presented to reveal important insights. Interestingly, they also reveal that the ED loses its optimality in fading (and diversity) channels, that is, $p = 2$ is not the best performing detector in these conditions.

[1] Chapter 4 has been published in the *IEEE Transactions on Vehicular Technology* as [89].

4.1 Introduction and Motivation

For the p-norm detector, recall that the decision variable is of the form

$$T_p = \frac{1}{N} \sum_{i=1}^{N} |y_i|^p. \tag{4.1}$$

Although the ED is one of the most popular detectors for spectrum sensing due to its blind characteristics and low implementation complexity, it is not necessarily the better performing detector, when it comes to comparison with the p-norm detector. The p-norm detector has several advantages compared to ED. First, choosing $p \neq 2$ may yield a performance gain and hence the best p value depends upon the probability of correct detection, the probability of false alarm, the SNR, and the received signal sample size [39]. Second, adaptive optimization of p yields remarkable performance gain over the ED with the resulting performance being closer (than ED) to the locally optimal detector[2] at very low SNRs [40]. Moreover, the optimal p that minimizes the total error rate is not equal to 2 in general, and other p values may provide more reliable (less erroneous) sensing performance [90], [91].

However, the existing p-norm detector performance analyses are limited by some ad hoc assumptions. For example, reference [39] assumes T_p as Gamma distributed, an approximation that is more accurate for lower p, higher N and relatively low SNR. For CR networks operating at low SNRs, reference [40] assumes a large N ($N \gg 1$) such that the CLT holds, and thus T_p is approximately Gaussian. However, in practice, the requirement of a low sensing time conflicts with the large sample assumption. The assumption of a single received signal sample ($N = 1$) per CR and per antenna used in [90] and [91] severely limits the reliability of detection. Overall, what is lacking is a more exact and general performance analysis of the p-norm detector.

Moreover, the existing analyses are limited to AWGN (non-fading) [39] and Rayleigh-fading [40], [90], [91]. However, spatially correlated non-homogeneous scattering occurs in real propagation environments [92], which are better modeled by the κ-μ and the α-μ distributions. The κ-μ distribution is a small-scale fading model where κ is associated with the LOS conditions and μ is associated with the number of multipath clusters [92]. The κ-μ model includes the Rayleigh, Rician and Nakagami-m fading models as special cases. On

[2] A locally optimal detector is asymptotically optimal at low SNR.

the other hand, the α-μ fading model relates α and μ to the non-linearity and to the number of multipath components, respectively [93]. Likewise, the α-μ model includes Weibull, Gamma, Nakagami-m, Rayleigh, exponential and one-sided Gaussian models as special cases. Moreover, field trials have confirmed that the κ-μ and the α-μ distributions outperform the classical fading models in fitting the experimental data due to the comprehensive range (versatility) of these models' parameter values [92], [93]. Thus, evaluation of the p-norm detection performance in these generalized fading models is useful

(i) to quantify the performance loss (relative to the non-fading case) incurred in realistic fading channels and, potentially, to help in designing detectors robust to such impacts, and

(ii) to determine the required SNR and related parameter values necessary to achieve a prescribed performance in non-homogeneous and non-linear propagation environments.

In addition, as wireless fading fundamentally limits performance, antenna diversity combining techniques are used to mitigate its impact [24]. Thus, achievable performance gains by integrating these techniques with the p-norm detector must be quantified. Hence, the p-norm detection performance analysis in generalized fading channels and with diversity reception is of interest.

Such analysis is challenging because the distribution of T_p in (4.1) appears intractable (in general). This distribution is necessary to obtain the detection probability, P_d, and the false alarm probability, P_f. Since the exact PDF-based analysis appears intractable, we consider utilizing the MGF of T_p. Fortunately, the MGF of T_p can be obtained as a product of MGFs of its summands (for statistically independent summands) and thus is more amenable to a tractable analysis. Furthermore, we show that this approach facilitates analysis in fading and diversity reception. To the best of our knowledge, no such comprehensive p-norm detection performance analysis is currently available. This chapter addresses the aforementioned issues in the following ways:

- First, for non-fading channels (i.e. channels with AWGN only), three solutions for P_d and P_f are developed: (i) for even-integer values of p, a closed-form MGF of the decision variable T_p is derived. Then, by using the Talbot's method for Laplace transform inversion [94], which is highly accurate and easy to program [95], a computationally

efficient solution is developed; (ii) for any arbitrary p, series-based MGF of T_p is derived and utilized to obtain accurate infinite series expressions with convergence acceleration based on the ϵ-algorithm [96]; (iii) a generalized Laguerre polynomial series [97] for the distribution of T_p is used to derive new approximate expressions. This approximation is more versatile than the Gamma approximation [39] and more accurate than the CLT approximation (for a few samples).[3]

- Second, to characterize the p-norm detector performance across a wide range of realistic multipath fading environments, the series MGF-based analysis is extended to obtain accurate series-form expressions for the average probability of detection over κ-μ and α-μ fading.

- Third, to assess the performance with antenna diversity reception (in fading), two non-coherent combining schemes, pLC and pLS, are proposed. These combiners are compared against the classical MRC and SC by deriving their performance in Nakagami-m fading channels. Interestingly, both pLC and pLS perform similarly to the traditional SC at low SNR but outperform it at relatively high SNR, with pLC performing closer to the optimal MRC. Furthermore, since pLC and pLS do not require any CSI, they are more useful than classical MRC and SC schemes for the p-norm detector (which functions without any CSI).

The organization of this chapter is as follows. The system model is described in Section 4.2. The detection and false alarm probabilities in the AWGN channel are derived in Section 4.3. The series MGF-based analysis is utilized to derive the average detection probabilities over κ-μ and α-μ fading and with antenna diversity reception over Nakagami-m fading in Section 4.4. Numerical results are discussed in Section 4.5. Concluding remarks are made in Section 4.6.

[3]The CLT approximation is a reference benchmark. It is considered for p-norm detection in [40] and in general, for signal detection, in [20].

4.2 System Model

After baseband down conversion and a sampling process, the i-th signal sample of $y(t)$ (2.6), $\forall i \in \{1, 2, ..., N\}$ can be expressed in the digital form as

$$y_i = \begin{cases} w_i & : H_0, \\ h_i S_i + w_i & : H_1, \end{cases}$$

where notations h_i, S_i and w_i indicate i-th sample of the complex fading channel gain, PU signal and noise, respectively. The signal and the noise samples are i.i.d. with $S_i \sim \mathcal{CN}(0, \sigma_S^2)$ [4] and $w_i \sim \mathcal{CN}(0, \sigma_w^2)$. The channel samples are i.i.d as well.[5] The signal, noise and the channel gain are statistically independent of each other.

Now we resort to the p-norm detector, whose decision variable given in (2.8), after normalization with respect to the noise variance, may be written as

$$T_p = \frac{1}{N} \sum_{i=1}^{N} Y_i^p \underset{H_0}{\overset{H_1}{\gtrless}} \lambda, \tag{4.2}$$

where we define $Y_i \triangleq |y_i|/\sigma_w$. Under the system model considered, the distribution of the i-th received signal sample under H_0 and H_1 follows complex Gaussian distribution with $y_i|H_0 \sim \mathcal{CN}(0, \sigma_w^2)$ and $y_i|H_1 \sim \mathcal{CN}(0, \sigma_w^2(1+\gamma_i))$, respectively, with $\gamma_i \triangleq |h_i|^2 \sigma_S^2/\sigma_w^2$ being the instantaneous received SNR of the i-th sample.

Note that P_d and P_f can be alternatively expressed as

$$\begin{aligned} P_d &= 1 - F_{T_p|H_1}(\lambda), \\ P_f &= 1 - F_{T_p|H_0}(\lambda). \end{aligned} \tag{4.3}$$

Clearly, P_d and P_f are the complementary CDFs (CCDFs) of T_p under hypothesis $H \in$

[4] Gaussian signal assumption is valid, for example, in an OFDM signal having a large number of sub-carriers [98], [99]; in frequency-shift keying (FSK) signals that can be reasonably approximated as Gaussian process due to the complex time-structure; in radio-spectroscopy where the radiation process can be approximated as a Gaussian process due to collision-broadening or other atomic effects; or in radio-astronomy where the signals generated from radio-stars or gas clouds can be modeled as Gaussian which has varying intensities over the radio spectrum[100].

[5] This assumption is valid for time-selective fading channels, which are typical in some practical situations (e.g., when there is relative motion between the transceiver pair [25], or when the transceiver pair have a carrier frequency offset due to their oscillators' mismatch [101]). Nevertheless, the analytical approach developed in the chapter can be readily extended for time-flat fading channels as well.

$\{H_1, H_0\}$, respectively, with $F_{T|H}(\cdot)$ denoting the CDF under hypothesis H. The baseline objective of this work is to develop expressions for both P_d and P_f. Recall that P_d depends on the received SNR whereas P_f does not. Thus, in the fading channels, only the detection probability needs to be averaged over the PDF of the received SNR.

4.3 Derivation of P_d and P_f in AWGN

In AWGN, $h_i = 1, \forall i \in \{1, 2, ..., N\}$ and thus we define $\gamma \triangleq \sigma_S^2/\sigma_w^2$ dropping the subscript 'i'. The results for AWGN derived in this section establish an upper bound on the achievable sensing performance and also facilitate the subsequent extension to multipath fading and diversity reception scenarios. Moreover, these results are important for a fair comparison with the existing Gamma approximation [39].

As the distribution of y_i under each hypothesis is complex Gaussian, the squared amplitude of normalized i-th sample Y_i^2 is exponentially distributed as $Y_i^2|H_0 \sim e^{-x}u(x)$ for H_0, and $Y_i^2|H_1 \sim [1/(1+\gamma)]e^{-x/(1+\gamma)}u(x)$ for H_1, where $u(\cdot)$ denotes the unit step funciton. The MGF of the detector's decision variable T_p under hypothesis H is defined as $\mathcal{M}_{T_p|H}(s) \triangleq \mathbb{E}_{T_p|H}\left[e^{-sT_p}\right]$. Since the noise samples as well as the signal samples are i.i.d. and mutually independent of each other, the MGF of T_p can be expressed as a product of the MGFs of $Y_i^p/N \; \forall i \in \{1, 2, ..., N\}$, given as

$$\mathcal{M}_{T_p|H}(s) = \left[\mathbb{E}_{T_p|H}\left(e^{-\frac{s}{N}\left(\frac{|y_i|}{\sigma_w}\right)^{2\cdot\frac{p}{2}}} \right) \right]^N = \left[\int_0^\infty e^{-\frac{s}{N}x^{p/2}} \cdot A_H e^{-A_H x} dx \right]^N, \quad (4.4)$$

where A_H is a parameter under hypothesis H defined as

$$A_H \triangleq \begin{cases} 1 & H_0, \\ 1/(1+\gamma) & H_1. \end{cases}$$

4.3.1 Closed-form MGF-based analysis for even-integer p

Talbot's method for Laplace Transform Inversion

To this end, we need to obtain the detection and the false alarm probabilities from the MGF (4.4), which are the CCDFs of T_p under H_1 and H_0 respectively. For this purpose, we resort to the relation between the CDF and MGF of T_p where the CDF of T_p under H, $F_{T_p|H}(\lambda)$,

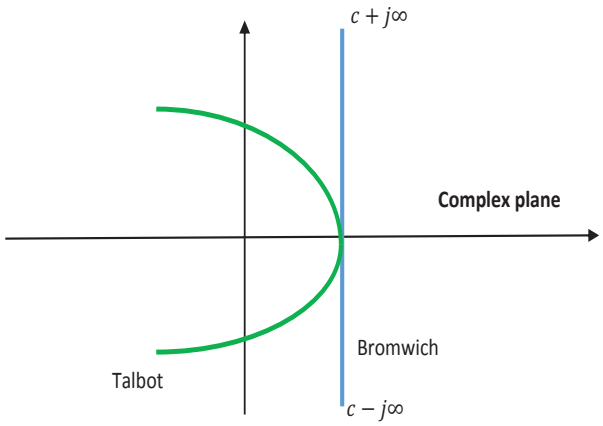

Fig. 4.1. Talbot's deformation of the Bromwich contour

can be obtained from the inverse Laplace transform of $\mathcal{M}_{T_p|H}(s)/s$ as

$$F_{T_p|H}(\lambda) = \frac{1}{2\pi\jmath}\int_B \frac{\mathcal{M}_{T_p|H}(s)}{s}\, e^{s\lambda} ds = \frac{1}{2\pi\jmath}\int_B \widehat{\mathcal{M}}_{T_p|H}(s)\, e^{s\lambda} ds, \tag{4.5}$$

where we define $\widehat{\mathcal{M}}_{T_p|H}(s) = \mathcal{M}_{T_p|H}(s)/s$, and B is the Bromwich contour as shown in blue in Fig. 4.1, which is a line defined by $s = c + \jmath w$ where $-\infty < w < \infty$ and c is a constant such that the singularities of $\widehat{\mathcal{M}}_{T_p|H}(s)$ are to the left of c [94]. Considering even-integer p and using [102, eq. (4)] to solve the integral in (4.4) results in a closed-form MGF of the form

$$\mathcal{M}_{T_p|H}(s) = \left[\frac{\sqrt{p/2}}{(\sqrt{2\pi})^{p/2-1}} G^{\frac{p}{2},1}_{1,\frac{p}{2}}\left(\frac{2^{p/2}A_H^{p/2}N}{p^{p/2}s}\middle|\begin{matrix}1\\ \frac{2}{p},\frac{4}{p},...,1\end{matrix}\right)\right]^N, \tag{4.6}$$

where $G^{\cdot,\cdot}_{\cdot,\cdot}(\cdot)$ is the Meijer's G-function [103, eq. (4)]. Thus, substitution of (4.6) into (4.5) suggest that an analytical expression for $F_{T_p|H}(\lambda)$ appears intractable. To add more, a direct computation of the integral (4.5) over the contour B is impractical due to possible oscillations of $e^{s\lambda}$ as $|w| \to \infty$. To address the difficulty in evaluating such integrals, Talbot, in his classical work [94] suggested deforming the Bromwich contour B to the form as depicted in green in Fig. 4.1. The motive of the deformation was to improve the convergence of the integral (4.5) by making the real component of s (negative) larger such that the contour B is wrapped around the negative real axis without crossing any singularities of $\widehat{\mathcal{M}}_{T_p|H}(s)$ in the deformation process. Thus, according to Cauchy's theorem [44], the deformed contour is still a valid one.

The classical numerical method suggested by Talbot attracted remarkable interest among researchers. To this end, to improve the numerical stability of such evaluation in a fixed-precision computing environment, a multi-precision method termed the "fixed Talbot method" was proposed by the work [95], which derived an alternative form of the integral as

$$F_{T_p|H}(\lambda) = \frac{1}{2\pi\jmath}\int_{-\pi}^{\pi} \widehat{\mathcal{M}}_{T_p|H}[s(\theta)] \cdot s'(\theta) e^{\lambda s(\theta)} d\theta, \tag{4.7}$$

where

$$s(\theta) = r\theta(\cot\theta + \jmath)$$

with $|\theta| < \pi$, $s'(\theta)$ being the derivative of $s(\theta)$ w.r.t. θ, and $r = 2\mathcal{W}/(5\lambda)$ with integer $\mathcal{W}$ controlling the desired precision for the fixed Talbot method [95]. The integral in (4.7) can then be evaluated by using the trapezoidal rule with step size $\pi/\mathcal{W}$ and $\theta_k = k\pi/\mathcal{W}$, and hence the CDF $F_{T_p|H}(\lambda)$ can be computed as [95], [104]

$$F_{T_p|H}(\lambda) = \frac{r}{\mathcal{W}}\left(\frac{1}{2}\widehat{\mathcal{M}}_{T_p|H}(r)e^{r\lambda} + \sum_{k=1}^{\mathcal{W}-1} \Re\{e^{\lambda s(\theta_k)}\widehat{\mathcal{M}}_{T_p|H}[s(\theta_k)]\,(1+\jmath\sigma(\theta_k))\}\right), \tag{4.8}$$

where $\sigma(\theta) = \theta + (\theta\cot\theta - 1)\cot\theta$. Based on [95], the number of significant digits of $F_{T_p|H}(\lambda)$ calculated in (4.8) is approximately equal to $0.6\mathcal{W}$. Then, the CCDF of $T_p|H$ can immediately be expressed as

$$\mathbb{P}(T_p \geq \lambda|H) = 1 - \frac{r}{\mathcal{W}}\left(\frac{1}{2}\widehat{\mathcal{M}}_{T_p|H}(r)e^{r\lambda} + \sum_{k=1}^{\mathcal{W}-1} \Re\{e^{\lambda s(\theta_k)}\widehat{\mathcal{M}}_{T_p|H}[s(\theta_k)]\,(1+\jmath\sigma(\theta_k))\}\right). \tag{4.9}$$

By substituting $A_H = 1/(1+\gamma)$ and $A_H = 1$, respectively, into (4.6) and subsequently using (4.9), P_d and P_f can be computed accurately. Note that a numerical software package such as MATHEMATICA can be readily used for the evaluation of (4.9). Hence, (4.9) offers a computationally attractive solution for both P_d and P_f when p is an even-integer.

4.3.2 Series MGF-based analysis for arbitrary p

In this section, starting from the derivation of a series-form MGF of T_p, novel series solutions are obtained for P_d and P_f which are valid for any arbitrary p. Substituting $e^{-x} = \sum_{v=0}^{\infty}(-1)^v x^v/v!$ inside the integral in (4.4), interchanging the order of integration

TABLE 4.1
THE ϵ-TABLE.

$c=-2$	$c=-1$	$c=0$	$c=1$	...
0	$\epsilon(0,0)=S_0$	$\epsilon(0,1)$	$\epsilon(0,2)$	...
0	$\epsilon(1,0)=S_1$	$\epsilon(1,1)$	$\epsilon(1,2)$	...
$\vdots$	$\vdots$	$\vdots$	$\vdots$	$\iddots$
0	$\epsilon(\eta-3,0)=S_{\eta-3}$	$\epsilon(\eta-3,1)$	$\epsilon(\eta-3,2)$	
0	$\epsilon(\eta-2,0)=S_{\eta-2}$	$\epsilon(\eta-2,1)$		
0	$\epsilon(\eta-1,0)=S_{\eta-1}$			

and summation, and using [103, eq. (3.326.2)], we have

$$\mathcal{M}_{T_p|H}(s)=\left[\frac{2}{p}\sum_{v=0}^{\infty}\frac{(-1)^v A_H^{v+1}N^{2(v+1)/p}}{v!\ s^{2(v+1)/p}}\Gamma\left(\frac{2(v+1)}{p}\right)\right]^N. \tag{4.10}$$

By using [103, eq. (0.314)] to further simplify (4.10), the series-form MGF can be obtained as

$$\mathcal{M}_{T_p|H}(s)=\frac{2^N}{p^N}\sum_{v=0}^{\infty}\frac{C_{v|H}N^{2(v+N)/p}}{s^{2(v+N)/p}}, \tag{4.11}$$

where

$$C_{v|H}=\frac{1}{v\,\Gamma(2/p)A_H}\sum_{k=1}^{v}(kN-v+k)\frac{(-1)^k}{k!}\Gamma\left(\frac{2(k+1)}{p}\right)A_H^{k+1}\ C_{v-k|H},\ \ v\geq 1,$$

and $C_{0|H}=[\Gamma(2/p)A_H]^N$. The CDF $F_{T|H}(\lambda)$ can then be obtained by using the inverse Laplace transform

$$\mathcal{L}^{-1}\left[\frac{\Gamma(a+1)}{s^{a+1}}\right]=t^a,\ \ a>-1,$$

on $\mathcal{M}_{T_p|H}(s)/s$, and subsequently, the CCDF under hypothesis H can be expressed as

$$\mathbb{P}(T_p>\lambda|H)=1-\frac{2^N}{p^N}\sum_{v=0}^{\infty}\frac{C_{v|H}(N\lambda)^{2(v+N)/p}}{\Gamma\left(\frac{2(v+N)}{p}+1\right)}. \tag{4.12}$$

Thus, the use of (4.12) after substituting $A_H=1/(1+\gamma)$ and $A_H=1$ for hypothesis H_1 and H_0 in the expression for $C_{v|H}$ yields the detection probability P_d and the false alarm probability P_f, respectively.

Moreover, (4.12) can be expressed as an alternating series-sum such that the CCDF

under hypothesis H is $\mathbb{P}(T_p > \lambda|H) = 1 - \sum_{v=0}^{\infty}(-1)^v D_{v|H}$, with

$$D_{v|H} \triangleq \frac{2^N}{p^N} \cdot \frac{|C_{v|H}|(N\lambda)^{2(v+N)/p}}{\Gamma\left(\frac{2(v+N)}{p}+1\right)}.$$

Our experiments show that $D_{v|H}$ is readily decreasing with increasing v. Thus, the infinite sum $\mathcal{S}_\infty = \sum_{k=0}^{\infty}(-1)^n D_{k|H}$ can be estimated by a partial sum of its n_t terms of the form $\mathcal{S}_{n_t} = \sum_{k=0}^{n_t}(-1)^n D_{k|H}$, and the truncation error E_{tr} can thus be upper-bounded as $|E_{tr}| < |D_{n_t+1|H}|$. Although the absolute truncation error $|E_{tr}|$ readily decreases with increasing n_t, the rate of convergence may be accelerated by using the powerful ϵ-algorithm. The ϵ-algorithm transforms the original series into convergents of its associated continued fractions thus resulting in a faster rate of convergence (i.e. fewer terms to achieve a given precision) [96].

The objective of the ϵ-algorithm is to estimate $\mathcal{S}_\infty$ by using as few partial sums as possible. This algorithm generates a two-dimensional triangular array called the ϵ-table as shown in Table 4.1 with entries $\epsilon(k, c+1)$, where $k = 0, 1, 2, ...$ is the row index and $c = -2, -1, 0, 1, 2, ...$ determines the column index. The first two columns (column '-2' and column '-1') are initialized as $\epsilon(k, -1) = 0$, $\epsilon(k, 0) = \mathcal{S}_k, \forall k \in \{0, 1, ..., \eta-1\}$, with η representing the total number of terms used in the partial sum. The remaining columns are updated as

$$\epsilon(k, c+1) = \epsilon(k+1, c-1) + [\epsilon(k+1, c) - \epsilon(k, c)]^{-1},$$

where $c \geq 0$. As the value of η is increased (which leads to the corresponding increase in the number of columns), the even columns of the ϵ-table contain increasingly accurate estimates of S_∞ [96]. The algorithm stops (no further increase in η) when the desired precision is attained at a particular even column (i.e., the values in the column converge with the desired precision). Then, any value in the column can be used as an estimated $\mathcal{S}_\infty$ and the corresponding value of η represents the number of terms needed in the ϵ-algorithm. For example, for a 2.5-norm detector at SNR of 0 dB, with $N = 4$ at $P_f = 0.01$, $\eta = 21$ terms are sufficient for the ϵ-algorithm applied to (4.12) for computing P_d with 4-decimal points accuracy, as compared to $n_t = 33$ terms without convergence acceleration. More examples in Table 4.2 (obtained with accuracy of 4-decimal points) clearly show the advantage of the

TABLE 4.2
NUMBER OF TERMS NEEDED IN (4.12) FOR COMPUTATION OF P_d WITH AND WITHOUT (W.O.) USING ϵ-ALGORITHM.

	$\gamma = -15$ dB, $\lambda = 5$						$\gamma = 0$ dB, $\lambda = 7$			$\gamma = 10$ dB, $\lambda = 7$			
p	1.8		2.5		3.5		1.8	2.5	3.5	1.5		4	
N	2	4	2	4	2	4	4	4	4	5	10	5	10
w.o. ϵ-algorithm	41	79	25	47	19	33	59	33	23	29	59	7	7
with ϵ-algorithm	21	63	15	23	13	19	27	19	13	15	33	5	3

ϵ-algorithm in increasing the convergence rate (hence reducing the computation time).

4.3.3 Generalized Laguerre polynomial series-based approximation

In the approximation theory literature, the random variables which exhibit non-linear and complex characteristics thus causing them to deviate from Gaussanity may be often approximated by using generalized PDF forms with the parameters depending upon the underlying statistical properties of the random variables to be approximated. The generalized Laguerre polynomial approximation is one of such approaches where the PDF of any random variable Z can be written in terms of a weighted sum of the generalized Laguerre polynomials as

$$f_Z(z) \approx \sum_{n=0}^{\infty} \omega_n L_n^{\alpha}(z) \tag{4.13}$$

where

$$L_n^{\alpha}(z) \triangleq \sum_{u=0}^{n} \frac{(-1)^u}{u!} \frac{\Gamma(\alpha+n+1)}{\Gamma(n-u+1)\Gamma(\alpha+u+1)} z^u$$

is the generalized Laguerre polynomial [105], and ω_n are the corresponding weights (details on their determination discussed shortly). The generalized Laguerre polynomial series approximation has been popularly used for addressing distribution problems in mathematical physics, atomic theory and transmission line electromagnetics [97]. For these problems, the weights in the Laguerre series sum have been chosen to depend upon the Gamma random variable which has often proven to be useful for approximating non-Gaussian PDFs [97].

The series (4.13) converges when $Z > 0$. For an extensive convergence analysis of the approximation, we refer the readers to [106]–[108]. However, we would like to emphasize on few important conditions for the series to represent $f_Z(z)$ as follows.

(i) $f_Z(z)$ is absolutely continuous in every finite interval, and

(ii) $\lim_{z\to 0} z^{\alpha+1} f_Z(z) = 0$.

Clearly, the decision variable T_p meets these conditions and thus it serves as a motivation to pursue the applicability of the approximation for our problem at hand. Thus, in this section, we derive approximate expressions for the detection and false alarm probabilities by using a generalized Laguerre polynomial series representation of the p-norm detector decision variable.

To this end, we propose approximating the PDF of the decision variable T_p by a weighted (N_g+1)-term sum of number of generalized Laguerre polynomials of the form [97]

$$f_{T_p}(z) \approx \frac{\beta z^{\alpha} e^{-z}}{\Gamma(\alpha+1)} \sum_{n=0}^{N_g} r_n L_n^{\alpha}(z), \;\; z \geq 0, \;\; \alpha \geq -1, \tag{4.14}$$

where the coefficient r_n is given by[6]

$$r_n = \frac{n!\,\Gamma(\alpha+1)}{\beta\,\Gamma(n+\alpha+1)} \sum_{\nu=0}^{n} \frac{(-1)^{\nu}\,\Gamma(\alpha+n+1)\beta^{\nu} m_{\nu}}{\nu!\,\Gamma(n-\nu+1)\Gamma(\alpha+\nu+1)}, \tag{4.15}$$

where $m_\nu = \mathbb{E}(T_p^\nu)$ is the ν-th moment of T_p, and the parameters α and β are given by

$$\alpha = \frac{2m_1^2 - m_2}{m_2 - m_1^2}, \;\; \beta = \frac{m_1}{m_2 - m_1^2}.$$

It is important to note that in this chapter, the usefulness of the Laguerre approximation is demonstrated by using only a few summands N_g.

Note that the moment m_ν depends on the hypothesis $H \in \{H_0, H_1\}$ and can be obtained by multinomial expansion of (4.2) followed by some algebra as

$$m_\nu | H = \frac{1}{N^\nu} \sum_{\mathbf{\Lambda}_\nu} \binom{\nu}{k_1, ..., k_N} \mathbb{E}_{Y_1, Y_2, ..., Y_N | H} \left[\prod_{i=1}^{N} Y_i^{k_i p} \right],$$

where $\mathbf{\Lambda}_\nu = [k_1, ..., k_N | k_1 + ... + k_N = \nu, k_1, ..., k_N \geq 0]$. Utilizing the i.i.d. property of $Y_i \; \forall i \in \{1, 2, ..., N\}$ followed by evaluation of the mathematical expectation, we can show

[6]Note that the factor β in the denominator outside the summation in (4.15) necessary to normalize the area under the PDF (4.14) to unity is missing in [97, eq. (10)].

that

$$m_\nu|H = \frac{1}{N^\nu} \sum_{\mathbf{\Lambda}_\nu} \binom{\nu}{k_1, ..., k_N} \prod_{i=1}^{N} A_H^{-\frac{k_i p}{2}} \Gamma\left(\frac{k_i p}{2} + 1\right). \tag{4.16}$$

By substituting the definition of $L_n^\alpha(z)$ into (4.14), integrating the resulting expression from $z = 0$ to $z = \lambda$, and changing the order of integration and summation followed by some algebra, the CDF of T_p can be obtained as

$$F_{T_p}^{\text{Lag}}(\lambda) = \sum_{n=0}^{N_g} \frac{r_n \beta}{\Gamma(\alpha+1)} \sum_{u=0}^{n} \zeta(u, n, \alpha, \lambda), \tag{4.17}$$

in which

$$\zeta(u, n, \alpha, \lambda) \triangleq \frac{(-1)^u \Gamma(\alpha+n+1)}{u!\Gamma(n-u+1)\Gamma(\alpha+u+1)} \mathcal{G}(\alpha+u+1, \lambda),$$

and $\mathcal{G}(a, x) = \int_0^x e^{-t} t^{a-1} dt$ is the lower incomplete Gamma function [26, eq. (6.5.2)].[7] Since the moments m_i of T_p are different under the two hypotheses as revealed by (4.16), the parameters α, β and r_n are also hypothesis-dependent. Using (4.16) for each hypothesis $H \in \{H_0, H_1\}$ in the definition of α and β, we get

$$\begin{aligned}
&\alpha|H_0 = \alpha|H_1 = \tfrac{(N+1)\Gamma^2(p/2+1) - \Gamma(p+1)}{\Gamma(p+1) - \Gamma^2(p/2+1)}, \\
&\beta|H_0 = \tfrac{N\Gamma(p/2+1)}{\Gamma(p+1) - \Gamma^2(p/2+1)}, \\
&\beta|H_1 = A_H^{p/2} \cdot \beta|H_0.
\end{aligned}$$

Since $\alpha|H_0 = \alpha|H_1$, we simply denote them by α. Thus, the probability of T_p exceeding λ under hypotheses H can be expressed as the CCDF of (4.17) as

$$\mathbb{P}^{\text{Lag}}(T_p > \lambda|H) = 1 - \sum_{n=0}^{N_g} \frac{r_n|H \cdot \beta|H}{\Gamma(\alpha+1)} \sum_{u=0}^{n} \zeta(u, n, \alpha, \lambda), \tag{4.18}$$

where $r_n|H$ for each $H \in \{H_1, H_0\}$ is obtained from (4.15) by replacing α, $\beta|H_1$ and $\beta|H_0$ for hypothesis H_1 and H_0, respectively. Hence, the resulting expressions under H_1 and H_0 yield the desired detection probability P_d^{Lag} and false alarm probability P_f^{Lag}, respectively.

Note that (4.18) is obtained by approximating the PDF of T_p by a weighted sum of

[7] The superscript 'Lag' is used as shorthand notation for 'Laguerre'.

a finite number (N_g) of identically distributed Gamma random variables whose weights depend on the corresponding Laguerre-polynomials. Interestingly, our numerical results in Section 4.5 reveal that the Laguerre approximation is more versatile than the Gamma approximation and more accurate than the CLT approximation (for a few samples).

4.4 Analysis in Fading and Diversity Combining

In this section, a unified approach based on the series-MGF obtained in Section 4.3.2 is developed for deriving the average detection probability in various fading and diversity reception scenarios. Specifically, average detection probabilities over the κ-μ and the α-μ fading are derived. As well, for a multiple-antenna p-norm detector, the performance of the two proposed schemes, the pLC and the pLS, and of the classical MRC and SC schemes are derived in Nakagami-m fading channels.

For fading channels, the instantaneous received SNRs $\gamma_i = |h_i|^2\sigma_S^2/\sigma_w^2, i = \{1, 2, ..., N\}$ are random variables whose PDFs depend on the fading channel (and/or diversity-combining) model. Then, the probability of detection would depend on the instantaneous SNRs $\boldsymbol{\gamma} = \{\gamma_1, \gamma_2, ..., \gamma_N\}$. Hence, the average probability of detection $\overline{P}_d$ must be obtained by integrating the instantaneous probability of detection $P_d(\boldsymbol{\gamma})$ over the joint PDF (JPDF) $f(\boldsymbol{\gamma})$. Using (4.3) and (4.5), $P_d(\boldsymbol{\gamma})$ can be expressed as

$$P_d(\boldsymbol{\gamma}) = 1 - \frac{1}{2\pi\jmath}\int_B \frac{\mathcal{M}_{T_p|H_1}(s,\boldsymbol{\gamma})}{s}\, e^{s\lambda} ds, \tag{4.19}$$

where $\mathcal{M}_{T|H_1}(s,\boldsymbol{\gamma})$ is the MGF of $T_p|H_1$ conditioned on $\boldsymbol{\gamma}$. Then, $\overline{P}_d$ can be obtained by integrating (4.19) over the JPDF $f(\boldsymbol{\gamma})$ as

$$\overline{P}_d = 1 - \frac{1}{2\pi\jmath}\int_{\boldsymbol{\gamma}}\int_B \frac{\mathcal{M}_{T_p|H_1}(s,\boldsymbol{\gamma})}{s}\, e^{s\lambda} f(\boldsymbol{\gamma}) ds d\boldsymbol{\gamma}. \tag{4.20}$$

Interchanging the order of integrations, (4.20) can be written as

$$\overline{P}_d = 1 - \frac{1}{2\pi\jmath}\int_B e^{s\lambda}\frac{\overline{\mathcal{M}}_{T_p|H_1}(s)}{s} ds, \tag{4.21}$$

where $\overline{\mathcal{M}}_{T_p|H_1}(s) = \int_{\boldsymbol{\gamma}} \mathcal{M}_{T_p|H_1}(s,\boldsymbol{\gamma}) f(\boldsymbol{\gamma}) d\boldsymbol{\gamma}$ is the unconditional[8] MGF of $T_p|H_1$. Thus,

[8]Henceforth, the term "unconditional" implies averaging (integration) over the JPDF $f(\boldsymbol{\gamma})$.

(4.21) suggests that the average detection probability can be easily obtained once we have the inverse Laplace transform of the unconditional MGF of $T_p|H_1$.

To evaluate (4.21), first, the need is to find $\overline{\mathcal{M}}_{T_p|H_1}(s)$. For independently faded samples, the JPDF $f(\boldsymbol{\gamma})$ can be expressed as the product of each individual PDFs $f(\gamma_i)$, $\forall i \in \{1, 2, ..., N\}$. Thus, we have $\overline{\mathcal{M}}_{T_p|H_1}(s) = \prod_{i=1}^{N} \overline{\mathcal{M}}_{Y_i^p/N|H_1}(s)$, in which $\overline{\mathcal{M}}_{Y_i^p/N|H_1}(s)$ is the unconditional MGF of Y_i^p/N under H_1 given as

$$\overline{\mathcal{M}}_{Y_i^p/N|H_1}(s) = \int_0^\infty \mathcal{M}_{Y_i^p/N|H_1}(s, \gamma_i) f(\gamma_i) d\gamma_i$$

with $f(\gamma_i)$ being the marginal PDF of the instantaneous SNR of the i-th sample while $\mathcal{M}_{Y_i^p/N|H_1}(s, \gamma_i)$ represents the conditional (on γ_i) MGF of Y_i^p/N under H_1. Here, we can see that $\mathcal{M}_{Y_i^p/N|H_1}(s, \gamma_i)$ can be expressed in a series-form following the steps similar to those used in the derivation of (4.10) after replacing $A_H = 1/(1 + \gamma_i)$ as

$$\mathcal{M}_{Y_i^p/N|H_1}(s, \gamma_i) = \frac{2}{p} \sum_{v=0}^{\infty} \frac{(-1)^v N^{2(v+1)/p}}{v!\ s^{2(v+1)/p}} \frac{\Gamma\left(\frac{2(v+1)}{p}\right)}{(1 + \gamma_i)^{v+1}}. \tag{4.22}$$

Thus, for i.i.d. fading, we can write $\overline{\mathcal{M}}_{T_p|H_1}(s) = [\overline{\mathcal{M}}_{Y_i^p/N|H_1}(s)]^N$. Then, the only need is to obtain $\overline{\mathcal{M}}_{Y_i^p/N|H_1}(s)$. As we will consider various statistical models for $f(\gamma_i)$, we rewrite the unconditional MGF $\overline{\mathcal{M}}_{Y_i^p/N|H_1}(s)$, with the abuse of notations as

$$\overline{\mathcal{M}}^{\text{fd}}_{Y_i^p/N|H_1}(s) = \int_0^\infty \mathcal{M}_{Y_i^p/N|H_1}(s, \gamma)\, f_{\text{fd}}(\gamma) d\gamma, \tag{4.23}$$

where the script 'fd' denotes the corresponding fading (and/or diversity-combining) model under consideration. Solution of (4.23) would subsequently yield $\overline{\mathcal{M}}^{\text{fd}}_{T_p|H_1}(s)$ and then the application of inverse Laplace transformation on $\overline{\mathcal{M}}^{\text{fd}}_{T_p|H_1}(s)/s$ (similarly to the application in Section 4.3.2) yields the average probability of detection $\overline{P_{d,\text{fd}}}$ for the corresponding fading (and/or diversity combining) scenario. In the following sections, the unconditional MGF (4.23) is derived for different channel models and various diversity-combining schemes on a case-by-case basis.

4.4.1 The κ-μ Fading-No Diversity

The κ-μ distribution can model a wide variety of fading environments with LOS propagation. The PDF of the instantaneous SNR for this fading model is given by [29]

$$f_{\kappa\text{-}\mu}(\gamma) = \frac{\mu(1+\kappa)^{\frac{\mu+1}{2}} e^{-\mu\kappa}\gamma^{\frac{\mu-1}{2}}}{\kappa^{\frac{\mu-1}{2}}\overline{\gamma}^{\frac{\mu+1}{2}} e^{-\frac{\mu(1+\kappa)}{\overline{\gamma}}\gamma}} I_{\mu-1}\left(2\mu\sqrt{\frac{\kappa(1+\kappa)\gamma}{\overline{\gamma}}}\right), \tag{4.24}$$

where $I_\nu(\cdot)$ is the ν-th order modified Bessel function of first kind [26], $\gamma \geq 0$, and $\overline{\gamma}$ is the average received SNR. The parameter $\kappa > 0$ is the ratio of the total power of the dominant components to that of the scattered waves, and

$$\mu = \frac{\mathbb{E}^2\{\gamma\}}{\text{Var}\{\gamma\}}\left(1 + \frac{2\kappa}{(1+\kappa)^2}\right)$$

represents the number of multipath clusters. By replacing the modified Bessel function of first kind in (4.24) with its infinite series representation [26, eq. (9.6.10)], substituting the resulting series for $f_{\kappa\text{-}\mu}(\gamma)$ into (4.23), interchanging the order of integration and summation, and finally, using the definition of the confluent hypergeometric function of the second kind [109],

$$U(a,b,z) = \frac{1}{\Gamma(a)}\int_0^\infty e^{-zt}t^{a-1}(1+t)^{b-a-1}dt, \quad a,\, z > 0, \tag{4.25}$$

to solve the resulting integral, the unconditional MGF over κ-μ fading $\overline{\mathcal{M}}^{\kappa\text{-}\mu}_{Y_i^p/N|H_1}(s)$ can be derived to be

$$\begin{aligned}\overline{\mathcal{M}}^{\kappa\text{-}\mu}_{Y_i^p/N|H_1}(s) &= \frac{2\,\mu^\mu(1+\kappa)^\mu}{p\,e^{\kappa\mu}\,\overline{\gamma}^\mu} \\ &\times \sum_{v=0}^{\infty}\Bigg[\frac{(-1)^v}{v!}\Gamma\left(\frac{2(v+1)}{p}\right)\left(\frac{N}{s}\right)^{\frac{2(v+1)}{p}} \\ &\times \sum_{j=0}^{\infty}\frac{\mu^{2j}\kappa^j(1+\kappa)^j}{\overline{\gamma}^j\,j!}U\left(\mu+j, \mu+j-v, \frac{\mu(1+\kappa)}{\overline{\gamma}}\right)\Bigg].\end{aligned} \tag{4.26}$$

The expression (4.26) is utilized to obtain the unconditional MGF of $T_p|H_1$ over κ-μ fading and subsequently used to deduce the expression for the average detection probability $\overline{P_{d,\kappa\text{-}\mu}}$ in Section 4.4.4. Truncation of the resulting infinite series occurring in $\overline{P_{d,\kappa\text{-}\mu}}$ is discussed in Section 4.4.5.

Note that for any other generalized fading model, say, η-μ fading model [92], (which is another generalized fading model for non-LOS conditions) is considered, the unconditional MGF similar to (4.26) can be obtained. Further, the subsequent analysis would be similar thus indicating the generality of our approach.

4.4.2 The α-μ Fading-No Diversity

In α-μ distribution, parameter $\alpha > 0$ models the non-linearity of the propagation medium, and parameter $\mu > 0$ denotes the number of multipath clusters. The PDF of the instantaneous SNR under this fading model is given by [110]

$$f_{\alpha\text{-}\mu}(\gamma) = \frac{\alpha\mu^{\mu}}{2\Gamma(\mu)\tilde{\gamma}^{\alpha\mu/2}}\gamma^{\alpha\mu/2-1}e^{-\mu\left(\frac{\gamma}{\tilde{\gamma}}\right)^{\alpha/2}}, \tag{4.27}$$

where $\gamma \geq 0$, and

$$\tilde{\gamma} = \frac{\mu^{2/\alpha}\Gamma(\mu)}{\Gamma(\mu + 2/\alpha)}\frac{E_b}{N_0},$$

in which E_b/N_0 is the energy per bit to noise power spectral density ratio. Substituting the PDF (4.27) into (4.23) gives

$$\begin{aligned}\overline{\mathcal{M}}^{\alpha\text{-}\mu}_{Y_i^p/N|H_1}(s) = \frac{2}{p}\sum_{v=0}^{\infty}\Bigg[&\frac{(-1)^v}{v!}\Gamma\left(\frac{2(v+1)}{p}\right)\left(\frac{N}{s}\right)^{\frac{2(v+1)}{p}} \\ &\times \frac{1}{\Gamma(\mu)}\int_0^{\infty}\frac{\alpha\mu^{\mu}}{2\tilde{\gamma}^{\alpha\mu/2}}\frac{\gamma^{\alpha\mu/2-1}e^{-\mu\left(\frac{\gamma}{\tilde{\gamma}}\right)^{\frac{\alpha}{2}}}}{(1+\gamma)^{v+1}}d\gamma\Bigg].\end{aligned} \tag{4.28}$$

Unfortunately, an exact closed-form solution for the integral in (4.28) appears to be intractable. However, by substituting

$$t = \frac{\mu}{\tilde{\gamma}^{\alpha/2}}\gamma^{\alpha/2},$$

the integral can be alternatively expressed as $\mathcal{I} = \int_0^{\infty} g(t)e^{-t}dt$ with

$$g(t) = t^{\mu-1}\left[1 + \frac{t^{2/\alpha}}{\mu^{2/\alpha}}\tilde{\gamma}\right]^{-v-1}.$$

The integral $\mathcal{I}$ can then be approximated by a Gaussian-Laguerre quadrature sum of the form

$$\mathcal{I} = \int_0^\infty g(t)e^{-t}dt \approx \sum_{q=1}^{N_Q} w_q g(t_q),$$

where t_q and w_q are the abscissas and weight factors for the Gaussian-Laguerre quadrature integration [26, eq. (25.4.45)]. Thus, (4.28) can be evaluated as

$$\overline{\mathcal{M}}^{\alpha\text{-}\mu}_{Y_i^p/N|H_1}(s) \approx \frac{2/p}{\Gamma(\mu)} \sum_{v=0}^{\infty} \left[\frac{(-1)^v}{v!} \Gamma\left(\frac{2(v+1)}{p}\right) \left(\frac{N}{s}\right)^{\frac{2(v+1)}{p}} \sum_{q=1}^{N_Q} w_q g(t_q) \right]. \quad (4.29)$$

The unconditional MGF (4.29) provides the basis for obtaining the average detection probability $\overline{P_d}_{,\alpha\text{-}\mu}$ in Section 4.4.4. As (4.29) is derived using Gaussian-Laguerre approximation for the integral in (4.28), the accuracy of the approximation is discussed in conjunction with the expression for $\overline{P_d}_{,\alpha\text{-}\mu}$ in Section 4.4.5.

4.4.3 Analysis for Antenna Diversity

In this section, the input to the p-norm detector comprises of a total of L antennas. Two non-coherent combining techniques, pLC and pLS, are proposed and compared against traditional MRC and SC. Note that the proposed schemes can be readily analyzed for κ-μ and α-μ channels. However, as the SNR of the MRC output is given by the sum of the individual branch SNRs (see Section 4.4.3.3), its analysis in κ-μ or α-μ channel requires an exact PDF of the sum of such variates. Such PDFs are not available in the literature.[9] As we are interested in analyzing the effect of diversity-combining on the p-norm detection performance and in determining the performance of pLC and pLS relative to classical MRC and SC, i.i.d. Nakagami-m fading over the diversity branches is considered for further analysis. Each of the diversity-combining scheme is treated separately in the following.

4.4.3.1 p-Law Combining (pLC)

A schematic diagram of the proposed pLC scheme is shown in Fig. 4.2 above. The received signal at each branch is input to its *p-norm device*, which raises each sample to the p-th power followed by sample-averaging. This yields a total of L independent decision

[9] Although approximations of the sum distributions of κ-μ and α-μ variates are available, respectively, in [111] and [112], they require moment matching for estimating the relevant parameters and are beyond the scope of this work.

variables $T_{p1}, T_{p_2}, ..., T_{p_L}$, which are added together to obtain the pLC decision variable

$$T_{\text{plc}} = \sum_{l=1}^{L} T_{p_l} = \frac{1}{N} \sum_{l=1}^{L} \sum_{i=1}^{N} (Y_{i,l})^p,$$

where $Y_{i,l}$ is the i-th normalized sample received at the l-th branch (this definition is similar to the definition of Y_i in (4.2) for a single branch).[10] The final decision is made after comparing T_{plc} against the threshold.

The PDF of the received SNR over a single branch Nakagami-m fading is given by [24]

$$f_{\text{Nak}}(\gamma) = \frac{1}{\Gamma(m)} \left(\frac{m}{\overline{\gamma}}\right)^m \gamma^{m-1} e^{-\frac{m}{\overline{\gamma}}\gamma}, \ \gamma \geq 0. \tag{4.30}$$

We define $\overline{\mathcal{M}}^{\text{plc}}_{(Y_{i,l})^p/N|H_1}(s)$ as the unconditional MGF of $(Y_{i,l})^p/N|H_1$, which can be obtained by substituting (4.30) into (4.23) and using the definition of the confluent hypergeometric function of the second kind (4.25) to solve the resulting integral as

$$\begin{aligned} \overline{\mathcal{M}}^{\text{plc}}_{(Y_{i,l})^p/N|H_1}(s) &= \frac{2}{p}\left(\frac{m}{\overline{\gamma}}\right)^m \\ &\times \sum_{v=0}^{\infty} \frac{(-1)^v}{v!} \Gamma\left(\frac{2(v+1)}{p}\right) \left(\frac{N}{s}\right)^{\frac{2(v+1)}{p}} U\left(m, m-v, \frac{m}{\overline{\gamma}}\right). \end{aligned} \tag{4.31}$$

As $(Y_{i,l})^p/N$ are i.i.d. for all samples $i \in \{1, 2, ..., N\}$ and for all branches $l \in \{1, 2, ..., L\}$, the unconditional MGF of the decision variable T_{plc} under H_1 can be expressed as a product of the unconditional MGFs $\overline{\mathcal{M}}^{\text{plc}}_{(Y_{i,l})^p/N|H_1}(s)$ such that $\overline{\mathcal{M}}_{T_{\text{plc}}|H_1} = [\overline{\mathcal{M}}^{\text{plc}}_{(Y_{i,l})^p/N|H_1}(s)]^{NL}$. Note that the MGF of T_{plc} under H_0 is $\mathcal{M}_{T_{\text{plc}}|H_0}(s) = [\mathcal{M}_{T_p|H_0}(s)]^L$, where $\mathcal{M}_{T_p|H_0}(s)$ is given by (4.10) with $A_H = 1$. These MGFs form the basis for obtaining the average detection probability $\overline{P_d}_{,\text{plc}}$ and the false alarm probability $P_{f,\text{plc}}$, respectively, in Section 4.4.4.

4.4.3.2 p-Law Selection (pLS)

The proposed pLS scheme is shown in Fig. 4.3. In this scheme, the received signal at each branch is passed through its p-norm device to obtain L decision variables $T_{p_1}, T_{p_2}, ..., T_{p_L}$. Then, only the branch with the largest decision variable is selected such that the pLS deci-

[10] This scheme may be considered as a generalization of SLC scheme used in the conventional ED [33].

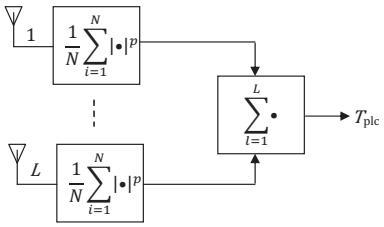

Fig. 4.2. The proposed pLC scheme

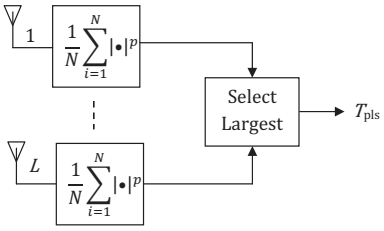

Fig. 4.3. The proposed pLS scheme

sion variable is given by $T_{\text{pls}} = \max\{T_{p_1}, T_{p_2}, ..., T_{p_L}\}$.[11] The final decision is made after comparing T_{pls} against the threshold. For the independent decision variables, the CDF of T_{pls} can be expressed as

$$\begin{aligned} F_{T,\text{pls}} = \mathbb{P}(T_{\text{pls}} \leq \lambda) &= \mathbb{P}(T_{p_1} \leq \lambda, T_{p_2} \leq \lambda, ..., T_{p_L} \leq \lambda) \\ &= \prod_{l=1}^{L}[1 - \mathbb{P}(T_{p_l} > \lambda)]. \end{aligned} \tag{4.32}$$

Since the branches are i.i.d., the false alarm probability of the pLS scheme can be expressed as

$$P_{f,\text{pls}} = 1 - [1 - P_f]^L, \tag{4.33}$$

where the P_f occurring in (4.33) is given by (4.12) for $H = H_0$. Similarly, it is easy to show that the average detection probability for the pLS scheme over Nakagami-m fading channels can be obtained as

$$\overline{P_d}_{,\text{pls}} = 1 - [1 - \overline{P_d}_{,\text{Nak}}]^L, \tag{4.34}$$

[11] This scheme may be thought of as generalization of the square-law selection (SLS) scheme used in the ED [33].

where $\overline{P_d}_{,\text{Nak}}$ is the average detection probability of a single-branch p-norm detector over Nakagami-m fading. Thus, to evaluate (4.34), only $\overline{P_d}_{,\text{Nak}}$ is needed, which can be obtained from the unconditional MGF (4.31). The derivation of $\overline{P_d}_{,\text{Nak}}$ is discussed in 4.4.4.

4.4.3.3 MRC

Recall that the MRC is a coherent combining scheme that requires the complete CSI at the receiver [24]. Although the p-norm detector can function without any CSI, the analysis in MRC is important mainly because of its optimality, which helps to establish an upper bound on the achievable sensing performance against which other combining schemes may be compared. For this case, each of the branches is weighted with the complex conjugate of the corresponding fading coefficient and combined to yield the signal $y_{\text{mrc}}(t) = \sum_{l=1}^{L} h_l^* y_l(t)$ where h_l^* and $y_l(t)$ denote the complex conjugate fading coefficient and the received signal respectively, for the l-th branch. The samples of $y_{\text{mrc}}(t)$ are then fed into the p-norm detector.

For a total of L antennas, the MRC output SNR is given by $\gamma^{\text{mrc}} = \sum_{l=1}^{L} \gamma_l$, where γ_l is the SNR of the l-th branch. For i.i.d. branches in Nakagami-m fading, the MRC output SNR is [24]

$$f_{\text{mrc}}(\gamma) = \frac{1}{\Gamma(Lm)} \left(\frac{m}{\overline{\gamma}}\right)^{Lm} \gamma^{Lm-1} e^{-\frac{m}{\overline{\gamma}}\gamma}, \ \gamma \geq 0. \tag{4.35}$$

Then, the unconditional MGF of the i-th sample of the combined signal, Y_i^p/N (with the abuse of notation), can be obtained by substituting (4.35) into (4.23) as

$$\begin{aligned} \overline{\mathcal{M}}^{\text{mrc}}_{Y_i^p/N|H_1}(s) = \frac{2}{p}\left(\frac{m}{\overline{\gamma}}\right)^{Lm} \sum_{v=0}^{\infty} \Bigg[\frac{(-1)^v}{v!} \Gamma\left(\frac{2(v+1)}{p}\right) \\ \times \left(\frac{N}{s}\right)^{\frac{2(v+1)}{p}} U\left(Lm, Lm-v, \frac{m}{\overline{\gamma}}\right) \Bigg], \end{aligned} \tag{4.36}$$

where the definition of the confluent hypergeometric function of second kind (4.25) is used to solve the resulting integral. The unconditional MGF of $T_p|H_1$ is then obtained as $\overline{\mathcal{M}}^{\text{mrc}}_{T_p|H_1}(s) = [\overline{\mathcal{M}}^{\text{mrc}}_{Y_i^p/N|H_1}(s)]^N$, which will be used to derive the corresponding average detection probability $\overline{P_d}_{,\text{mrc}}$ in Section 4.4.4.

4.4.3.4 SC

For an L-branch SC, the resulting SNR is given by $\gamma^{\text{sc}} = \max\{\gamma_1, \gamma_2..., \gamma_L\}$. Then, the PDF of output SNR for an SC receiver in i.i.d. Nakagami-m fading channels with integer m is given by [113]

$$f_{\text{sc}}(\gamma) = \frac{L}{\Gamma(m)} \sum_{l=0}^{L-1} \left[(-1)^l \binom{L-1}{l} e^{-\frac{(l+1)m}{\overline{\gamma}}\gamma} \sum_{\nu=0}^{l(m-1)} \mathcal{B}(\nu, l, m) \left(\frac{m}{\overline{\gamma}}\right)^{m+\nu} \gamma^{m+\nu-1} \right] \tag{4.37}$$

for $\gamma \geq 0$, where $\mathcal{B}(\nu, l, m)$ is defined as

$$\mathcal{B}(\nu, l, m) = \sum_{\imath=\nu-m+1}^{\nu} \frac{\mathcal{B}(\imath, l-1, m)}{(\nu-\imath)!} I_{[0,(l-1)(m-1)]}(\imath),$$

with $\mathcal{B}(0, 0, m) = \mathcal{B}(0, l, m) = 1$, $\mathcal{B}(\nu, 1, m) = 1/(\nu!)$, $\mathcal{B}(1, l, m) = l$, and

$$I_{[a,b]}(\imath) = \begin{cases} 1 & a \leq \imath \leq b, \\ 0 & \text{otherwise.} \end{cases}$$

By substituting (4.37) into (4.23) and then using (4.25) to solve the resulting integral, the unconditional MGF of Y_i^p/N can be expressed in the form

$$\begin{aligned} \overline{\mathcal{M}}^{\text{sc}}_{Y_i^p/N|H_1}(s) = \frac{2L}{p\Gamma(m)} \sum_{v=0}^{\infty} \Bigg[\frac{(-1)^v}{v!} \Gamma\left(\frac{2(v+1)}{p}\right) \\ \times \left(\frac{N}{s}\right)^{\frac{2(v+1)}{p}} \sum_{l=0}^{L-1} (-1)^l \binom{L-1}{l} \sum_{\nu=0}^{l(m-1)} \rho(m, \overline{\gamma}, l, v, \nu) \Bigg], \end{aligned} \tag{4.38}$$

where $\rho(m, \overline{\gamma}, l, v, \nu)$ is defined as

$$\rho(m, \overline{\gamma}, L, v, \nu) \triangleq \mathcal{B}(\nu, l, m) \left(\frac{m}{\overline{\gamma}}\right)^{m+\nu} \Gamma(m+\nu) U\left(m+\nu, m+\nu-v, \frac{(l+1)m}{\overline{\gamma}}\right).$$

Similar to MRC, the unconditional MGF of $T_p|H_1$ is then given by

$$\mathcal{M}^{\text{sc}}_{T_p|H_1}(s) = [\mathcal{M}^{\text{sc}}_{Y_i^p/N|H_1}(s)]^N,$$

which will be used to derive the corresponding average detection probability $\overline{P_{d,\text{sc}}}$ in Section 4.4.4.

4.4.4 Unified Expression for Average Detection Probability Over Fading and Diversity Cases

The derived unconditional MGFs of the decision variables for the respective cases can be expressed in a series-form similar to (4.11) after using [103, eq. (0.314)]. We denote this form by $\mathcal{M}^{\text{fd}}_{T_p|H_1}(s)$. Then, by applying the inverse Laplace transform on $\mathcal{M}^{\text{fd}}_{T_p|H_1}(s)/s$ as in Section 4.3.2, the average detection probability for each of the fading and diversity-combining cases, $\overline{P_d}_{,\text{fd}}$, can be expressed in a single compact form as

$$\overline{P_d}_{,\text{fd}} = 1 - \frac{2^N \xi_{\text{fd}}}{p^N} \sum_{v=0}^{\infty} \frac{C_{v,\text{fd}} \cdot (N\lambda)^{2(v+N)/p}}{\Gamma\left(\frac{2(v+N)}{p}\right)}, \tag{4.39}$$

with

$$C_{v,\text{fd}} = \frac{1}{v\,\Gamma(2/p) a_{0,\text{fd}}} \sum_{u=1}^{v} (uN - v + u) \frac{(-1)^u}{u!} \Gamma\left(\frac{2(u+1)}{p}\right) a_{u,\text{fd}} C_{v-u,\text{fd}}, \;\; u \geq 1,$$

and $C_{0,\text{fd}} = [\Gamma(2/p) a_{0,\text{fd}}]^N$. The coefficients $a_{u,\text{fd}}$ appearing in the expression of $C_{v,\text{fd}}$ are dependent on the respective fading and diversity-combining cases and are derived to be

$$\begin{aligned}
a_{u,\kappa\text{-}\mu} &= \sum_{j=0}^{\infty} \frac{\mu^{2j} \kappa^j (1+\kappa)^j}{\overline{\gamma}^j j!} U\left(\mu + j, \mu + j - u, \frac{\mu(1+\kappa)}{\overline{\gamma}}\right), \\
a_{u,\alpha\text{-}\mu} &= \sum_{q=1}^{N_Q} w_q g(t_q), \;\; a_{u,\text{mrc}} = U\left(Lm, Lm - u, \frac{m}{\overline{\gamma}}\right), \\
a_{u,\text{sc}} &= \sum_{l=0}^{L-1} (-1)^l \binom{L-1}{l} \sum_{\nu=0}^{l(m-1)} \rho(m, \overline{\gamma}, l, v, \nu),
\end{aligned} \tag{4.40}$$

with ξ_{fd} for the corresponding cases defined as

$$\begin{aligned}
\xi_{\kappa\text{-}\mu} &\triangleq \left(\frac{\mu(1+\kappa)}{e^{\kappa}\overline{\gamma}}\right)^{N\mu}, \quad \xi_{\alpha\text{-}\mu} \triangleq \left(\frac{1}{\Gamma(\mu)}\right)^N, \\
\xi_{\text{mrc}} &\triangleq \left(\frac{m}{\overline{\gamma}}\right)^{NLm}, \quad \xi_{\text{sc}} \triangleq \left(\frac{L}{\Gamma(m)}\right)^N.
\end{aligned} \tag{4.41}$$

For the pLC scheme, the average detection probability $\overline{P_d}_{,\text{plc}}$ is given by (4.39) with $a_{u,\text{plc}} = a_{u,\text{mrc}}|_{L=1}$, and the false alarm probability $P_{f,\text{plc}}$ is given by (4.12) (for $H = H_0$), with each N occurring in (4.39) and (4.12) replaced by NL except the one occurring as $N\lambda$ inside the

TABLE 4.3
NUMBER OF TERMS IN (4.39) FOR COMPUTING $\overline{P_{d,\kappa\text{-}\mu}}$ WITH 4-DECIMAL POINTS ACCURACY ($\lambda = 7$).

SNR (dB)	p	N	κ	μ	$V_{\kappa\text{-}\mu}$	J
-15	4.5	6	1.5	2.4	19	15
0	2.7	3	3.2	1.5	25	16
5	1.8	2	4	3.2	36	31
5	3.3	4	1.5	2.2	17	12

TABLE 4.4
NUMBER OF TERMS IN (4.39) FOR COMPUTING $\overline{P_{d,\alpha-\mu}}$ WITH 4-DECIMAL POINTS ACCURACY.

(SNR (dB), λ)	p	N	α	μ	$V_{\alpha\text{-}\mu}$	N_Q
$(-10, 7)$	4	3	1.5	2.5	18	21
$(-5, 5)$	3	3	1.5	1	23	10
$(3, 5)$	2.5	6	3	2	25	14
$(3, 5)$	1.8	6	2	3.3	74	5

summation. For the pLS scheme, the average detection probability $\overline{P_{d,\text{pls}}}$ in (4.34) requires only $\overline{P_{d,\text{Nak}}}$, which is given by (4.39) for MRC with $a_{u,\text{mrc}}|_{L=1}$ and $\xi_{\text{mrc}}|_{L=1}$.

4.4.5 Computation of $\overline{P_{d,\text{fd}}}$ in (4.39)

As is clear from (4.39) and (4.40), the final expressions for $\overline{P_{d,\text{plc}}}$ $\overline{P_{d,\text{pls}}}$, $\overline{P_{d,\text{mrc}}}$ and $\overline{P_{d,\text{sc}}}$ require the evaluation of only a single infinite series-sum similar to that for the AWGN case in (4.12). The series expression for these cases can then be truncated with a finite number of terms, and the truncation error can be upper bounded in a similar manner.

The expression of $\overline{P_{d,\kappa\text{-}\mu}}$ contains two infinite series-sums in v and j, which have to be truncated with a finite number of terms for computation. A tight truncation error upper bound for $\overline{P_{d,\kappa\text{-}\mu}}$ is difficult to obtain due to occurrence of infinite sums in both the numerator and denominator of the recursively computed coefficients $C_{v,\kappa\text{-}\mu}$. Nevertheless, our numerical experiments reveal that the sums are readily converging and can be truncated with a finite number of terms, which can be chosen to achieve the desired precision. For example, the number of terms in v and j (denoted by $V_{\kappa\text{-}\mu}$ and J respectively) for computing $\overline{P_{d,\kappa\text{-}\mu}}$ with 4-decimal points accuracy are shown in Table 4.3.

Similarly, the expression of $\overline{P_{d,\alpha\text{-}\mu}}$ requires the evaluation of an infinite series-sum in v and further includes the computation of the Gaussian-Laguerre quadrature sum. Accurate

computation of $\overline{P_{d,\alpha\text{-}\mu}}$ is possible by truncating the infinite series in v with $V_{\alpha\text{-}\mu}$ terms and simultaneously choosing a suitable number of terms N_Q in the quadrature sum to satisfy the overall precision requirement. Some examples with various sets of values for 4-decimal points accuracy are shown in Table 4.4.

4.5 Numerical results and discussions

In this section, the p-norm detector performance is characterized with several P_d vs. SNR curves, and the ROC curves, which are the plots of P_d against P_f. Since a low probability of false alarm is highly desirable (for example, in IEEE 802.22, a CR requires $P_f \leq 0.1$ [23]), we set $P_f = 0.01$ for all of the P_d vs. SNR plots. The detection threshold λ is determined based on this requirement and used for the computation of P_d. On the other hand, the ROC curves are obtained by varying the threshold from a low to a high value (theoretically, from 0 to ∞), and plotting the corresponding P_d against P_f. Thus, the ROC curves are important to jointly observe how P_d and P_f vary with the detector parameters (SNR, p, sample size, fading severity, and/or the number of antennas).

A numerical analysis to provide insights into the derived results is presented next. Results of Monte-Carlo simulation performed in MATLAB with 10^6 iterations are included wherever necessary for validating the analysis.

4.5.1 Performance in AWGN (Fig. 4.4)

In Fig. 4.4, the Talbot method (4.9), the series solution (4.12), the Laguerre approximation (4.18), the Gamma approximation [39] (see Appendix B.1), and the CLT-based approximation (see Appendix B.2) are compared. The results plotted for two different combinations of (p, N), namely $(p = 2, N = 2)$ and $(p = 4, N = 5)$, give the following insights:

(i) The Talbot solution (4.9) and the series-based solution (4.12) match exactly with the simulation results for both sets of (p, N), thus validating the accuracy (exactness) of these solutions.

(ii) For $p = 2$, the Gamma approximation is exact since the decision variable is then a Gamma-distributed sum of N independent exponential random variables. However, for another p ($p = 4$), the decision variable is no longer Gamma distributed, and

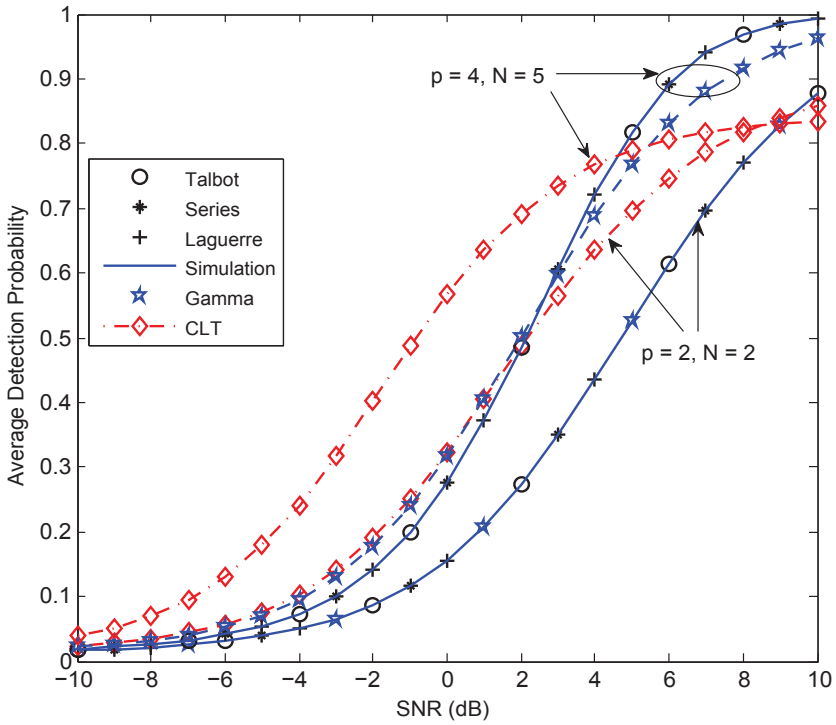

Fig. 4.4. Comparison of the derived Talbot solution (4.9), series solution (4.12) and the Laguerre approximation (4.18) against the existing Gamma (Appendix B.1) and CLT (Appendix B.2) approximations for AWGN.

the Gamma approximation deviates from the simulation. Interestingly, the proposed Laguerre approximation matches the simulation for both p values.

(iii) The Laguerre approximation has remarkably better accuracy than the CLT approximation.

Hence, from (ii)-(iii), we can say that the Laguerre approximation is more versatile than the Gamma approximation and is more accurate than the CLT approximation (for small sample size).

4.5.2 Effect of sample size N (Fig. 4.5)

The sample size N is a critical performance-determining parameter of the detector. Hence, the effect of N on the average detection probability over the Rayleigh fading channel (obtained from $\overline{P_{d,\kappa\text{-}\mu}}$ in (4.39) with $\kappa \to 0$, $\mu = 1$) is studied in Fig. 4.5 for a 3.5-norm detector. The CLT approximation is plotted for comparison. The results reveal the following.

(i) The reliability of spectrum sensing improves drastically with the number of received

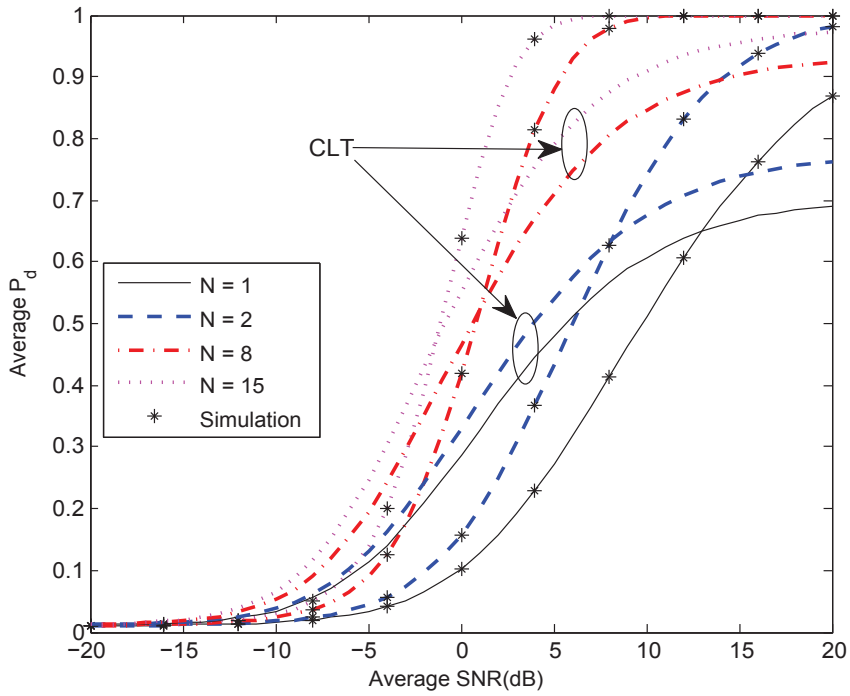

Fig. 4.5. Average detection probability ($\overline{P_d}$) vs. average SNR ($\overline{\gamma}$) for 3.5-norm detector in Rayleigh fading (using (4.39) with $\kappa \to 0$, $\mu = 1$) for various samples, compared to the CLT approximation and simulation.

signal samples as compared to the reliability of the detector with one sample ($N = 1$) considered in [90] and [91]. For example, at SNR of 10 dB, the 2-samples-based detector ($N = 2$) yields about 45% higher detection probability than the one-sample detector. Furthermore, even at a low SNR of -10 dB, the 15-samples-based detector obtains about an 86% gain in detection probability compared to the single sample-based detector.

(ii) The CLT approximation[12] deviates significantly, although its accuracy improves with an increase in sample size.

4.5.3 Analysis in κ-μ fading (Fig. 4.6 and Fig. 4.7)

The effect of p on the detection probability $\overline{P_{d,\kappa\text{-}\mu}}$ in (4.39) for a fixed LOS ($\kappa = 1.5$) and fixed multipath ($\mu = 2.2$) condition is illustrated in Fig. 4.6. The following observations are made:

[12]Obtained by numerically integrating $P_{d,\text{CLT}}$ (see Appendix B.2) over the Rayleigh fading PDF $f(\gamma) = 1/\overline{\gamma} \cdot \exp(-\gamma/\overline{\gamma})$, $\gamma \geq 0$.

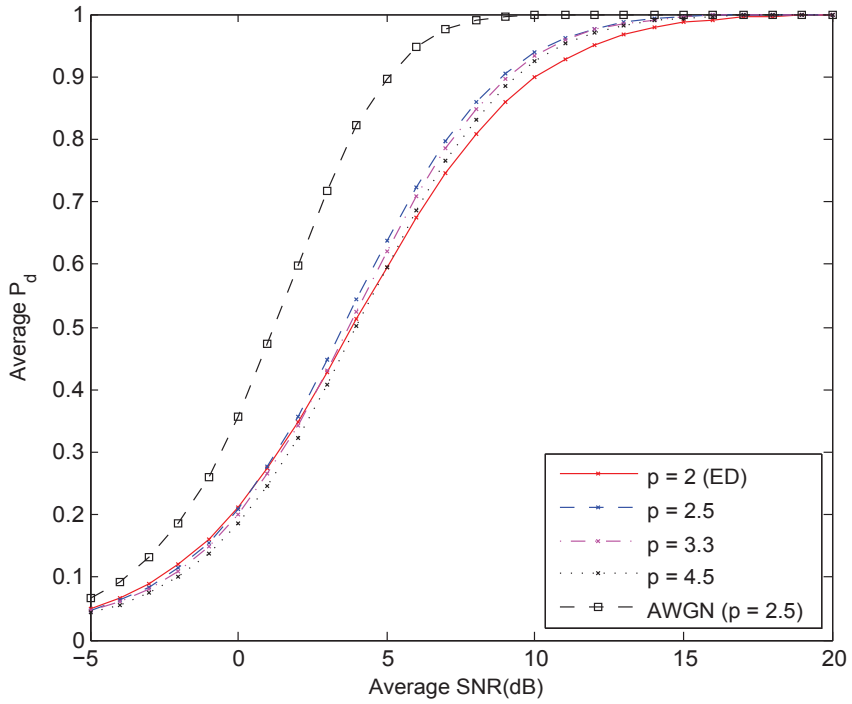

Fig. 4.6. Average detection probability ($\overline{P_{d,\kappa\text{-}\mu}}$) vs. average SNR ($\overline{\gamma}$) in a $\kappa = 1.5$, $\mu = 2.2$ fading channel for various p with $N = 6$. The AWGN plot is included for comparison. Discrete marks indicate simulation values.

(i) The ED ($p = 2$) does not necessarily yield the best sensing performance in κ-μ fading channels compared to other detectors with $p \neq 2$. For example, at SNR of 7 dB with $N = 6$, the 2.5-norm detector achieves 7% higher $\overline{P_{d,\kappa\text{-}\mu}}$ than that of the ED. The 3.3-norm detector is the second-best one, when the SNR exceeds 2 dB. Even the 4.5-norm detector possesses a higher $\overline{P_{d,\kappa\text{-}\mu}}$ than that of the ED for a received SNR above 6 dB. Thus, the ED is not necessarily the best choice among all p in non-homogeneous LOS propagation.

(ii) The comparison with the AWGN (no fading) reveals that multipath fading severely affects the p-norm detection performance. For example, at an SNR of 2 dB, the detection probability reduces by as much as 40% compared to the corresponding case without fading for a 2.5-norm detector.

In Fig. 4.7, the ROC curves (plotted in log-log scale for clarity) of a 3-norm detector with $N = 3$ for several LOS and multipath conditions are shown. For a fixed multipath effect (fixed μ), the detector performs better at stronger LOS (higher κ) conditions. Likewise, the performance improves with the increased multipath effect (higher μ) for a given LOS

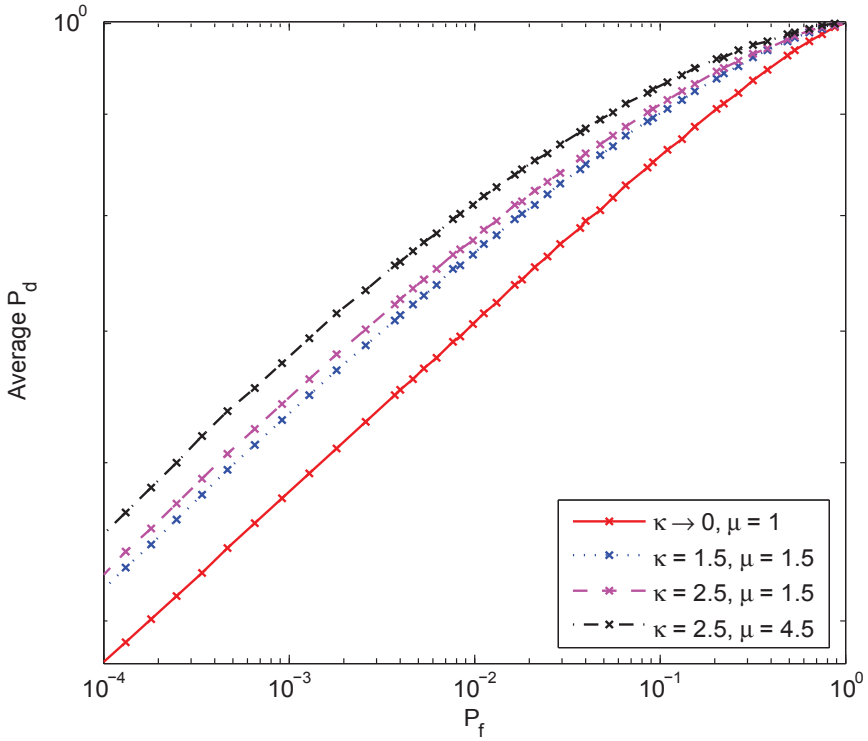

Fig. 4.7. ROC curves (in log-log scale) for a 3-norm detector with $N = 3$ for various κ-μ channels at SNR of 7 dB. The discrete marks indicate the simulation results.

strength (fixed κ). These results indicate the advantages of propagation environments having a stronger LOS and a higher number of multipath components on the sensing performance.

4.5.4 Analysis in α-μ fading (Fig. 4.8)

The effect of non-linear propagation on the p-norm detection performance ($p = 2.7$) is presented in Fig. 4.8 for various instances of the α-μ fading channel. Additionally, an ED ($p = 2$) plot and the simulation results are included for comparison. The following observations are made:

(i) The analytical results for $\overline{P_{d,\alpha\text{-}\mu}}$ in (4.39) and the simulation results match, thus validating the accuracy of the Gaussian-Laguerre quadrature integration used for deriving $\overline{P_{d,\alpha\text{-}\mu}}$.

(ii) The increased non-linearity of the propagation medium (higher α) for a fixed multipath effect (fixed μ) has a positive effect on the sensing performance. As well, the performance is better for a larger multipath effect (higher μ) at a given non-linearity

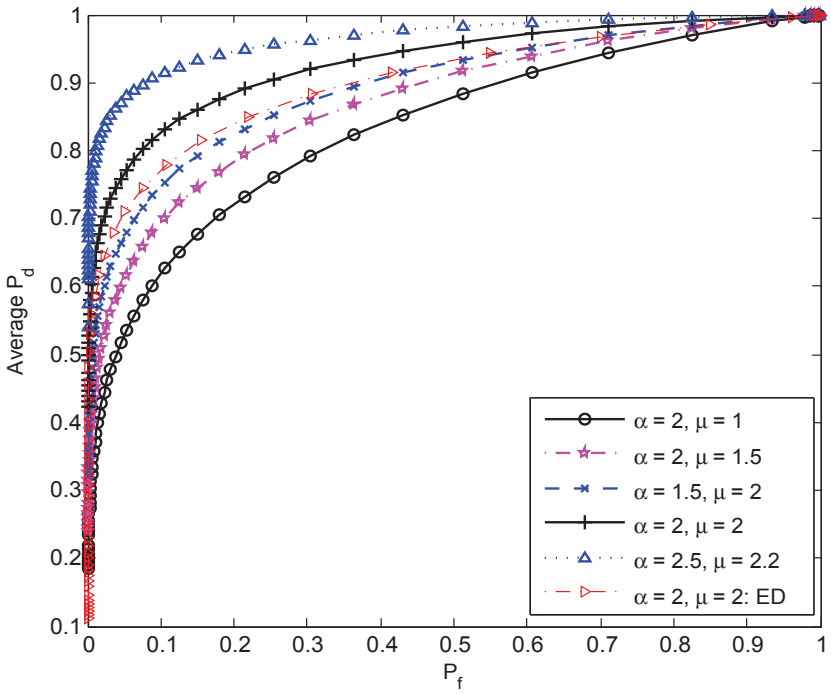

Fig. 4.8. ROC curves of a 2.7-norm detector for various α-μ channels at SNR $= 3$ dB, $N = 5$. The ED ($p = 2$) plot is included for comparison. The discrete marks on the graphs indicate the simulation results.

(fixed α). For example, at $P_f \approx 0.1$, when α increases from 1.5 to 2 at $\mu = 2$, an approximately 11% gain in $\overline{P_{d,\alpha\text{-}\mu}}$ is obtained. Likewise, about a 20% increase in $\overline{P_{d,\alpha\text{-}\mu}}$ results when μ increases from 1 to 1.5 at $\alpha = 2$.

(iii) The results also suggest that ED ($p = 2$) is not necessarily the best choice (among all p) for detecting signals affected by the non-linearity of the wireless channel. For example, at $P_f \approx 0.1$, over a channel with $\alpha = 2$ and $\mu = 2$, the 2.7-norm detector yields about a 7.5% higher $\overline{P_{d,\alpha\text{-}\mu}}$ than the ED.

4.5.5 Analysis with diversity-combining (Fig. 4.9)

The boost in p-norm detection performance due to antenna diversity is depicted in Fig. 4.9. Furthermore, to assess the relative performance gains of the pLC, pLS, MRC and SC schemes, they are compared against each other and with the no-diversity (single-antenna) case as well. The following insights are evident:

(i) Antenna diversity boosts the p-norm detection performance: Even at a low SNR of -10 dB with $P_f \approx 0.1$, the 2.5-norm detector deploying a 3-branch MRC yields

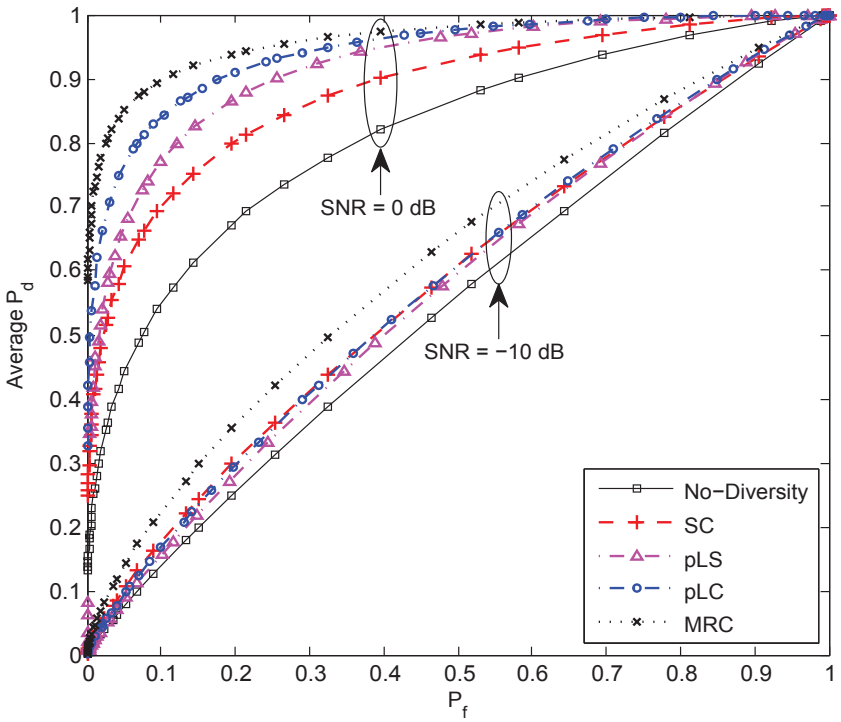

Fig. 4.9. Two sets of ROC curves at SNR -10 dB ($p = 2.5$, $N = 3$) and 0 dB ($p = 3$, $N = 4$) for various diversity-combining schemes in Nakagami-3 fading channels with $L = 3$. No-diversity curves are included for comparison. The discrete marks on the graphs indicate the simulation results.

about a 53% increase in detection probability compared to the no-diversity case.

(ii) Performance of pLC, pLS, MRC and SC: As expected, MRC has the best performance among all the schemes. Interestingly, the proposed pLC and pLS schemes perform quite similarly to the traditional SC at low SNR (plots at -10 dB), while both of them outperform SC at a relatively high SNR (plots at 0 dB). For instance, at an SNR of 0 dB for $P_f \approx 0.1$, the 3-norm detector ($N = 4$) with SC, pLS, pLC and MRC schemes yields, respectively, about 28%, 40%, 54% and 66% increase in detection probability compared to the no-diversity case. Note that the pLC performs closer (than pLS and SC) to the optimal MRC. As a final note, the MRC relies on the availability of full CSI for each branch while the SC requires constant monitoring of all the branches in order to find the branch with the maximum SNR [24]. However, these requirements lead to higher complexity and cost for practical implementation. Thus, the proposed pLC and pLS schemes may offer better alternatives than the MRC and SC schemes, particularly, for a non-coherent device like the p-norm detector.

4.6 Conclusion

In this chapter, a comprehensive p-norm detector performance analysis for non-fading (AWGN), generalized fading and with several antenna diversity-combining schemes is presented by developing several analytical/numerical solutions for P_d and P_f. To evaluate P_d and P_f for AWGN channels, the MGF of the decision variable is derived in two forms: (i) closed-form for even-integer p, and (ii) series-form for arbitrary p. A numerical method utilizing the Talbot inversion is developed for case (i), and infinite series expansion with convergence acceleration based on the ϵ-algorithm is derived for case (ii). Additionally, a new approximation based on the Laguerre polynomial series is shown to be more versatile compared to the existing Gamma approximation and more accurate than the CLT approximation. To quantify the impact of the fading channels, the series MGF-based analysis is extended to cover the κ-μ and α-μ fading channels, thus helping to quantify the sensing performance in more realistic fading environments. To capitalize on antenna diversity, non-coherent pLC and pLS schemes which do not require any CSI are proposed. Their performances along with those of the traditional MRC and SC schemes are derived for Nakagami-m fading. Interestingly, both pLC and pLS perform similar to the SC at low SNR, while outperforming it at relatively high SNR. Further, pLC performs the closest (among all the schemes) to the optimal MRC at higher SNR. Moreover, the proposed pLC and pLS schemes are more suitable than the MRC and SC schemes for the p-norm detector, which can function without any CSI.

Chapter 5

Approximations for Performance of Energy Detector and p-norm Detector

Although the CLT approximations for the detection probability of the ED and the p-norm detector are accurate for large sample sizes, their accuracy is poor otherwise. A recent work has addressed this problem by developing the CGA. However, CGA is not the only option and thus this chapter introduces five other classical approximations for P_d. They tightly match the exact values even for few samples and thus are more accurate than CLT. These approximations have been unnoticed in the spectrum sensing research community and this chapter [1] aims at making them known to a wider audience. Because the range of their potential applications could be diverse, to demonstrate their utility, we derive a novel AUC expression for the p-norm detector. Finally, the derived AUC is subsequently extended to characterize the effect of noise variance uncertainty on the p-norm detection performance.

5.1 Introduction and Motivation

Spectrum sensing must focus on yielding quick decisions on the presence or absence of the spectrum opportunities. As ED and the p-norm detector can operate blindly, they are capable of quickly sensing the spectrum. Thus, these detectors must operate with as few

[1] Chapter 5 has been published in the *IEEE Communications Letters* as [114].

number of samples as possible, and at the same time, ensure high sensing reliability.

As the IEEE 802.22 based CRs must detect potential spectrum opportunities rapidly, the ED and the p-norm detector must operate with fewest possible samples while offering high detection reliability. However, their probability of detection, P_d, is widely approximated by using the CLT [27] which yields P_d in terms of the well-known Gaussian-Q function. The CLT-based approximation has found widespread applications in solving practical problems such as sensing-throughput tradeoff [47], multiple-band spectrum sensing [48], low SNR spectrum sensing [115], [40], and numerous others. However, it is not accurate enough for small sample sizes [116]. Small sample size based analysis is particularly important, say, for highly delay-sensitive applications such as mission critical MTC in future 5G networks [2].

Exact P_d (without approximations) has also been analyzed extensively. For example, works in [30], [35], [36], [117], [118] treat ED with fading, shadowing, multiple antennas, cooperative diversity, and other factors. For the p-norm detector, since exact closed-form P_d and P_f are intractable, several computational methods were developed in Chapter 4. However, such exact analyses often lead to complicated expressions (residues, infinite series, and so on) rather than closed-forms, which may hinder their rapid use in optimization and low-SNR design [40], [47], [48], [115].

Thus, simple and accurate P_d approximations valid for arbitrary sample size are necessary. To the best of our knowledge, only the work in [116] has attacked this problem with the CGA, originally proposed by Abdel-Aty [119] for approximating non-central chi-square distributions. However, the CGA is not the only option, and other more robust approximations may exist. Thus, in this chapter, we investigate five other classical approximations to derive P_d. These approximations

(i) yield accurate P_d in closed form;

(ii) apply to an arbitrary number of samples;

(iii) need only the first few moments/cumulants, and thus are applicable to deterministic or random signal model; and

(iv) may be extended to other applications, say, the p-norm detector for which we will derive an approximate, compact expression for the AUC.

A brief review of the problem is given in Section 5.2. The proposed approximations are described in Section 5.3. Some important insights are discussed in Section 5.5. The AUC performance of p-norm detector is treated in Section 5.6. The chapter is concluded with Section 5.6.

5.2 Problem Statement

For the unknown deterministic signal based ED, recall the detection probability

$$P_d = Q_N(\sqrt{2\gamma}, \sqrt{\lambda}). \tag{5.1}$$

The conditional decision variables $T|H_0$ and $T|H_1$ are distributed as χ^2_{2N} and $\chi^2_{2N}(2\gamma)$, respectively. Thus, the problem at hand is to find accurate approximations to (5.1) for arbitrary sample size, unlike CLT, which is limited to ($N \gg 1$).

5.3 New Approximations

As expression (5.1) results from the CCDF of $T|H_1$ which is $\chi^2_{2N}(2\gamma)$ distributed, we seek accurate approximations for this CCDF by approximating the distribution of $T|H_1$. Let Y denote $T|H_1$. Among the numerous approximations available in the statistical literature, we next consider five important ones to find accurate approximations to the distribution of Y [120]–[124]. Note that for some of our derivations, the cumulant generating function of Y is needed which is obtained as [125] $g(t) = \ln \mathbb{E}\left(e^{tY}\right) = \frac{t}{1-2\gamma t} - N\ln(1-2\gamma t), \quad t \leq \frac{1}{2\gamma}$. Then, the Taylor expansion of $g(t)$ yields the first three cumulants of Y to be $\kappa_1 = 2(N+\gamma)$, $\kappa_2 = 4(N+2\gamma)$, $\kappa_3 = 16(N+3\gamma)$. On the other hand, for some of the approximations, the method of moments is utilized and thus the moments of Y are needed. To this end, the r-th moment of Y can be shown to be $m_r = 2^r e^{-\gamma}\Gamma(r+N)_1\tilde{F}_1(r+N; N; \gamma)$. Next, we present the five approximations for deriving P_d.

5.3.1 Patnaik's approximation

The first approximation that we present is the Patnaik's approximation which essentially relies on the method of moments for approximating the non-central chi-square distribution by a scaled central chi-square distribution with its degrees of freedom and the scaling factor determined by moment matching such that they depend upon the non-centrality parameter

and the degrees of freedom of the non-central chi-square distribution. In particular, Patnaik [120] proposed approximating the non-central chi-square random variable Y by a scaled central one denoted $Z_1 \sim \chi^2_v$, as

$$Y \approx \rho Z_1. \tag{5.2}$$

The problem then is to find the scaling factor ρ and the new degree of freedom v. By matching the first two moments of both sides of (5.2), these parameters are found to be

$$\rho = \frac{2(N+2\gamma)}{N+\gamma}, \quad v = \frac{2(N+\gamma)^2}{N+2\gamma}.$$

Then, the approximate detection probability, denoted P_d^{pn}, can be expressed as

$$P_d^{\text{pn}} = \mathbb{P}(\rho Z_1 > \lambda) = \int_{\lambda/\rho}^{\infty} f_{Z_1}(z)dz = \frac{1}{\Gamma(v/2)}\Gamma\left(\frac{v}{2}, \frac{\lambda}{2\rho}\right). \tag{5.3}$$

Clearly, P_d^{pn} is in terms of the upper-incomplete Gamma function (as opposed to the more complicated generalized Marcum-Q function (5.1)) and thus may further lead to tractable analysis (e.g., when averaging P_d over fading, shadowing, antenna/cooperative diversity, or in other applications such as sensing-throughput tradeoff) for arbitrary sample size unlike the CLT which is valid only for large sample sizes. The accuracy of (5.3) will be investigated in Section 5.4.

5.3.2 Pearson's approximation

Another approximation based on the method of moments is the Pearson's approximation which is similar to Patnaik's approximation with an additional parameter introduced for a possibly attaining a better accuracy than Patnaik's approximation. In particular, Pearson's method is a generalization of Patnaik's idea where Y is approximated with a linear transformation of a central chi-square random variable denoted $\mathcal{X} \sim \chi^2_{v'}$, as

$$Y \approx Z_2 = a\mathcal{X} + b,$$

where a, b and v' are to be determined via moment matching. By matching the first two moments on both sides, we get [121]

$$Z_2 = \frac{\mathcal{X} - v'}{\sqrt{2v'}}\text{Var}(Y) + \mathbb{E}(Y) = \frac{N+3\gamma}{N+2\gamma}\mathcal{X} - \frac{2\gamma^2}{N+3\gamma}. \tag{5.4}$$

Parameter v' is obtained by matching the third moments of Z_2 (5.4) and Y as

$$v' = \frac{2(N+2\gamma)^3}{(N+3\gamma)^2}.$$

Then, the approximate detection probability, $P_d^{\text{ps}} = \mathbb{P}(a\mathcal{X} + b > \lambda)$, is obtained as

$$P_d^{\text{ps}} = \frac{1}{\Gamma(v'/2)}\Gamma\left(\frac{v'}{2}, \left(\lambda + \frac{2\gamma^2}{N+3\gamma}\right) \cdot \frac{N+2\gamma}{2(N+3\gamma)}\right). \tag{5.5}$$

Despite matching the first three moments, the final P_d^{ps} expression has a form similar to P_d^{pn} (5.3) and thus has the same computational ease. Intuitively, we expect (5.5) to be highly accurate as it utilizes the first three exact moments.

5.3.3 Three-parameter Gamma

In this subsection, we present another approximation by using cumulants. The underlying principle is to approximate the non-central chi-square distribution by a three-parameter Gamma distribution, which is one of the classical distributions arising in the problems involving heavy-tailed distributions [126]. The three-parameter Gamma distribution has been known to have shapes similar to Weibull, Log-normal and Inverse Gaussian distribution thus suggesting that it is well-suited for approximating diverse class of (non-Gaussian) distributions.

To this end, we utilize the three-parameter Gamma PDF to approximate the PDF of Y as [122]

$$f_Y(y) = \frac{(y-\delta)^{\alpha-1}e^{-(y-\delta)/\beta}}{\beta^\alpha \Gamma(\alpha)}, \tag{5.6}$$

where $\delta < y < \infty$, $\alpha = 4\kappa_2^3/\kappa_3^2$, $\beta = \kappa_3/(2\kappa_2)$ and $\delta = \kappa_1 - 2\kappa_2^2/\kappa_3$. Thus, the parameters α, β and δ in (5.6) are readily obtained from the cumulants of Y. The approximate detection probability, P_d^{tg}, can hence be expressed as

$$P_d^{\text{tg}} = \int_\lambda^\infty f_Y(y)dy = \frac{1}{\Gamma(\alpha)}\Gamma\left(\alpha, \frac{\lambda-\delta}{\beta}\right). \tag{5.7}$$

Since both (5.7) and (5.5) utilize third-order statistics, their accuracy is expected to be similar.

So far, we have presented all the approximations based on moment/cumulant matching. In contrast, the next two approximations are based upon finding a rapid transformation of

Y that approaches a Gaussian random variable. The basis is as follows. If we denote Y as $Y(N)$ (a function of N), then we know $Y(N)$ converges to a Gaussian random variable when $N \to \infty$. However, this condition requires a large number of samples. Alternatively, if a transform $\mathcal{F}(\cdot)$ can be found which makes $\mathcal{F}(Y)$ Gaussian without the large-sample assumption, that forms the basis for approximating the non-central chi-square tail probability. Transforms of type $\mathcal{F}(x) = (ax+b)^{\beta}$ have been used in the literature with its variations as discussed next.

5.3.4 Sankaran's third approximation

Following the principle of transformation of the non-central chi-square random variable to Gaussian as stated above, Sankaran proposed the transformation of the form $\mathcal{F}(Y) = (aY)^{\beta}$ with β chosen such that the coefficient in the expansion of the third cumulants of $\mathcal{F}(Y)$ vanishes [123]. Inherently, the underlying concept of this approximation is based on the Mann-Wald theorem which states that any continuous function of Y tends to a normal distribution as $\kappa_1 \to \infty$ [124].

To this end, Sankaran proposed the following transformation of Y

$$X = \left(\frac{Y}{\kappa_1}\right)^h = \left(\frac{Y}{2(N+\gamma)}\right)^h,$$

to be Gaussian with mean

$$\mu_{\text{sk}} = 1 + \frac{h(h-1)(N+2\gamma)}{2(N+\gamma)^2} - \frac{h(h-1)(2-h)(1-3h)(N+2\gamma)^2}{8(N+\gamma)^4},$$

and variance

$$\sigma^2_{\text{sk}} = \frac{h^2(N+2\gamma)}{(N+\gamma)^2}\left[1 - (1-h)(1-3h)\frac{(N+2\gamma)}{2(N+\gamma)^2}\right],$$

where

$$h = 1 - \frac{2(N+\gamma)(N+3\gamma)}{3(N+2\gamma)^2}.$$

As X is Gaussian distributed, the desired approximate detection probability, P_d^{sk}, can thus be obtained in terms of the Gaussian-Q function after some algebraic manipulations to be

$$P_d^{\text{sk}} = \mathbb{P}(Y > \lambda) = Q\left(\frac{\lambda^h - \mu_{\text{sk}} 2^h (N+\gamma)^h}{\sigma_{\text{sk}} 2^h (N+\gamma)^h}\right). \tag{5.8}$$

Similar to the CLT approximation, expression (5.8) avoids occurrence of the generalized Marcum-Q function (in P_d), yet does not invoke the large-sample assumption needed for the CLT. Thus, expression (5.8) should work for any number of samples (low to high).

5.3.5 Moschopoulos' approximation

Another approximation utilizing the transformation of the non-central chi-square random variable to a Gaussian random variable is the Moschopoulos' approximation. This approach builds upon the same principle of Mann Wald's theorem and improves the normal approximation compared to that obtained using Sankaran by exploiting the following more generalized transformation of Y (abusing the notation X)

$$X = \left(\frac{Y+b}{\kappa_1}\right)^h,$$

where h (abusing previous notations) and b are determined from the first three cumulants of Y as $h = 1 - \kappa_1\kappa_3/(3\kappa_2^2)$ and $b = \kappa_2/(2\kappa_1) - \kappa_3/(4\kappa_2)$. Then, X is Gaussian distributed with mean

$$\mu_{\text{mo}} = 1 + \frac{h}{\kappa_1}\left(\frac{(h-1)\kappa_2}{2\kappa_1} + b\right),$$

and variance

$$\sigma^2_{\text{mo}} = h^2\frac{\kappa_2}{\kappa_1^2}.$$

Then, similar to (5.8), the desired approximate detection probability, P_d^{mo}, is given by

$$P_d^{\text{mo}} = \mathbb{P}(Y > \lambda) = Q\left(\frac{(\lambda+b)^h - \kappa_1^h\mu_{\text{mo}}}{\kappa_1^h\sigma_{\text{mo}}}\right). \tag{5.9}$$

Since the detection probabilities (5.8) and (5.9) both utilize up to third-order statistics of Y and have the same functional complexity, these approximations may possess similar accuracy.

5.4 Numerical Results and Discussions

Section 5.3 presented five approximations for detection probability. Before moving into the comparisons, it is important to note that for the CGA, the approximate detection probability,

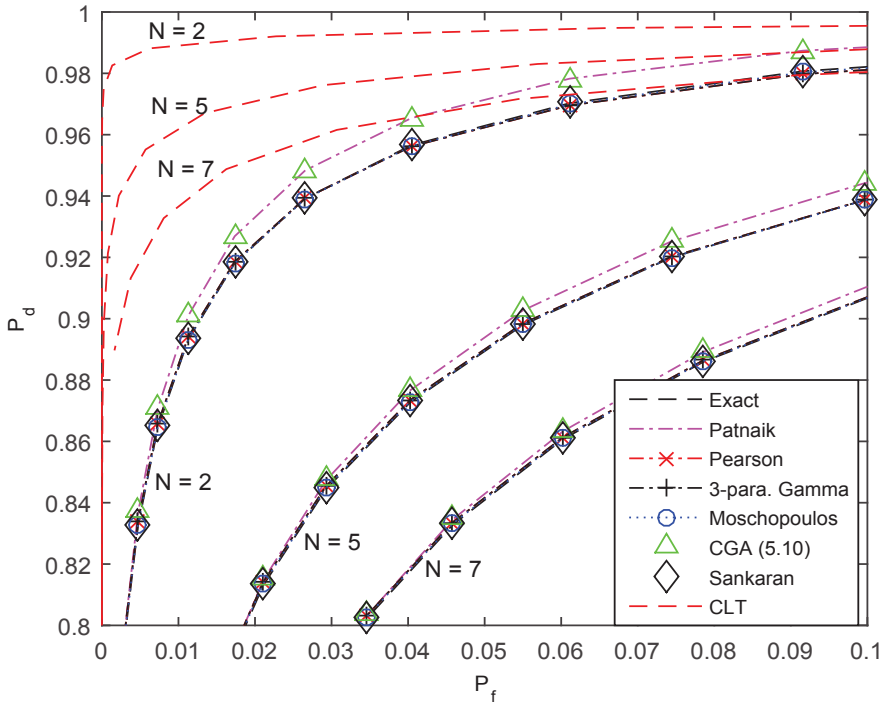

Fig. 5.1. ROC curves for various sample sizes for $P_f \leq 0.1$, $\gamma = 10\,\text{dB}$.

P_d^{cga}, can be derived following the transformation of Y to Gaussian as given in [119] to be

$$P_d^{\text{cga}} = Q\left(\left[\left(\frac{\lambda}{2(N+\gamma)}\right)^{1/3} + \frac{N+2\gamma}{9(N+\gamma)^2} - 1\right]\sqrt{\frac{9(N+\gamma)^2}{N+2\gamma}}\right). \tag{5.10}$$

Fig. 5.1 compares the ROC curves for the six approximations (along with the CLT approximation) and the exact P_d (5.1). Note that we restrict $P_f \leq 0.1$ (for example, as per the specifications in IEEE 802.22 [27]). While the CLT is the least accurate, P_d^{cga} (5.10) and P_d^{pn} (Patnaik) almost match the exact values and become more accurate with increasing N. The other proposed approximations tightly match the exact values.

Fig. 5.2 shows the AEs of the six approximations and of the approximation method in [116] which uses CGA for both P_d and P_f. Here, AE is given as $|P_d^{\text{ex}} - P_d^{\text{app}}|$, where P_d^{ex} is the exact (5.1) and P_d^{app} is the approximate. Clearly, for $4 \leq \gamma\,\text{dB} \leq 14$, all except the Patnaik and the two CGA approximations have AE $\leq 10^{-3}$. The average (over all SNRs) AEs of the Pearson's and the three-parameter Gamma are the lowest. Note that the CGA [116] has lower AE than CGA (5.10) for $\gamma < -1\,\text{dB}$. Another interesting observation is that for low SNRs ($\gamma \leq -5\,\text{dB}$), the Patnaik approximation outperforms Sankaran's,

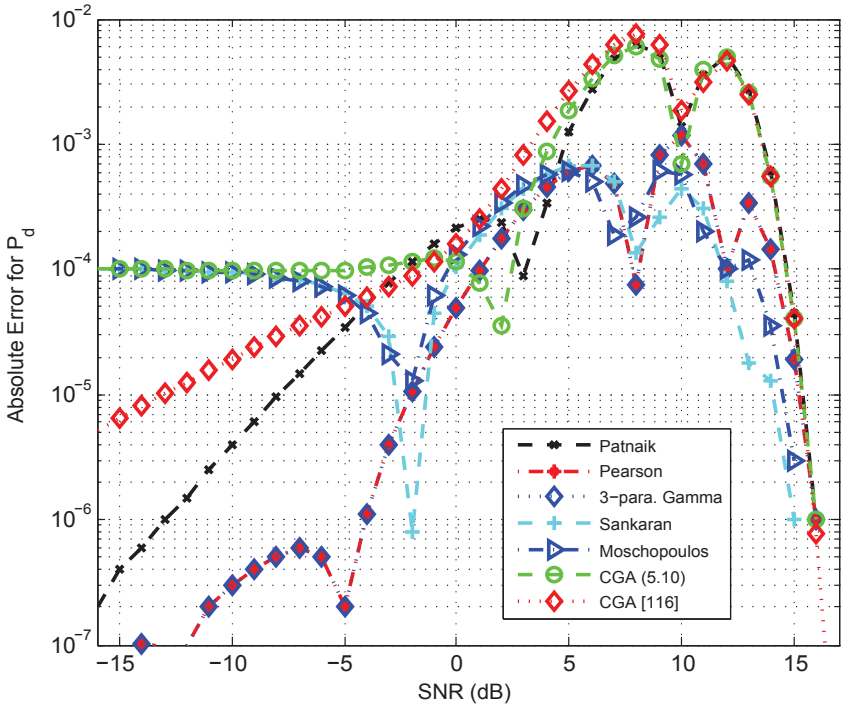

Fig. 5.2. Absolute error for P_d vs. γ for $P_f = 0.01$, $N = 5$.

Moschopoulos' and the CGA approximations.

5.5 AUC of the p-norm Detector

Recall the p-norm detector decision variable as $T_p = 1/N \sum_{i=1}^{N} |y_i|^p$. Clearly, the general form of T_p makes the exact closed-form performance analysis of the p-norm detector intractable. To demonstrate the applicability of one of the approximations, we thus consider the p-norm detector in this section and derive its approximate AUC performance, its exact AUC being analytically intractable.

Section 5.4 shows that P_d^{pn} is highly accurate at low SNRs (with AE $< 3 \times 10^{-6}$ at SNRs below -15 dB). For instance, IEEE 802.22 requires spectrum sensing at SNRs as low as -22 dB [27]. We thus adopt P_d^{pn} to derive the AUC of the p-norm detector. Similar to [39], [40], we consider a random PU signal model [27], [47], [115]. In this model, the PU signal samples and the AWGN samples are assumed to be $s_i \sim \mathcal{CN}(0, \sigma_s^2)$ and $n_i \sim \mathcal{CN}(0, \sigma_w^2)$, respectively, $\forall i \in \{1, 2, ..., N\}$. Recall that the exact distribution of T_p is intractable as $p > 0$ is an arbitrary real number. In contrast, the Patnaik's approximation

for $T_p|H_1$ and $T_p|H_0$ yields (see Appendix C.1)

$$P_d = \frac{1}{\Gamma(\theta/2)}\Gamma\left(\frac{\theta}{2}, \frac{\lambda}{2\psi_1}\right), \quad P_f = \frac{1}{\Gamma(\theta/2)}\Gamma\left(\frac{\theta}{2}, \frac{\lambda}{2\psi_0}\right), \tag{5.11}$$

with the parameters expressed as

$$\theta = \frac{2N\Gamma^2(p/2+1)}{\Gamma(p+1)-\Gamma^2(p/2+1)}, \ \psi_j = \frac{\Gamma(p+1)-\Gamma^2(p/2+1)}{2N\Gamma(p/2+1)A_j^{p/2}},$$

for $j = 0, 1$, with $A_0 \triangleq 1$, $A_1 \triangleq 1/(1+\gamma)$, and $\gamma \triangleq \sigma_s^2/\sigma_w^2$. Then, by substituting (5.11) into the definition of the AUC [27] AUC $= -\int_0^\infty P_d(\gamma, \lambda)\frac{\partial P_f}{\partial \lambda}d\lambda$, and then using [103, eq. (6.455.1)] to solve the integral, the AUC can be expressed as

$$\text{AUC} = \frac{2\Gamma(\theta)(1+\gamma)^{p\theta/4}{}_2F_1\left(1, \theta; \frac{\theta}{2}+1; \frac{(1+\gamma)^{p/2}}{(1+\gamma)^{p/2}+1}\right)}{\theta\Gamma^2(\theta/2)(1+(1+\gamma)^{p/2})^\theta}. \tag{5.12}$$

This new expression (5.12) helps to study the dependence of AUC on SNR, N and p as depicted in Fig. 5.3 and Fig. 5.4.

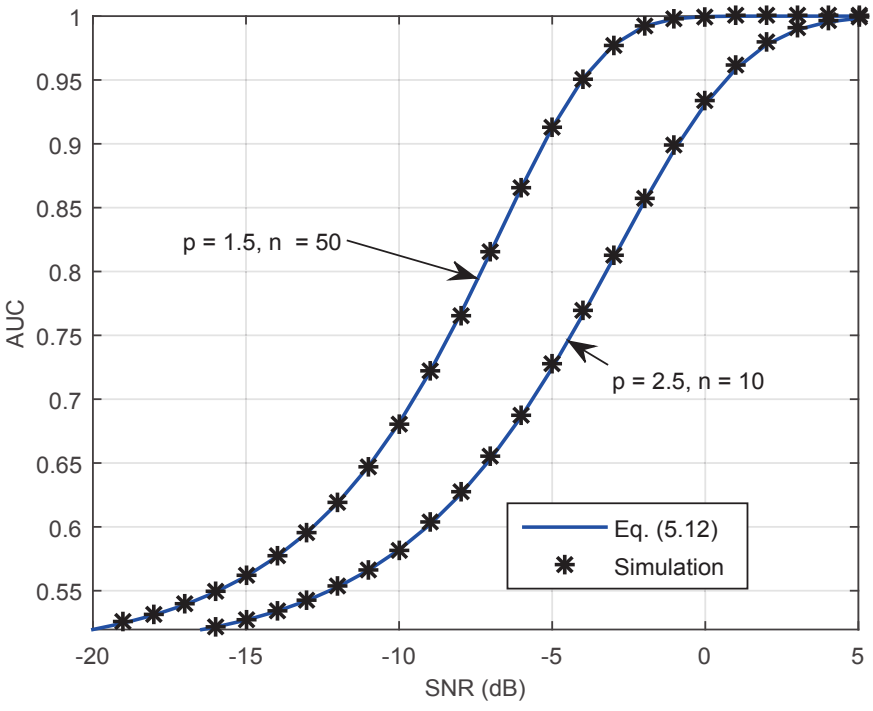

Fig. 5.3. AUC vs. SNR for different p and N.

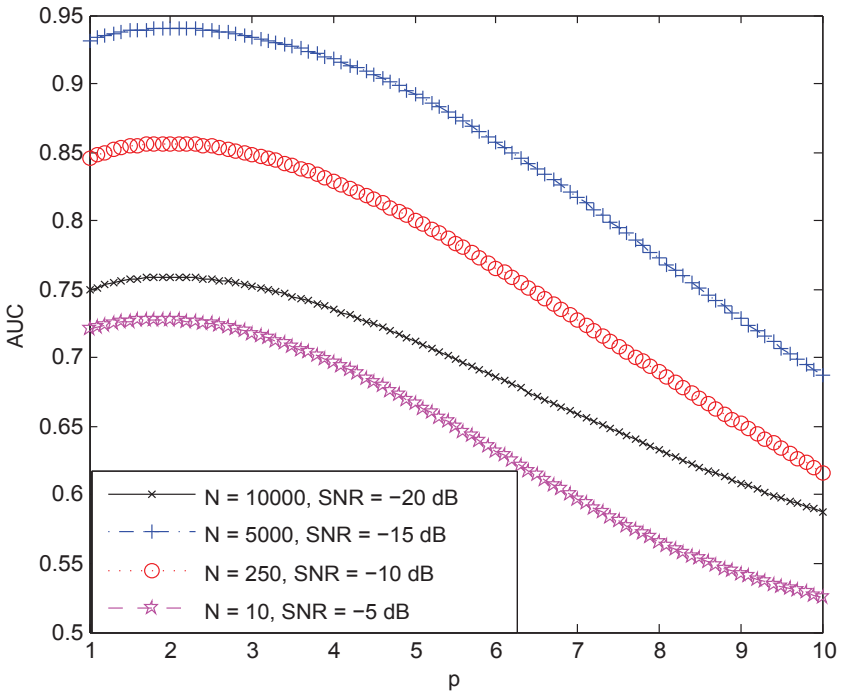

Fig. 5.4. AUC vs. p for different sample sizes and SNRs

In Fig. 5.3, (5.12) is compared against the simulation results for $p = 1.5$ and $p = 2.5$. The close match between (5.12) and the simulation results is evident, thus validating its accuracy.

The dependence of AUC on p is depicted in Fig. 5.4 for a wide range of parameter values: SNRs as low as -20 dB and N in the orders of 10^1 to 10^4. Clearly, it can be seen that a 15 dB drop in SNR (from -5 dB to -20 dB) requires N to be increased by 3 orders of magnitude (10^1 to 10^4) to maintain a similar performance. Thus, (5.12) accurately facilitates the p-norm AUC performance analysis for any SNR and any N.

5.5.1 Effect of noise variance uncertainty on AUC

In the previous analyses, we implicitly assumed a perfect knowledge of the noise variance. However, the background noise in communication systems often comprises of thermal noise, leaked signals from adjacent bands, aliasing due to imperfect filters, interfering transmissions from other users in the vicinity, noise variance estimation errors, and others [20], [127]. This causes the actual noise power (denoted by σ_a^2) to be different from the nominal

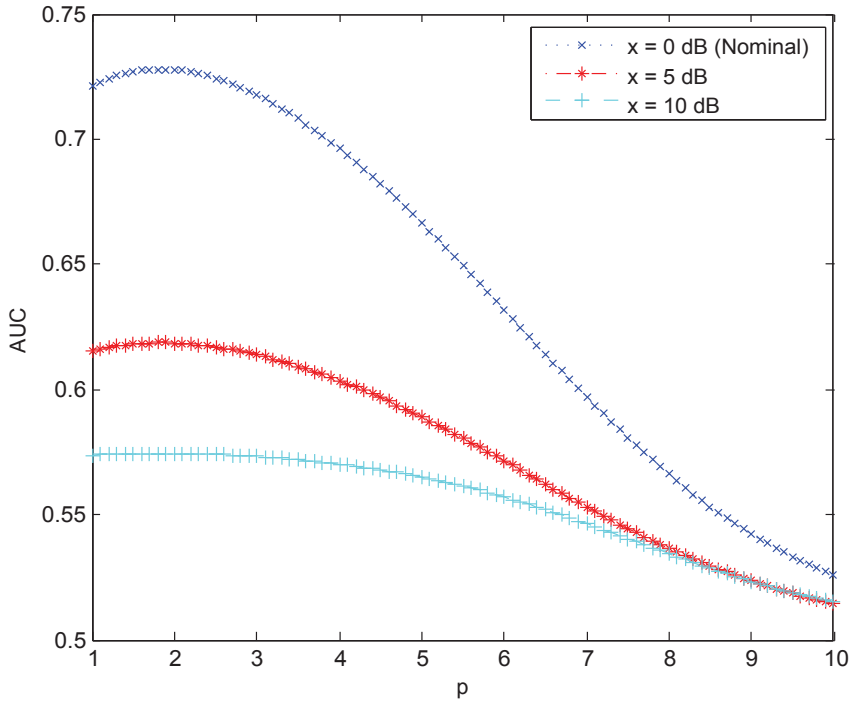

Fig. 5.5. AUC vs. p for various noise uncertainty levels x dB for $N = 10$ at $\gamma = -5$ dB.

level of noise (denoted by σ_n^2) such that $\sigma_a^2 \in [(1/\xi)\sigma_n^2, \xi\sigma_n^2]$, where $\xi = 10^{x/10} > 1$ for x dB uncertainty in the noise power [20]. The work [20] discovered that the ED performance degrades in presence of noise variance uncertainty. We thus seek to find the effect of noise variance uncertainty for the case of p-norm detector.

The actual noise variance is assumed to take any of the K possible values, that is, $\sigma_a^2 \in \{\sigma_k^2 | 1 \leq k \leq K\}$, such that $\sigma_L^2 = \sigma_1^2 < \sigma_2^2 < ... < \sigma_1^K = \sigma_H^2$ with probability of occurrence of each σ_k^2 denoted by $\mathbb{P}(\sigma_k^2)$ [128]. Thus, the AUC averaged over the noise variance uncertainty, denoted by $\overline{\text{AUC}}$, can be expressed in the form

$$\overline{\text{AUC}} = \sum_{k=1}^{K} \mathbb{P}(\sigma_k^2)\text{AUC}(\sigma_k), \tag{5.13}$$

where $\text{AUC}(\sigma_k)$ can be easily derived following (5.12) to be

$$\text{AUC}(\sigma_k) = \frac{2\Gamma(\theta)}{\theta\Gamma^2(\theta/2)} \cdot \frac{[\sigma_k^p(\sigma_k^2+\sigma_s^2)^{p/2}]^{\theta/2}}{(\sigma_k^p + (\sigma_k^2+\sigma_s^2)^{p/2})^\theta} {}_2F_1\left(1, \theta; \frac{\theta}{2}+1; \frac{(\sigma_k^2+\sigma_s^2)^{p/2}}{\sigma_k^p + (\sigma_k^2+\sigma_s^2)^{p/2}}\right). \tag{5.14}$$

The derived $\overline{\text{AUC}}$ (5.13) is used to study the effect of uncertain noise variance as shown in Fig. 5.5 where a set of AUC vs. p curves are plotted for $\mathbb{P}(\sigma_L^2) = 0.1, \mathbb{P}(\sigma_H^2) = 0.9$

(that is, $K = 2$). Clearly, increased levels of noise variance uncertainty severely impacts the p-norm detection performance (about 15% and 21% degradation for $5\,\text{dB}$ and $10\,\text{dB}$ uncertainty respectively, compared to the nominal case).

5.6 Conclusion

The CLT approximation for P_d, although offering computational ease, is not accurate for small sample sizes. A previous remedy has been the CGA. This chapter investigates five more classical approximations. As a further application, the Patnaik's approximation is utilized to derive a novel AUC expression of the p-norm detector. The AUC analysis is further extended to quantify the effect of noise variance uncertainty on the p-norm detector performance. These analyses hence indicate the possibilities of potential applications of the approximations to problems other than energy detection. This chapter thus introduces these important but unnoticed approximations to the research community. Other than detection performance analysis, these approaches may be applicable to more general performance analysis problems involving antenna/co-operative diversity, stochastic interference networks, relaying schemes, and others, which remain as interesting open research problems for researchers to explore further.

Chapter 6

Spectrum Sensing Performance of p-norm Detector in Random Network Interference

The traditional ED's spectrum sensing performance is known to degrade in presence a number of interferers around the sensing CR, where both the number as well as locations of the interfering nodes from the CR are random. In such situations, the p-norm detector could potentially yield improved spectrum sensing performance. Thus, this chapter [1] investigates the p-norm detector performance in a more generalized setup where the received signal at the CR is subject to the cumulative effects of path-loss, fading and random network interference. Interestingly, fine tuning p in response to changes in the critical parameters of operations, especially to the change in interferer density, is found to yield substantial performance gains. Motivated by this and with the goal of further improving the sensing performance, cooperative spectrum sensing is also investigated. To this end, significant performance gains compared to the single CR based sensing are reported.

6.1 Introduction and Motivation

The near future concept of "networked everything" [2], where every wireless user (device) is virtually connected to every other user, creates massive networks of interconnected de-

[1] Chapter 6 has been published in the *Proceedings of IEEE International Conference on Communications* as [129].

vices. This leads to leakage of powers from undesired transmitters in space over relatively large distances thus causing interference to the sensing CR node [31]. Such scenarios may typically arise in heterogeneous network settings, for example, while enabling co-existence between IEEE 802.22 WRANs and IEEE 802.11af Super Wi-Fi in the TV white spaces where an IEEE 802.11af based small-cell access point (AP) may receive interference from other similar APs or even from the IEEE 802.22 based incumbents [130]. However, 802.22 and 802.11af based systems have different specifications. For example, maximum transmit power of an 802.22 PU could go upto $1\,\text{kW}$ while that for an 802.11af AP is $100\,\text{mW}$ [31]. Thus, despite such disparate operating conditions, the CR must make correct decisions on the presence/absence of vacant bands. Moreover, in addition to such disparities, the CR must operate in the presence of a network of interferers where both the number and locations (distances) of the interferers vary randomly. Clearly, such random network interference impairs the spectrum sensing accuracy of the CR.

Although numerous works on ED [27], [33]–[37], [58], [59], [67] have uncovered interesting insights on channel impairments and diversity configurations, the investigation of the impact of random network interference on ED is extremely limited [74], [131], [132]. While these studies show that random interference from secondary users clearly degrades ED's ability to identify unused spectrum bands, [74], [131], [132] do not treat the inherent effects of fading (which, henceforth refers to multipath/shadowing). Moreover, methods to improve the sensing performance against the cumulative effects of fading/shadowing and random network interference have not yet been reported.

To address these issues, we investigate the CR spectrum sensing performance in path-loss, fading and random network interference. We consider the p-norm detector, which being more versatile than the ED (regarding the choice of p) also outperforms the ED in multipath-fading (Chapter 4). However, to the best of our knowledge, the performance of p-norm detector has never been studied in presence of random network interference. In summary, the contributions of this chapter are as follows:

(i) As the exact distribution of the p-norm detector decision variable is analytically intractable, we utilize the Patnaik's approximation developed in Chapter 5, which leads to conditional detection probability P_d (conditioned on fading and random network parameters) and false alarm probability P_f (conditioned on random network parameters) expressions as functions of path-loss, fading and network parameters of interest.

(ii) Further, the average P_d over fading channels is derived. The derived expression and P_f (from (i)) are then utilized to devise semi-analytical evaluation of the detection performance averaged over the random network model. The devised method saves simulation run-times drastically compared to exhaustive Monte-Carlo iterations performed over all random parameters (noise, fading, interferers).

(iii) Finally, the developed framework is extended to cooperative spectrum sensing to explore further possible gains with multiple collaborating CR nodes.

The system model is introduced in Section 6.2. Approximate conditional expressions for P_d and P_f are derived in Section 6.3. Average P_d and P_f over fading and random network interference are derived in Section 6.4. Novel insights are discussed for single CR based sensing in Section 6.5 and for cooperative sensing in Section 6.6 before concluding the chapter with Section 6.7.

6.2 System Model

6.2.1 Network Model

The network model is shown in Fig. 6.1. Consider a CR located at the center of a circular disc of radius R so that it can sense the presence/absence of PU transmission within the area $A = \pi R^2$. The PU transmitter is operating at a fixed distance $r_0 \leq R$ from the CR node. Within the same area A, there exist K interferers located at distances $\mathbf{r} = [r_1, r_2, ..., r_K]$ from the sensing CR such that both K and $\mathbf{r}$ vary randomly. Such topological randomness in network interference can be modeled via spatial point processes [133]. While our proposed semi-analytical method is not limited to any particular point process model, we will consider the popular (homogeneous) Poisson point process (PPP) in this work [133] (Section 6.5). The PPP model is valid when the interferers are randomly distributed over a large area without any correlation between their locations. However, even for correlated locations, the PPP model is known to be accurate to within 1-2 dB of the performance of an actual LTE network [133].

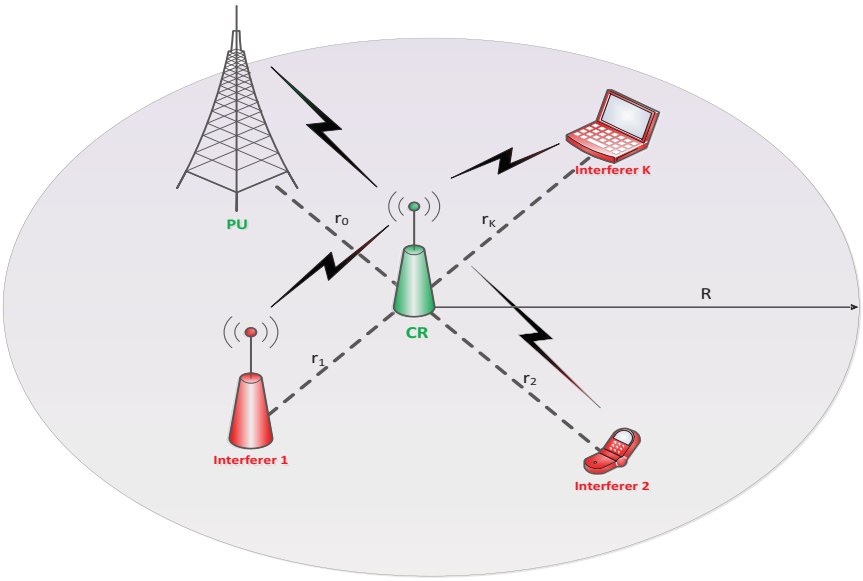

Fig. 6.1. Network Model. The total number of interferers K and the distances r_k, $\forall k \in \{1, 2, ...K\}$ are random.

6.2.2 Link Model

Denoting the true presence and absence of the PU signal within the CR sensing region by H_1 and H_0, respectively, the n-th received signal sample y_n, $\forall n \in \{1, 2, ..., N\}$, conditioned on K, $\mathbf{r}$ and the PU-CR random fading channel coefficient h, can be expressed as

$$y_n = \begin{cases} w_n + \sum_{k=1}^{K} r_k^{-\alpha/2} s_{k,n} & : H_0, \\ h r_0^{-\alpha/2} s_{P,n} + w_n + \sum_{k=1}^{K} r_k^{-\alpha/2} s_{k,n} & : H_1, \end{cases} \tag{6.1}$$

where α is the path-loss exponent, $s_{k,n} \sim \mathcal{CN}(0, P_i)$ is the k-th interfering signal sample assumed to be conditionally (on K and $\mathbf{r}$) complex Gaussian with mean zero and variance P_i, $w_n \sim \mathcal{CN}(0, \sigma_w^2)$ AWGN sample and $s_{P,n} \sim \mathcal{CN}(0, P_s)$ is complex Gaussian PU signal sample. Note that the statistical modeling of transmit signals as Gaussian is a widely used approach [39], [47], [74], [115], [116], [131], [132], [134]. Also, we disregard the effect of fading on the interfering signals since deep fading of the PU signal (rather than interfering signals) is what limits the sensing performance. Without loss of generality, the PU signal, noise and interfering signals are assumed to be mutually independent.

6.3 Conditional Performance of the p-norm detector

As the p-norm detector decision variable T_p is a sum of arbitrary p-th powered random variables, the distributions $T_p|H_1$ and $T_p|H_0$ are not amenable to an exact closed-form analysis even in non-random (non-fading, AWGN) channels as demonstrated in Chapter 4. Thus, to date, three distinct approaches for performance analysis of p-norm detector exist, however, with some limitations as follows.

(i) Although highly accurate methods based on the moment-generating function, Laguerre polynomials, and series-sum have been developed for evaluating P_d and P_f in Chapter 4, the extension of these techniques to the random network and link model at hand appears difficult.

(ii) The CLT approximation for the distribution of T_p [40] is only suitable for large samples ($N \gg 1$) and does not facilitate the small-sample performance which is critical to determine the minimum samples (to maintain low sensing times) required for attaining the target sensing performance [116].

(iii) Another approach based on approximating T_p by a Gamma random variable [39] does not limit the sample size (as in CLT). However, it only considers AWGN channels without encompassing path-loss, fading and/or random network interference.

To circumvent these limitations, we derive approximate P_d and P_f expressions to facilitate analysis of the problem at hand.

We resort to the Patnaik's approximation introduced in Chapter 5 to approximate the scaled (by ρ) version of T_p by a central chi-square random variable Y with u degrees of freedom as

$$Y = \frac{1}{\rho} \cdot T_p. \tag{6.2}$$

The scaling factor ρ and the degrees of freedom u can be determined by matching the first two exact moments of T_p/ρ to those of Y. Then, the CCDFs of Y under hypotheses H_0 and H_1 yield P_f and P_d, respectively.

For the random signal model considered, the distribution of y_n, $\forall n \in \{1, 2, ..., N\}$, under hypotheses H_0 and H_1, can be expressed as $y_n|H_0 \sim \mathcal{CN}(0, v_0)$ and $y_n|H_1 \sim \mathcal{CN}(0, v_1)$, respectively. The variables v_0 and v_1 denote variances conditioned on the ran-

dom variables K, $\mathbf{r} = [r_1, r_2, ..., r_K]$ under H_0, and additionally on h under H_1, as

$$\begin{aligned} v_0 &= \sigma_w^2 + \sum_{k=1}^{K} P_i r_k^{-\alpha} \\ v_1 &= \sigma_w^2 + \sum_{k=1}^{K} P_i r_k^{-\alpha} + |h|^2 P_s r_0^{-\alpha}. \end{aligned} \tag{6.3}$$

Since y_n is conditionally complex Gaussian distributed, its squared amplitude $|y_n|^2$ is exponentially distributed under each hypothesis H_j with the PDF $f_{|y_n|^2}(x) = 1/v_j e^{-x/v_j}$, $j = \{0, 1\}$. Since the samples are i.i.d., the mean of $T_p|H_j$, denoted by μ_j, can be expressed after interchanging the order of integration and summation as

$$\mu_j = \frac{1}{N} \sum_{i=1}^{N} \int_0^\infty x^{p/2} \frac{1}{v_j} e^{-x/v_j} dx = v_j^{p/2} \Gamma\left(\frac{p}{2} + 1\right), \tag{6.4}$$

where definition of Gamma function, $\Gamma(a) = \int_0^\infty x^{a-1} e^{-x} dx$, is used. The variance of $T_p|H_j$, denoted by $var(T_p|H_j)$, can be obtained similarly as

$$var(T_p|H_j) = \frac{v_j^p}{N} \left[\Gamma(p+1) - \Gamma^2\left(\frac{p}{2} + 1\right) \right]. \tag{6.5}$$

Then, by using the transformation (6.2), matching the corresponding means and variances under each H_j, and solving the resulting equations for u and $\rho|H_j$ denoted by ρ_j, $j = \{0, 1\}$ we get

$$u = \frac{2N\Gamma^2(p/2+1)}{\Gamma(p+1) - \Gamma^2(p/2+1)},\ \rho_j = v_j^{p/2} g(N, p), \tag{6.6}$$

where $g(N, p) \triangleq [\Gamma(p+1) - \Gamma^2(p/2+1)]/[2N\Gamma(p/2+1)]$. Then, the CCDFs of Y, for $j = \{0, 1\}$, can be readily derived in terms of the upper-incomplete Gamma function $\Gamma(a, x) = \int_x^\infty t^{a-1} e^{-t} dt$, to yield P_d and P_f, respectively, as

$$P_d \simeq \frac{1}{\Gamma(u/2)} \Gamma\left(\frac{u}{2}, \frac{\lambda}{2\rho_1}\right), P_f \simeq \frac{1}{\Gamma(u/2)} \Gamma\left(\frac{u}{2}, \frac{\lambda}{2\rho_0}\right). \tag{6.7}$$

These approximate expressions (6.7) are simple enough to lend analysis in the random network/link model of interest as will be discussed in the next section where we evaluate the average of these metrics over the corresponding random variables.

Before proceeding to the next section, the derived expressions (6.7) are numerically compared against the simulation results via the ROC curves (Fig. 6.2) for two p-norm de-

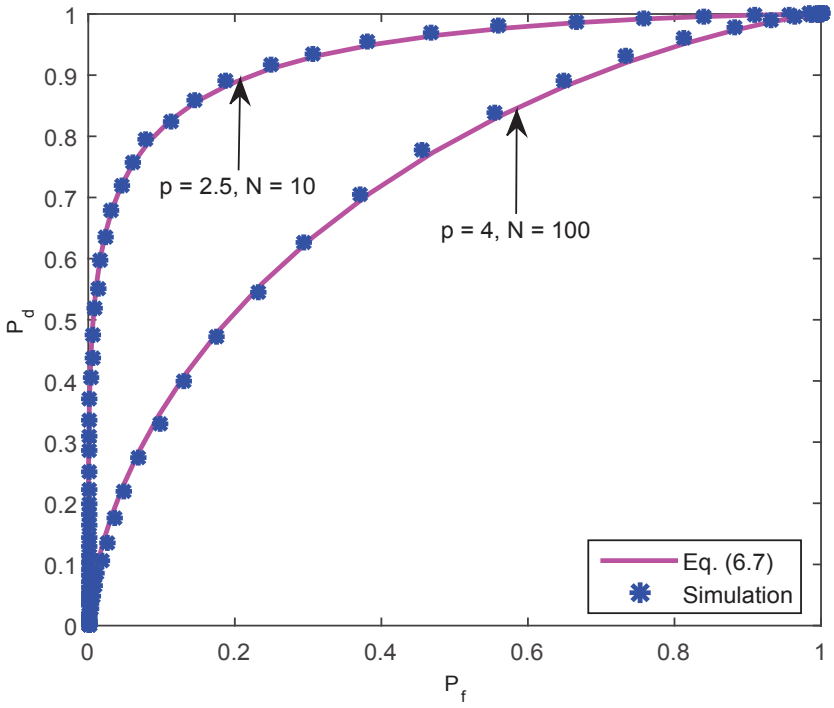

Fig. 6.2. ROC curves comparing (6.7) and simulation. The $p = 4$, $N = 100$ graph is plotted for SINR $= -10$ dB and $p = 2.5$, $N = 10$ is obtained with SINR $= 0$ dB.

tectors with different sample sizes and conditional (on K, $\mathbf{r}$ and h) SINRs, where SINR $\triangleq P_s r_0^{-\alpha}/[\sigma_w^2 + \sum_{k=1}^{K} P_i r_k^{-\alpha}]$. For both cases, (6.7) and simulations match closely, thus validating the accuracy of (6.7).

6.4 Average Detection Performance

As discussed in Section 6.3, P_f is conditioned on the number of interferers K and their distances $\mathbf{r}$ while P_d is additionally conditioned on channel gain h. Thus, exhaustive simulations would require averaging over realizations of the random signals, channel gain, noise and the point process, which would result in long run-times, particularly for high interferer densities where the number of interfering nodes can be very large. Thus, simulation-only based evaluations are prohibitively expensive for multiple-parameter design perspectives which require inter-relationship among various parameters (such as α, P_s, P_i, p, N and others) with wide range of values. This motivates us to develop a semi-analytical method for faster computation of average P_f (over K and $\mathbf{r}$), denoted by $\overline{P}_f$, and average P_d, denoted by $\overline{P}_d$ (over K, $\mathbf{r}$ and h), next.

Substituting ρ_1 from (6.6) into the conditional P_d (6.7) and integrating over the PDF of the squared amplitude of channel coefficient $|h|^2$, denoted by $f_{|h|^2}(x)$, results into

$$P_{d|\text{PP}} = \frac{1}{\Gamma(u/2)} \int_0^\infty \Gamma\left(\frac{u}{2}, \frac{\lambda/[2g(N,p)]}{(\sigma_a^2 + xP_s r_0^{-\alpha})^{p/2}}\right) f_{|h|^2}(x)dx, \tag{6.8}$$

where we define $\sigma_a^2 = \sigma_w^2 + \sum_{k=1}^K P_i r_k^{-\alpha}$ and the subscript PP indicates conditioning on the point process (i.e. on K and $\mathbf{r}$). Since $p > 0$ is a critical parameter of interest, imposing any limitations on its range is unrealistic (for example, assuming p as an integer or confining it to a particular interval, for ease of analysis) for achieving gains resulting from fine tuning of p. Unfortunately, this requirement renders the integral in (6.8) virtually intractable. However, with further algebraic manipulations, the integral can be simplified to obtain $P_{d|\text{PP}}$ as an integral over a finite support of the form

$$P_{d|\text{PP}} = \int_0^{\pi/2} \Gamma\left(\frac{u}{2}, \frac{\lambda/[2g(N,p)]}{(\sigma_a \sec\theta)^p}\right) f_{|h|^2}\left(\frac{\sigma_a^2 \tan^2\theta}{P_s r_0^{-\alpha}}\right) \xi(\theta)d\theta \tag{6.9}$$

where we define $\xi(\theta) = \frac{2\sigma_a^2 \tan\theta \sec^2\theta}{P_s r_0^{-\alpha}\Gamma(u/2)}$. Note that (6.9) is a very general expression valid for any multipath-fading, shadowing or diversity combining model with a known PDF $f_{|h|^2}(x)$. Moreover, it can be readily computed in software packages such as MATLAB. Finally, (6.9) averaged over the point process yields $\overline{P}_d$ as

$$\overline{P}_d = \mathbb{E}_{K,\mathbf{r}}(P_{d|\text{PP}}), \tag{6.10}$$

where $\mathbb{E}_{K,\mathbf{r}}(\cdot)$ denotes the expectation over the random variables K and $\mathbf{r}$. Thus, (6.10) only needs to be iteratively averaged over the realizations of the point process while simulations-only based evaluations would require additional iterative simulations over random signals, channel gain h and noise. Note that since P_f (6.7) is independent of h, it only needs averaging over the point process. Thus, $\overline{P}_f$ is given by

$$\overline{P}_f = \mathbb{E}_{K,\mathbf{r}}(P_f). \tag{6.11}$$

The main advantage of (6.10) and (6.11) is a drastic reduction in simulation time compared to the direct (exhaustive) simulations over random signals, h, noise, and the point process. For instance, for a homogeneous PPP with average interferer density β over the

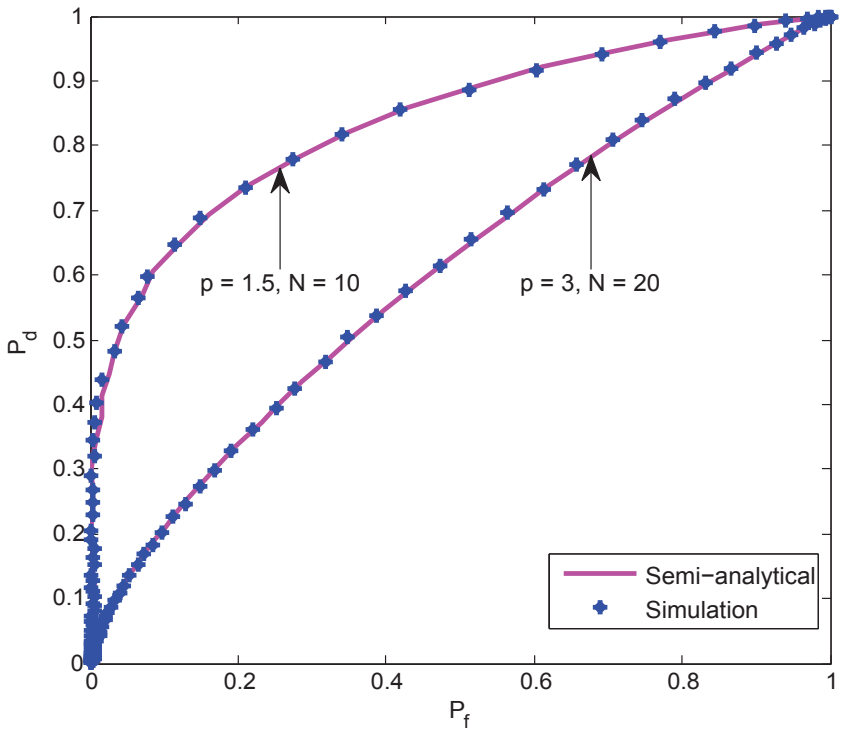

Fig. 6.3. ROC curves: semi-analytical (6.10) and (6.11) vs. simulations for 3-norm, $N = 20$ detector with $\beta = 0.0001$ $\alpha = 4$, $P_i = 10$ dB, $P_s = -10$ dB; and for 1.5-norm $N = 10$ detector with $\beta = 0.005$, $\alpha = 2.5$, $P_i = 5$ dB, $P_s = 0$ dB; $m = 2$, $\sigma_s = 4.66$ dB.

disc of radius R with the PU-CR link modeled by a Gamma-shadowed Nakagami-m channel (see Section 6.5), in order to attain a 3-digit accuracy for $\beta = 0.0001$ and $\beta = 0.01$ with $R = 150$, the direct simulations require 148 and 1555 seconds, respectively, while our semi-analytical solutions only require 4 and 51 seconds, respectively (on an Intel® Core i7™, 2.4 GHz CPU). Moreover, say, for $\beta = 0.1$, the average number of interferers is in the order of thousands (7069) and simulations could take more than one day to complete, while our solution only takes 127 seconds.

6.5 Numerical Setup and Discussions

In this section, we present novel, interesting insights into how the p-norm detector performs under the system model at hand. For numerical purpose, the interfering network is generated via a homogeneous PPP. The PU-CR channel is modeled as a Gamma-shadowed Nakagami-m fading channel. The CR sensing performance is illustrated via ROC curves and the average probability of error, defined as $\overline{P}_e = \mathbb{P}(H_1)(1 - \overline{P}_d) + \mathbb{P}(H_0)P_f$ where

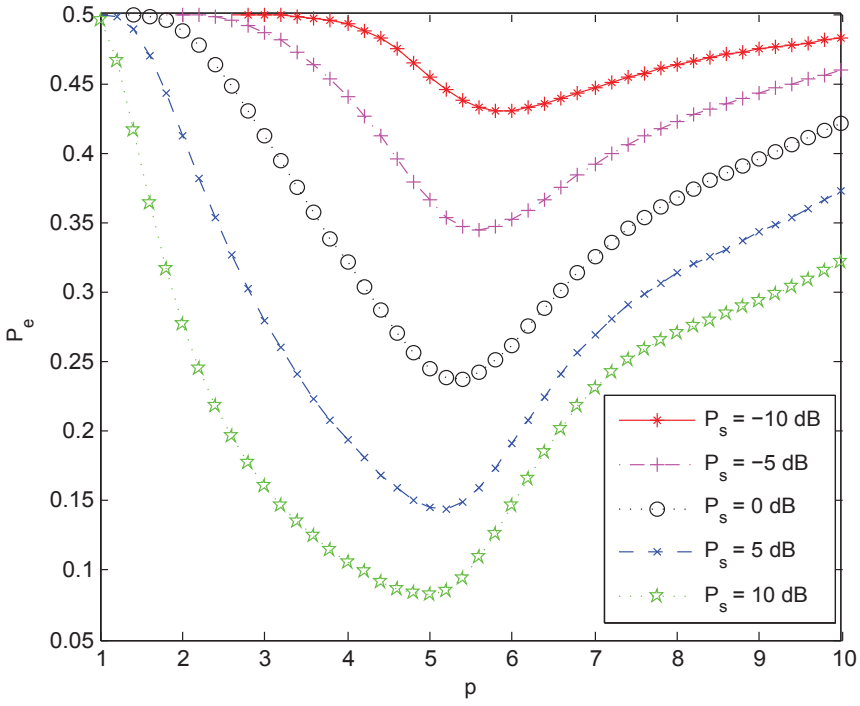

Fig. 6.4. $\overline{P}_e$ vs. p for various P_s with $N = 20$, $\lambda = 10$, $\beta = 0.0001$, $\alpha = 4$, $P_i = 4$ dB, $\sigma_s = 8.686$ dB and $m = 4.5$.

$\mathbb{P}(H_j)$, $j = \{0, 1\}$ denotes the probability of occurrence of H_j. Without loss of generality, the $\overline{P}_e$ results are obtained assuming equally-likely hypotheses.

For a homogeneous PPP with an average interferer density β, the total number of interferers K is a Poisson distributed random variable with probability mass function $\mathbb{P}(K = k) = (\beta A)^k e^{-\beta A}/k!$, while the distance r_k of the k-th interferer $\forall k \in \{1, 2, ..., K\}$ from the sensing CR is uniformly distributed in the disc of radius R with PDF $f_{r_k}(x) = 2x/R^2$, $0 < x < R$, and $f_{r_k}(x) = 0$, $x \geq R$.

The PDF of the squared envelope $|h|^2$ for the Gamma-shadowed Nakagami-m fading channel is given by [28]

$$f_{|h|^2}(x) = \frac{2b^{\frac{m+m_s}{2}} x^{\frac{m+m_s}{2}-1}}{\Gamma(m)\Gamma(m_s)} \mathcal{K}_{m_s-m}(2\sqrt{bx}) \tag{6.12}$$

with $b = m_s m/\Omega_s$, where for a shadowing standard deviation σ_s, $m_s = 1/[\exp(\sigma_s^2) - 1]$ represents the inverse shadowing severity, $\Omega_s = \sqrt{(m_s + 1)/m_s}$ is the shadowed area mean power, m is the Nakagami fading severity index, and $\mathcal{K}_\nu(\cdot)$ is the modified Bessel function of second kind of order ν.

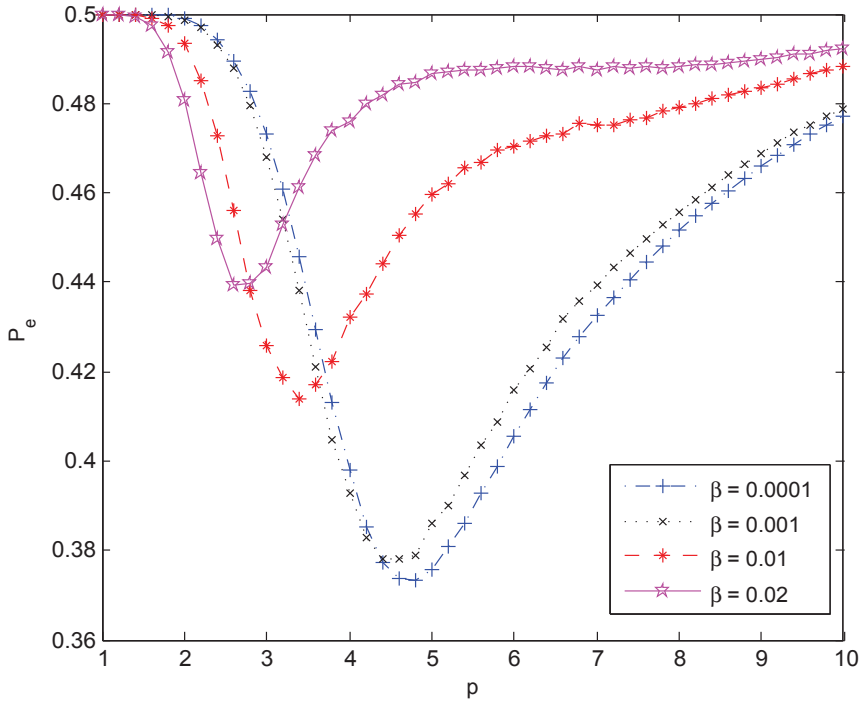

Fig. 6.5. $\overline{P}_e$ vs. p for various interferer densities β with $N = 10$, $\lambda = 10$ $P_s = 5\,\text{dB}$, $P_i = 5\,\text{dB}$, $\alpha = 2$, $\sigma_s = 6.52\,\text{dB}$ and $m = 2.5$.

Without loss of generality, we normalize the distances with respect to the PU's location $r_0 = 1$ and set $R = 150$. To validate our semi-analytical approach, ROCs obtained using (6.10) and (6.11) are numerically compared with those generated from simulations (Fig. 6.3) A tight match between the two clearly indicates the accuracy of our method.

The dependence of $\overline{P}_e$ on p for various PU signal powers (Fig. 6.4) clearly indicates that the ED ($p = 2$) is non-optimal in minimizing $\overline{P}_e$ with its performance getting worse for low PU power levels. An optimal p of 5, denoted by $p^* = 5$, attains 71% lower $\overline{P}_e$ than that of ED when $P_s = 10\,\text{dB}$. In fact, another $p^* = 5.4$ detector possesses 15% lower $\overline{P}_e$ than the ED even at $10\,\text{dB}$ lower (than that for the ED) P_s levels.

Another set of graphs (Fig. 6.5) illustrate the effect of interferer density on the choice of optimal p, which in general, is not equal to 2 (ED). For example, with an optimal $p = 4.8$, 25% lower $\overline{P}_e$ (than ED) is attained at $\beta = 0.0001$. More interestingly, the optimal p is inversely proportional to β.

Although the p-norm detector performance in multipath-fading channels was well studied in Chapter 4, its performance in shadowing is not known. Motivated by this, the effect

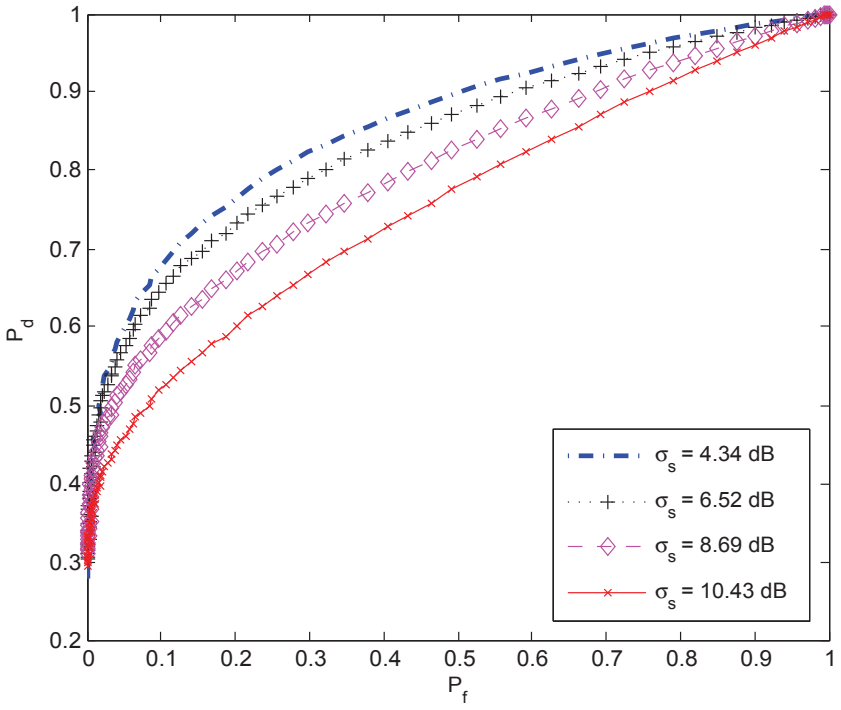

Fig. 6.6. ROC curves for a 3-norm, $N = 10$ detector for various σ_s dB with $\beta = 0.0001$, $\alpha = 2$, $P_i = 5$ dB, $P_s = 0$ dB and $m = 2.5$.

of shadowing is studied by varying the shadowing standard deviation, σ_s dB, as shown in Fig. 6.6 for a typical outdoor environment (where $4 \leq \sigma_s \text{ dB} \leq 12$). Clearly, largely shadowed PU signals are more difficult to detect. For example, with a 6.1 dB increase in the shadowing standard deviation, $\overline{P}_d$ drops by about 23% (at $P_f = 0.01$). A typical solution to mitigate the effects of shadowing is to exploit cooperation among a number of CRs, rather than having a single CR detect the PU, as discussed next.

6.6 Cooperative Spectrum Sensing Performance

In cases when the PU is heavily shadowed from the sensing CR, cooperation among multiple CRs remarkably improves the sensing performance [21]. Thus, to mitigate shadowing and more importantly, to explore further enhancements in the sensing performance, we now allow multiple CRs to cooperate.

We now consider multiple CRs participating along with a FC to decide on the presence/absence of PU in the spectrum of interest. Since our primary interest is to evaluate the benefits of cooperation rather than a particular fusion scheme, we do not seek any opti-

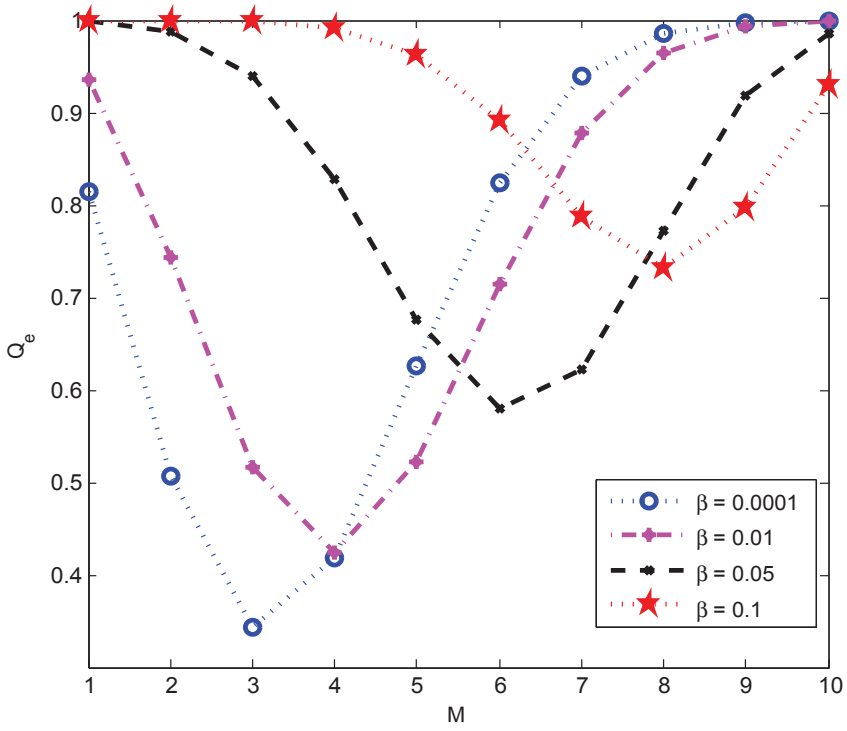

Fig. 6.7. $\overline{Q}_e$ vs. M with $C = 10$ for various β for a $N = 10$, 4.8-norm detector with $\lambda = 5.5$, $\alpha = 2$, $P_s = -5$ dB, $\sigma_s = 8.69$ dB, $P_i = 5$ dB and $m = 2.5$.

mal fusion scheme but simply choose the M out of C fusion rule for the purpose. A more detailed discussion of other common fusion rules can be found in [27]. For the M out of C fusion rule, the co-operative (fused) detection probability and false alarm probability, denoted by $\overline{Q}_d$ and $\overline{Q}_f$, respectively, are [135].

$$\overline{Q}_d = \sum_{l=M}^{C} \binom{C}{l} \overline{P}_d^l (1-\overline{P}_d)^{C-l}; \; \overline{Q}_f = \sum_{l=M}^{C} \binom{C}{l} \overline{P}_f^l (1-\overline{P}_f)^{C-l}, \tag{6.13}$$

where C is the total number of CRs and M is the threshold of cooperative detection such that if the sum of individual 1-bit CR decisions (1 or 0) exceeds (or equals) M, the FC decides in favor of H_1, else it decides on H_0.

Interestingly, cooperative spectrum sensing is advantageous for minimizing the overall probability of error given by $\overline{Q}_e = 1 - \overline{Q}_d + \overline{Q}_f$ (Fig. 6.7). Say, for $\beta = 0.05$, an optimal M, $M^* = 6$ reduces the probability of error ($\overline{Q}_e$) by 30% as compared to that for single CR ($\overline{P}_e = 0.42$) . Moreover, at larger interferer densities, having a higher M is better. For example, as much as 27% reduction in $\overline{Q}_e$ can be obtained when M is increased from 1 to

8 for a relatively large interferer density ($\beta = 0.1$).

6.7 Conclusion

Spectrum sensing with p-norm detector based CR under cumulative effects of path-loss, multipath-/shadow- fading and random network interference has been considered. Adaptive tuning of p in response to varying PU signal power yields better performance, as compared to the traditional ED ($p = 2$) Also, p can be chosen inversely to the interferer density to reduce the impact of random network interference on the sensing performance. Increased levels of shadow-fading degrades the p-norm performance. Additionally, cooperation further improves the sensing performance even in the presence of random network interference. The improvement is achieved by adapting the threshold of cooperative detection at the FC in proportion to the interferer density. Thus, our technique can serve as a robust tool to design, analyze and improve CR spectrum sensing performance which is pivotal for promoting coexistence among current and next-generation wireless networks.

Chapter 7

Conclusion and Future Work

In this thesis, several important open problems in performance analysis of two non-coherent detectors, the ED and the p-norm detector, were considered.

7.1 Conclusion and contributions summary

- In Chapter 3, a novel asymptotic technique accurate over a wider SNR range as compared to the existing asymptotic analysis valid only for high SNRs was proposed for characterizing the ED performance. The technique offered unified analysis in fading channels with and without diversity, in cooperative networks and interference. Furthermore, the proposed asymptotic analysis served as a unified tool to evaluate an alternative figure of merit, the CAUC of the ED. Our proposed asymptotic also yielded explicit expressions for the sensing gain, which is important to impart a quick estimate of the ED performance in the operating conditions of interest.

- The lack of comprehensive analysis of the p-norm detector performance in fading, diversity and AWGN was treated in Chapter 4. Several accurate tools were developed to overcome the limitations on the SNR range and the sample size, prevalent in the existing analyses. The analysis was further extended to obtain novel performance expressions for the p-norm detector in non-homogeneous and non-linear propagation environments represented by two of the generalized channel models. These expressions revealed that the ED is not the optimal detector in such environments. Furthermore, two new, non-coherent antenna diversity combining techniques were developed

for the p-norm detector which outperformed the existing SC combining technique at high SNRs while maintaining a performance similar to the SC at lower SNRs.

- To facilitate finite (small) sample performance of the ED and the p-norm detector, five classical approximations were first introduced for ED performance, in Chapter 5. The approximations were compared against the CLT approximation and the only existing finite sample approximation based on the CGA. The proposed approximations, which yielded simple expressions for the detection probability, were found to tightly match the exact detection probability expression based on the generalized Marcum-Q function. One of the proposed approximation was further applied to derive novel, finite sample AUC expression for the p-norm detector. The expression was found to be versatile for any number of samples (low to high). As a further application, the AUC analysis was extended to study the effect of noise variance uncertainty on the p-norm detector performance.

- To address performance degradation in presence of random network interference, where both the number as well as locations of the interfering nodes, are random, the p-norm detector was considered in Chapter 6. Furthermore, the comprehensive performance of spectrum sensing in an environment cumulatively affected by path-loss, fading and random network interference was lacking previously. In Chapter 6, these two issues were treated by devising a semi-analytical, unified framework for detection performance analysis in path-loss, fading and random network interference, without any restrictions on the fading or the random network model. Our devised semi-analytical framework was exploited to quantify significant performance gains (compared to ED) achievable by fine tuning the parameter p in response to the interferer density. Furthermore, the framework was extended to cooperative spectrum sensing, which yielded additional performance gains compared to single CR based spectrum sensing.

For completeness, the contributions are summarized in Table 7.1 below.

TABLE 7.1
SUMMARY OF CONTRIBUTIONS FOR CHAPTERS 3 - 6

Chapter	**Contributions**	**Applied to**
3	(a) Novel approximate $f(\beta)$ (b) Unified asymptotic analysis (c) High accuracy across wider SNR range (d) Reveals sensing gain	ED Unknown deterministic signal Nakagami-m/q MRC, EGC, SC Amplify-and-forward relays Interference
4	(a) Novel exact analytical framework (b) Unified exact analysis (c) Generalized fading channels (d) Analysis in diversity	p-norm detector Random signal κ-μ, α-μ pLC (new), pLS (new), MRC, SC
5	(a) Five accurate, finite-sample approximations for non-central chi-square (b) Simple closed-form for P_d with reduced functional complexity (compared to Marcum-Q) (c) Novel, compact AUC (p-norm)	ED p-norm detector Noise variance uncertainty effect on p-norm detector AUC
6	(a) Comprehensive, novel, semi-analytical framework under cumulative effects of random network interference, path-loss fading and shadowing (b) Cooperative spectrum sensing (c) Significant performance boost by fine tuning p (compared to ED)	p-norm detector Random signal Gamma-shadowed Nakagami-m Log-distance path-loss model Poisson field of interferers

7.2 Impact of the study

This thesis study developed several novel analytical frameworks for the spectrum sensing performance characterization of the low-cost, low-complexity detectors such as ED and the p-norm detector which are practically implementable detectors of interest to the wireless research community. The thesis primarily contributed in devising novel analytical techniques for quantifying and characterizing the spectrum sensing performance of CR networks. The quantification of the sensing performance of such detectors in fading channels, noise and interference uncertainty is of utmost importance to any system designer for enabling the overall concept of dynamic spectrum access using CR networks. Ultimately, the techniques developed in this research will serve for the design and analysis of efficient spectrum sensing systems for dynamic spectrum access in next generation wireless networks. Next, we present two example usage scenarios where the concepts developed in this this work can be of critical importance.

Example 1: Application to sensing-throughput tradeoff in spectrum sensing

To this end, one direct application of our devised methods for characterizing the reliability of spectrum sensing is in efficient resource utilization for CR networks. Our devised analytical methods are pivotal to evaluate the performance metrics such as P_d, P_f, P_e and AUC, which directly reflect the reliability of spectrum sensing. The spectrum sensing reliability, in turn, determines the duration of the sensing and transmission phases of the CR device. For instance, let us consider a scenario in a TDMA CR network where a specific time slot is allocated to each CR such that within this slot, a CR needs to: (i) sense the channel and (ii) transmit in case the channel is vacant. The sensing and transmission phases are mutually exclusive with the length of the sensing phase affecting the transmission phase such that a longer sensing time would result in a reduced transmission time and vice versa. This gives rise to the fundamental sensing-throughput tradeoff in CR networks [47]. In such situation, if the sensing reliability (for example, P_d) is low (say, due to operation in low SNRs) the CR may have to sense the channel for a longer period in order to collect enough samples for the sensing reliability to increase to an acceptable margin. Sensing for a longer period, however, reduces the allowable transmission period thus negatively impacting the CR throughput (due to increased delay in start of a transmission). On the other hand, if

the P_d for a given channel is sufficiently high (meeting the a pre-specified requirement), it allows reduction of the channel sensing period which gives the CR more time to transmit thus increasing the CR throughput. Thus, the sensing-throughput tradeoff analysis is one of the most critical applications where the contributions of this thesis can impact crucially.

Example 2: Application to energy efficient spectrum sensing

Another example where the reliability of spectrum sensing is critical, is while determining the energy consumption of the CR device. It is important to note that the increase/decrease of sensing phase duration has a more dominant impact (than the transmission phase) on the increase/decrease of the CR device's energy consumption since the sensing phase consumes more energy (up to 50% more) than the transmission phase [136]. To this end, one practical usage scenario where spectrum sensing could impact critically is the energy efficient opportunistic communication. In practice, the PU often switches from active (ON) to idle (OFF) states and vice versa over time which may be regarded as the PU activity. When the impact of PU activity is considered on spectrum sensing, the ON/OFF duration of the PU plays a critical role in determining the frequency (periodicity) of the CR sensing phase, which directly affects the energy consumed by the CR. The ON/OFF behavior of the PU could be estimated by the CR based on creation and maintenance of a database of the correctly detected ON instants of the PU in the channel of interest. Such database reflects the PU activity at the CR based on which the CR may be able to increase/decrease the frequency (periodicity) of its sensing phase whenever the PU is active for a longer/shorter time. In case the PU is active very sparsely, the sensing database would reflect such sparse PU behavior and thus would allow the CR to decrease the sensing periodicity and increase the transmission periodicity. Reduction of the sensing periodicity thus reduces the CR energy consumption. Hence, our devised analytical frameworks which contribute in creating and maintaining such PU activity database via spectrum sensing, enable the computation and establishment of energy-throughput tradeoff regions, which eventually can be used for optimizing the CR device's energy efficiency.

Before concluding the chapter, we outline some of the interesting open problems related to the thesis in the next section, which can be of interest in future research.

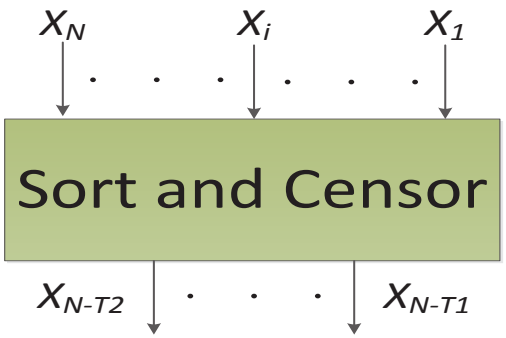

Fig. 7.1. TMOSCFAR detector principle.

7.3 Future work

- The approximate PDF proposed in Chapter 3 was explicitly used for asymptotic analysing of ED performance only. However, other potential applications of the technique could include evaluation and analysis of other crucial metrics to characterize wireless system performance. For example, applications of the proposed technique for analyzing the symbol error rate, outage probability, or channel capacity of systems deploying space-time coding and modulations, MIMO, antenna/relay selection schemes, and numerous other techniques are of high interest to wireless communication researchers and engineers.

- In this thesis, the decision variables of both the ED and the p-norm detector were constructed by utilizing all N received signal samples X_1, X_2, ..., X_N. However, in presence of noise variance or interference uncertainty, the quality of the received samples may vary across the sample space. Thus, as shown in Fig. 7.1, the received signal samples may be ordered from smallest to largest in magnitude as $|X_1| < |X_2| < ... < |X_N|$ and trimmed from both upper end (discard the largest T_2 samples) and lower end (discard the smallest T_1 samples) such that the resulting sample space is a subset of the original sample space, but with more reliable samples. These samples are then fed to the ED or the p-norm detector to yield the final decision which may be more robust to noise and interference uncertainty. This detector can be referred to as the trimmed-mean ordered statistics constant false alarm rate (TMOSCFAR) detector. The TMOSCFAR has been traditionally utilized in radar communications to yield improved target detection performance [137]. However, its performance in the context of spectrum sensing for broadband wireless networks remains unexplored.

Bibliography

[1] Cisco. [Online]. Available: http://www.cisco.com/c/en/us/solutions/collateral/service-provider/visual-networking-index-vni/white_paper_c11-520862.pdf

[2] Ericsson. [Online]. Available: urlhttp://www.ericsson.com/res/docs/whitepapers/wp-5g.pdf

[3] Q. Wang and D.-W. Yue, "A general parameterization quantifying performance in energy detection," *IEEE Signal Process. Lett.*, vol. 16, no. 8, pp. 699–702, Aug. 2009.

[4] A. Zanella, N. Bui, A. Castellani, L. Vangelista, and M. Zorzi, "Internet of things for smart cities," *IEEE Internet of Things Journal*, vol. 1, no. 1, pp. 22–32, Feb. 2014.

[5] F. Boccardi, R. Heath, A. Lozano, T. Marzetta, and P. Popovski, "Five disruptive technology directions for 5G," *IEEE Comm. Mag.*, vol. 52, no. 2, pp. 74–80, Feb. 2014.

[6] B. Bangerter, S. Talwar, R. Arefi, and K. Stewart, "Networks and devices for the 5G era," *IEEE Commun. Mag.*, vol. 52, no. 2, pp. 90–96, Feb. 2014.

[7] E. Dahlman, G. Mildh, S. Parkvall, J. Peisa, J. Sachs, Y. Selén, and J. Sköld, "5G wireless access: requirements and realization," *IEEE Commun. Mag.*, vol. 52, no. 12, pp. 42–47, Dec. 2014.

[8] H. Shi, R. Prasad, V. Rao, I. Niemegeers, and M. Xu, "Spectrum- and energy-efficient D2DWRAN," *IEEE Comm. Mag.*, vol. 52, no. 7, pp. 38–45, July 2014.

[9] G. Bartoli, R. Fantacci, K. Letaief, D. Marabissi, N. Privitera, M. Pucci, and J. Zhang, "Beamforming for small cell deployment in LTE-Advanced and beyond," *IEEE Wireless Commun.*, vol. 21, no. 2, pp. 50–56, Apr. 2014.

[10] A. Ghosh, R. Ratasuk, B. Mondal, N. Mangalvedhe, and T. Thomas, "LTE-Advanced: next-generation wireless broadband technology [invited paper]," *IEEE Wireless Commun.*, vol. 17, no. 3, pp. 10–22, June 2010.

[11] Federal Communications Commission, "Spectrum Policy Task Force," Rep. ET Docket no. 02-135, Nov. 2002.

[12] C. Cordeiro, K. Challapali, D. Birru, and N. Sai Shankar, "IEEE 802.22: the first worldwide wireless standard based on cognitive radios," in *Proc. IEEE Int. Symp. Dynamic Spectrum Access Netw. (DySPAN)*, 2005, pp. 328–337.

[13] J. Mitola and J. Maguire, G.Q., "Cognitive radio: making software radios more personal," *IEEE Personal Commun. Mag.*, vol. 6, no. 4, pp. 13–18, Aug. 1999.

[14] S. Haykin, "Cognitive radio: brain-empowered wireless communications," *IEEE J. Sel. Areas Commun.*, vol. 23, no. 2, pp. 201–220, Feb. 2005.

[15] A. Goldsmith, S. Jafar, I. Maric, and S. Srinivasa, "Breaking spectrum gridlock with cognitive radios: an information theoretic perspective," *Proc. IEEE*, vol. 97, no. 5, pp. 894–914, May 2009.

[16] I. F. Akyildiz, W.-Y. Lee, M. C. Vuran, and S. Mohanty, "Next generation/dynamic spectrum access/cognitive radio wireless networks: a survey," *Comput. Netw.*, vol. 50, no. 13, pp. 2127 – 2159, Sep. 2006.

[17] K. Shin, H. Kim, A. Min, and A. Kumar, "Cognitive radios for dynamic spectrum access: from concept to reality," *IEEE Wireless Commun.*, vol. 17, no. 6, pp. 64–74, 2010.

[18] D. Cabric, S. Mishra, and R. Brodersen, "Implementation issues in spectrum sensing for cognitive radios," in *Proc. Asilomar Conf. Signal, Syst. and Comput.*, vol. 1, 2004, pp. 772–776.

[19] H. Urkowitz, "Energy detection of unknown deterministic signals," *Proc. IEEE*, vol. 55, no. 4, pp. 523–531, Apr. 1967.

[20] R. Tandra and A. Sahai, "SNR walls for signal detection," *IEEE J. Sel. Areas Commun.*, vol. 2, no. 1, pp. 4–17, Feb. 2008.

[21] K. Letaief and W. Zhang, "Cooperative communications for cognitive radio networks," *Proc. IEEE*, vol. 97, no. 5, pp. 878–893, May 2009.

[22] Y. Zeng and Y.-C. Liang, "Covariance based signal detections for cognitive radio," in *Proc. IEEE Int. Symp. on Dynamic Spectrum Access Netw. (DySPAN).*, 2007, pp. 202–207.

[23] S. J. Shellhammer, "Spectrum sensing in IEEE 802.22," in *Proc. 1st IAPR Workshop on Cognitive Inf. Process.*, 2008.

[24] M. K. Simon and M.-S. Alouini, *Digital Communication over Fading Channels*, 2nd ed. New York: Wiley, 2005.

[25] G. L. Stuber, *Prinicples of Mobile Communication*, 2nd ed. Kluwer Academic Publishers, Norwell, MA, USA, 2001.

[26] M. Abramowitz and I. A. Stegun, *Handbook of Mathematical Functions with Formulas, Graphs and Mathematical Tables*. National Bureau of Standards, Nov. 1970.

[27] S. Atapattu, C. Tellambura, and H. Jiang, *Energy Detection for Spectrum Sensing in Cognitive Radio*. Springer, New York, 2014.

[28] I. Kostic, "Analytical approach to performance analysis for channel subject to shadowing and fading," *IEE Proc. Commun.*, vol. 152, no. 6, pp. 821–827, Dec. 2005.

[29] S. Atapattu, C. Tellambura, and H. Jiang, "A mixture gamma distribution to model the SNR of wireless channels," *IEEE Trans. Wireless Commun.*, vol. 10, no. 12, pp. 4193–4203, Dec. 2011.

[30] F. Digham, M.-S. Alouini, and M. K. Simon, "On the energy detection of unknown signals over fading channels," in *Proc. IEEE Int. Conf. Commun. (ICC)*, vol. 5, 2003, pp. 3575–3579.

[31] C. Ghosh, S. Roy, and D. Cavalcanti, "Coexistence challenges for heterogeneous cognitive wireless networks in TV white spaces," *IEEE Wireless Commun.*, vol. 18, no. 4, pp. 22–31, Aug. 2011.

[32] V. Kostylev, "Energy detection of a signal with random amplitude," in *IEEE Proc. Int. Conf. Commun. (ICC)*, vol. 3, 2002, pp. 1606–1610.

[33] F. Digham, M.-S. Alouini, and M. K. Simon, "On the energy detection of unknown signals over fading channels," *IEEE Trans. Commun.*, vol. 55, no. 1, pp. 21–24, Jan. 2007.

[34] S. P. Herath, N. Rajatheva, and C. Tellambura, "Energy detection of unknown signals in fading and diversity reception," *IEEE Trans. Commun.*, vol. 59, no. 9, pp. 2443–2453, Sep. 2011.

[35] S. Atapattu, C. Tellambura, , and H. Jiang, "Performance of an energy detector over channels with both multipath fading and shadowing," *IEEE Trans. Wireless Commun.*, vol. 9, no. 12, pp. 3662–3670, Dec. 2010.

[36] S. Atapattu, C. Tellambura, and H. Jiang, "Energy detection based cooperative spectrum sensing in cognitive radio networks," *IEEE Trans. Wireless Commun.*, vol. 10, no. 4, pp. 1232–1241, Apr. 2011.

[37] ——, "Analysis of area under the ROC curve of energy detection," *IEEE Trans. Wireless Commun.*, vol. 9, no. 3, pp. 1216–1225, Mar. 2010.

[38] ——, "Performance of energy detection: A complementary AUC approach," in *Proc. IEEE Global Telecommun. Conf. (GLOBECOM)*, 2010.

[39] Y. Chen, "Improved energy detector for random signals in Gaussian noise," *IEEE Trans. Wireless Commun.*, vol. 9, no. 2, pp. 558–563, Feb. 2010.

[40] F. Moghimi, A. Nasri, and R. Schober, "Adaptive L_p norm spectrum sensing for cognitive radio networks," *IEEE Trans. Commun.*, vol. 59, no. 7, pp. 1934–1945, July 2011.

[41] C. Helstrom, *Statistical Theory of Signal Detection*. Pergamon Press, 1960.

[42] A. Annamalai and C. Tellambura, "A simple exponential integral representation of the generalized Marcum Q-function $Q_M(a, b)$ for real-order M with applications," in *Proc. IEEE Military Commun. Conf. (MILCOM)*, 2008.

[43] C. Tellambura, A. Annamalai, and V. Bhargava, "Contour integral representation for generalized Marcum-Q function and its application to unified analysis of dual-branch selection diversity over correlated Nakagami-m fading channels," in *Proc. IEEE Veh. Technol. Conf. (VTC)*, vol. 2, 2000, pp. 1031–1034.

[44] R. Agarwal, K. Perera, and S. Pinelas, *An Introduction to Complex Analysis*. Springer, 2011.

[45] H. V. Poor, *An Introduction to Signal Detection and Estimation*. New York: Springer-Verlag, 1988.

[46] H. Kobayashi, B. L. Mark, and W. Turin, *Probability, Random Processes, and Statistical Analysis.* New York : Cambridge University Press, 2012.

[47] Y.-C. Liang, Y. Zeng, E. Peh, and A. T. Hoang, "Sensing-throughput tradeoff for cognitive radio networks," *IEEE Trans. Wireless Commun.*, vol. 7, no. 4, pp. 1326–1337, Apr. 2008.

[48] Z. Quan, S. Cui, A. Sayed, and H. Poor, "Optimal multiband joint detection for spectrum sensing in cognitive radio networks," *IEEE Trans. Signal Process.*, vol. 57, no. 3, pp. 1128–1140, 2009.

[49] A. Pandharipande and J. P. M. G. Linnartz, "Performance analysis of primary user detection in a multiple antenna cognitive radio," in *Proc. IEEE Int. Conf. Commun. (ICC)*, 2007, pp. 6482–6486.

[50] D. Cabric, "Addressing feasibility of cognitive radios," *IEEE Signal Process. Mag.*, vol. 25, no. 6, pp. 85–93, Nov. 2008.

[51] S. Mishra, A. Sahai, and R. Brodersen, "Cooperative sensing among cognitive radios," in *Proc. IEEE Int. Conf. Commun. (ICC)*, 2006, pp. 1658–1663.

[52] A. Ghasemi and E. Sousa, "Collaborative spectrum sensing for opportunistic access in fading environments," in *Proc. IEEE Int. Symp. Dynamic Spectrum Access Netw. (DySPAN)*, 2005, pp. 131–136.

[53] G. Ganesan and Y. Li, "Cooperative spectrum sensing in cognitive radio, part I: two user networks," *IEEE Trans. Wireless Commun.*, vol. 6, no. 6, pp. 2204–2213, June 2007.

[54] ——, "Cooperative spectrum sensing in cognitive radio, part II: multiuser networks," *IEEE Trans. Wireless Commun.*, vol. 6, no. 6, pp. 2214–2222, June 2007.

[55] T. Nechiporenko, P. Kalansuriya, and C. Tellambura, "Performance of optimum switching adaptive M-QAM for amplify-and-forward relays," *IEEE Trans. Veh. Technol.*, vol. 58, no. 5, pp. 2258–2268, 2009.

[56] V. Sharma Banjade, C. Tellambura, and H. Jiang, "Asymptotic performance of energy detector in fading and diversity reception," *IEEE Trans. Commun.*, vol. 63, no. 6, pp. 2031–2043, 2015.

[57] ——, "New asymptotics for performance of energy detector," in *Proc. IEEE Global Commun. Conf. (GLOBECOM)*, 2014, pp. 4020–4024.

[58] A. Annamalai, O. Olabiyi, S. Alam, O. Odejide, and D. Vaman, "Unified analysis of energy detection of unknown signals over generalized fading channels," in *Proc. IEEE Int. Wireless Commun. and Mobile Comput. Conf. (IWCMC)*, July 2011, pp. 636–641.

[59] O. Olabiyi and A. Annamalai, "Further results on the performance of energy detector over generalized fading channels," in *Proc. IEEE Int. Symp. Personal Indoor and Mobile Radio Commun. (PIMRC)*, Sep. 2011, pp. 604–608.

[60] Z. Wang and G. Giannakis, "A simple and general parameterization quantifying performance in fading channels," *IEEE Trans. Commun.*, vol. 51, no. 8, pp. 1389–1398, Aug. 2003.

[61] "IEEE standard for local and metropolitan area networks part 16: Air interface for broadband wireless access systems," IEEE Std 802.16-2009.

[62] A. H. Nuttall, "Some integrals involving the Q function," Naval Underwater Systems Center (NUSC), Tech. Rep., Apr. 1972.

[63] J. Callahan, K. Hoffman, D. Cox, D. O'Shea, H. Pollaatsek, and L. Senechal, *Calculus In Context*. Five Colleges, Inc., 2008.

[64] G. Smyth, *Polynomial Approximation*. John Wiley and Sons, 2014.

[65] Y. Dhungana and C. Tellambura, "New simple approximations for error probability and outage in fading," *IEEE Commun. Lett.*, vol. 16, no. 11, pp. 1760–1763, Nov. 2012.

[66] D. V. Widder, *The Laplace Transform.* Princeton University Press, N.J., 1941.

[67] V. Sharma Banjade, N. Rajatheva, and C. Tellambura, "Performance analysis of energy detection with multiple correlated antenna cognitive radio in Nakagami-m fading," *IEEE Commun. Lett.*, vol. 16, no. 4, pp. 502–505, 2012.

[68] C. Tellambura, A. Annamalai, and V. Bhargava, "Closed form and infinite series solutions for the MGF of a dual-diversity selection combiner output in bivariate Nakagami fading," *IEEE Trans. Commun.*, vol. 51, no. 4, pp. 539–542, Apr. 2003.

[69] Y. Lu and A. Duel-Hallen, "Channel-adaptive sensing strategy for cognitive radio ad hoc networks," in *Proc. IEEE Consum. Commun. and Netw. Conf.*, Jan. 2013, pp. 466–471.

[70] Wolfram. [Online]. Available: `http://functions.wolfram.com/HypergeometricFunctions/Hypergeometric1F1/`

[71] A. Nosratinia, T. Hunter, and A. Hedayat, "Cooperative communication in wireless networks," *IEEE Commun. Mag.*, vol. 42, no. 10, pp. 74–80, Oct. 2004.

[72] A. Bletsas, A. Lippnian, and D. Reed, "A simple distributed method for relay selection in cooperative diversity wireless networks, based on reciprocity and channel measurements," in *Proc. IEEE Veh. Technol. Conf. (VTC)*, 2005.

[73] J. Andrews, R. Ganti, M. Haenggi, N. Jindal, and S. Weber, "A primer on spatial modeling and analysis in wireless networks," *IEEE Commun. Mag.*, vol. 48, no. 11, pp. 156–163, Nov. 2010.

[74] A. Makarfi and K. Hamdi, "Interference analysis of energy detection for spectrum sensing," *IEEE Trans. Veh. Technol.*, vol. 62, no. 6, pp. 2570–2578, July 2013.

[75] Y. Tokgoz and B. Rao, "The effect of imperfect channel estimation on the performance of maximum ratio combining in the presence of cochannel interference," *IEEE Trans. Veh. Technol.*, vol. 55, no. 5, pp. 1527–1534, Sep. 2006.

[76] Wolfram. [Online]. Available: `http://functions.wolfram.com/HypergeometricFunctions/Hypergeometric1F1Regularized/02/`

[77] ——. [Online]. Available: `http://functions.wolfram.com/HypergeometricFunctions/Hypergeometric2F1Regularized/09/`

[78] M. Ramezani, M. Hajiaghayi, C. Tellambura, and M. Ardakani, "Receive antenna selection for unitary space-time modulation over semi-correlated Ricean channels," *IEEE Trans. Commun.*, vol. 58, no. 2, pp. 521–530, Feb. 2010.

[79] G. Amarasuriya, C. Tellambura, and M. Ardakani, "Performance analysis framework for transmit antenna selection strategies of cooperative MIMO AF relay networks," *IEEE Trans. Veh. Technol.*, vol. 60, no. 7, pp. 3030–3044, Sep. 2011.

[80] G. Amarasuriya, M. Ardakani, and C. Tellambura, "Output-threshold multiple-relay-selection scheme for cooperative wireless networks," *IEEE Trans. Veh. Technol.*, vol. 59, no. 6, pp. 3091–3097, July 2010.

[81] G. Amarasuriya, C. Tellambura, and M. Ardakani, "Multi-way MIMO amplify-and-forward relay networks with zero-forcing transmission," *IEEE Trans. Commun.*, vol. 61, no. 12, pp. 4847–4863, 2013.

[82] O. Amin, S. Ikki, and M. Uysal, "On the performance analysis of multirelay cooperative diversity systems with channel estimation errors," *IEEE Trans. Veh. Technol.*, vol. 60, no. 5, pp. 2050–2059, June 2011.

[83] A. Nezampour and R. Schober, "Asymptotic analysis of space-time codes in generalized fading channels," *IEEE Commun. Lett.*, vol. 13, no. 8, pp. 561–563, Aug. 2009.

[84] W. Xu, J. Zhang, P. Zhang, and C. Tellambura, "Outage probability of decode-and-forward cognitive relay in presence of primary user's interference," *IEEE Commun. Lett.*, vol. 16, no. 8, pp. 1252–1255, 2012.

[85] S. Atapattu, Y. Jing, H. Jiang, and C. Tellambura, "Relay selection schemes and performance analysis approximations for two-way networks," *IEEE Trans. Commun.*, vol. 61, no. 3, pp. 987–998, 2013.

[86] Y. Dhungana and C. Tellambura, "Uniform approximations for wireless performance in fading channels," *IEEE Trans. Commun.*, vol. 61, no. 11, pp. 4768–4779, 2013.

[87] D. Senaratne and C. Tellambura, "Generalized singular value decomposition for coordinated beamforming in MIMO systems," in *Proc. IEEE Global Commun. Conf. (ICC)*, 2010, pp. 1–6.

[88] T. Duong, K. J. Kim, H.-J. Zepernick, and C. Tellambura, "Opportunistic relaying for cognitive network with multiple primary users over Nakagami-m fading," in *Proc. IEEE Int. Conf. Commun.*, 2013, pp. 5668–5673.

[89] V. Sharma Banjade, C. Tellambura, and H. Jiang, "Performance of p-norm detector in AWGN, fading and diversity reception," *IEEE Trans. Veh. Technol.*, vol. 63, no. 7, pp. 3209–3222, Sep. 2014.

[90] A. Singh, M. Bhatnagar, and R. Mallik, "Optimization of cooperative spectrum sensing with an improved energy detector over imperfect reporting channels," *Proc. IEEE Veh. Technol. Conf. (VTC)*, 2011.

[91] A. Singh, M. R. Bhatnagar, and R. K. Mallik, "Cooperative spectrum sensing in multiple antenna based cognitive radio network using an improved energy detector," *IEEE Commun. Lett.*, vol. 16, no. 1, pp. 64–66, Jan. 2012.

[92] M. D. Yacoub, "The κ-μ distribution and the η-μ distribution," *IEEE Antennas Propag. Mag.*, vol. 49, no. 1, pp. 68–81, Feb. 2007.

[93] ——, "The α-μ distribution: a physical fading model for the Stacy distribution," *IEEE Trans. Veh. Technol.*, vol. 56, no. 1, pp. 27–34, Jan. 2007.

[94] A. Talbot, "The accurate numerical inversion of Laplace transforms," *IMA Journal of Applied Mathematics*, vol. 23, no. 1, pp. 97–120, 1979.

[95] J. Abate and P. P. Valkó, "Multi-precision Laplace transform inversion," *International Journal for Numerical Methods in Engineering*, vol. 60, pp. 979–993, May 2004.

[96] P. Wynn, "On the convergence and stability of the epsilon algorithm," *SIAM Journal on Numerical Analysis*, vol. 3, no. 1, pp. 91–122, Mar. 1966.

[97] H. Mustafa and R. Dimitrakopoulos, "Generalized Laguerre expansions of multivariate probability densities with moments," *ACM Journal of Computer and Mathematics with Applications*, vol. 60, no. 7, pp. 2178–2189, Oct. 2010.

[98] A. Taherpour, M. Nasiri-Kenari, and S. Gazor, "Multiple antenna spectrum sensing in cognitive radios," *IEEE Trans. Wireless Commun.*, vol. 9, no. 2, pp. 814–823, Feb. 2010.

[99] S. Wei, D. Goeckel, and P. Kelly, "Convergence of the complex envelope of bandlimited OFDM signals," *IEEE Trans. Inf. Theory*, vol. 56, no. 10, pp. 4893–4904, Oct. 2010.

[100] D. Middleton, "On the detection of stochastic signals in additive normal noise–I," *IRE Trans. Inf. Theory*, vol. 3, no. 2, pp. 86–121, June 1957.

[101] Z. Liu, X. Ma, and G. Giannakis, "Space-time coding and Kalman filtering for time-selective fading channels," *IEEE Trans. Commun.*, vol. 50, no. 2, pp. 183–186, Feb. 2002.

[102] J. Cheng, C. Tellambura, and N. C. Beaulieu, "Performance of digital modulations on Weibull slow-fading channels," *IEEE Trans. Commun.*, vol. 52, no. 8, pp. 1265–1268, Aug. 2004.

[103] I. S. Gradshteyn and I. Ryzhik, *Tables of Integrals, Series and Products*, 7th ed. London: Academic, 2007.

[104] R. C. Palat, A. Annamalai, and J. H. Reed, "An efficient method for evaluating information outage probability and ergodic capacity of OSTBC system," *IEEE Commun. Lett.*, vol. 12, no. 3, pp. 191–193, Mar. 2004.

[105] Wolfram. [Online]. Available: http://functions.wolfram.com/Polynomials/LaguerreL3/02/

[106] E. Hille, "On Laguerre's series: first note," *Proc. Natl. Acad. Sci., USA*, vol. 12, pp. 261–265, 1926.

[107] ——, "On Laguerre's series: second note," *Proc. Natl. Acad. Sci., USA*, vol. 12, pp. 265–269, 1926.

[108] ——, "On Laguerre's series: third note," *Proc. Natl. Acad. Sci., USA*, vol. 12, pp. 348–352, 1926.

[109] E. W. Weisstein, "Confluent hypergeometric function of the second kind." [Online]. Available: http://mathworld.wolfram.com/ConfluentHypergeometricFunctionoftheSecondKind.html

[110] A. M. Magableh and M. Matalgah, "Moment generating function of the generalized α-μ distribution with applications," *IEEE Commun. Lett.*, vol. 13, no. 6, pp. 411–413, June 2009.

[111] D. da Costa and M. Yacoub, "Accurate approximations to the sum of generalized random variables and applications in the performance analysis of diversity systems," *IEEE Trans. Commun.*, vol. 57, no. 5, pp. 1271–1274, May 2009.

[112] D. da Costa, M. Yacoub, and J. C. S. S. Filho, "Highly accurate closed-form approximations to the sum of α-μ variates and applications," *IEEE Trans. Wireless Commun.*, vol. 7, no. 9, pp. 3301–3306, Sep. 2008.

[113] A. Annamalai and C. Tellambura, "Performance evaluation of generalized selection diversity systems over Nakagami-m fading channels," *Wireless Commun. Mobile Comput.*, vol. 3, no. 1, pp. 99–116, Feb. 2003.

[114] V. Sharma Banjade, C. Tellambura, and H. Jiang, "Approximations for performance of energy detector and p-norm detector," *IEEE Commun. Lett.*, vol. 19, no. 10, pp. 1678–1681, 2015.

[115] S. Atapattu, C. Tellambura, and H. Jiang, "Spectrum sensing via energy detector in low SNR," in *Proc. IEEE Int. Conf. Commun. (ICC)*, 2011.

[116] L. Rugini, P. Banelli, and G. Leus, "Small sample size performance of the energy detector," *IEEE Commun. Letters*, vol. 17, no. 9, pp. 1814–1817, Sep. 2013.

[117] S. Herath, N. Rajatheva, and C. Tellambura, "On the energy detection of unknown deterministic signal over Nakagami channels with selection combining," in *Proc. IEEE Canadian Conf. Electr. and Comput. Eng.*, May 2009.

[118] P. Sofotasios, E. Rebeiz, L. Zhang, T. Tsiftsis, D. Cabric, and S. Freear, "Energy detection based spectrum sensing over κ-μ and κ-μ extreme fading channels," *IEEE Trans. Veh. Technol.*, vol. 62, no. 3, pp. 1031–1040, Mar. 2013.

[119] S. H. Abdel-Aty, "Approximate formulae for the percentage points and the probability integral of the non-central χ^2 distribution," *Biometrika*, vol. 41, no. 3-4, pp. 538–540, Dec. 1954.

[120] P. B. Patnaik, "The non-central χ^2- and F-distributions and their applications," *Biometrika*, vol. 36, no. 1-2, pp. 202–232, 1949.

[121] E. S. Pearson, "Note on an approximation to the distribution of non-central χ^2," *Biometrika*, vol. 46, no. 3/4, p. p. 364, Dec. 1959.

[122] P. W. Mielke Jr. and K. J. Berry, "Non-asymptotic inferences based on the chi-square statistic for r by c contingency tables," *Journal of Statistical Planning and Inference*, vol. 12, pp. 41 – 45, 1985.

[123] M. Sankaran, "On the non-central chi-square distribution," *Biometrika*, vol. 46, no. 1-2, pp. 235–237, 1959.

[124] P. G. Moschopoulos, "On a new transformation to normality," *Communications in Statistics - Theory and Methods*, vol. 12, no. 16, pp. 1873–1878, 1983.

[125] A. Papoulis, *Probability, Random Variables, and Stochastic Processes*. Mc-Graw Hill, 1984.

[126] W. Chen and S. Kotz, "The Riemannian structure of the three-parameter Gamma distribution," *Applied Mathematics*, vol. 4, no. 3, pp. 514–522, 2013.

[127] T. Cui, J. Tang, F. Gao, and C. Tellambura, "Moment-based parameter estimation and blind spectrum sensing for quadrature amplitude modulation," *IEEE Trans. Commun.*, vol. 59, no. 2, pp. 613–623, 2011.

[128] W. Lin and Q. Zhang, "A design of energy detector in cognitive radio under noise uncertainty," in *Proc. IEEE Int. Conf. Commun. Syst.*, Nov. 2008, pp. 213–217.

[129] V. Sharma Banjade, C. Tellambura, and H. Jiang, "Spectrum sensing performance of p-norm detector in random network interference," in *Proc. IEEE Int. Conf. Commun. (ICC)*, 2015, pp. 7474–7479.

[130] X. Feng, Q. Zhang, and B. Li, "Enabling co-channel coexistence of 802.22 and 802.11af systems in TV white spaces," in *Proc. IEEE Int. Conf. Commun. (ICC)*, June 2013, pp. 6040–6044.

[131] A. Makarfi and K. Hamdi, "Efficiency of energy detection for spectrum sensing in a Poisson field of interferers," in *Proc. IEEE Wireless Commun. and Netw. Conf. (WCNC)*, 2012, pp. 1023–1028.

[132] ——, "Efficiency of energy detection for spectrum sensing in the presence of non-cooperating secondary users," in *Proc. IEEE Global Commun. Conf. (GLOBECOM)*, Dec. 2012, pp. 4939–4944.

[133] H. ElSawy, E. Hossain, and D. I. Kim, "HetNets with cognitive small cells: user offloading and distributed channel access techniques," *IEEE Commun. Mag.*, vol. 51, no. 6, pp. 28–36, June 2013.

[134] A. Mariani, A. Giorgetti, and M. Chiani, "Effects of noise power estimation on energy detection for cognitive radio applications," *IEEE Trans. Commun.*, vol. 59, no. 12, pp. 3410–3420, Dec. 2011.

[135] V. Sharma Banjade and N. Rajatheva, "Primary user capacity maximization in cooperative detection network using m out of N fusion rule," in *Proc. Int. Symp. Wireless Commun. Syst. (ISWCS)*, 2011, pp. 482–486.

[136] C. Jiang, H. Zhang, Y. Ren, and H.-H. Chen, "Energy-efficient non-cooperative cognitive radio networks: micro, meso, and macro views," *IEEE Commun. Mag.*, vol. 52, no. 7, pp. 14–20, 2014.

[137] P. Gandhi and S. Kassam, "Analysis of CFAR processors in homogeneous background," *IEEE Trans. Aerosp. Electron. Syst.*, vol. 24, no. 4, pp. 427–445, July 1988.

[138] R. P. Agarwal, K. Perera, and S. Pinelas, *An Introduction to Complex Analysis*. Springer, New York, 2011.

[139] Wolfram. [Online]. Available: `http://functions.wolfram.com/HypergeometricFunctions/HypergeometricPFQRegularized/`

Appendix A

Derivations for Chapter 3

A.1 Derivation of $\overline{P}_{md}^{\text{asy}}$ (3.16)

Substituting the contour integral representation for the generalized Marcum-Q function given by [68, eq. (1)] into (3.3), we get

$$\overline{P}_{md} = 1 - \frac{e^{-\frac{\lambda}{2}}}{2\pi\jmath} \oint_{\Delta} \mathcal{M}_{\gamma}\left(1 - \frac{1}{z}\right) \frac{e^{\frac{\lambda}{2}z}}{z^{N}(1-z)} dz, \tag{A-1}$$

where Δ is a circular contour of radius r such that $0 < r < 1$, and $\jmath$ denotes the imaginary unit. The MGF of γ, $\mathcal{M}_{\gamma}(s)$, in (A-1) can be expressed in terms of the MGF of β as $\mathcal{M}_{\gamma}(s) = \mathcal{M}_{\beta}(s\overline{\gamma})$. Then, substituting the MGF $\mathcal{M}_{\beta}^{\text{app}}(s)$ from (3.14) into the resulting expression, and following some algebraic manipulations, we get

$$\overline{P}_{md}^{\text{asy}} = 1 - \frac{a\Gamma(t+1)e^{-\frac{\lambda}{2}}}{2\pi\jmath} \oint_{\Delta} [g_1(z) + g_2(z)] dz, \tag{A-2}$$

where $g_i(z) = \frac{1}{(\theta_i+\overline{\gamma})^{t+1}} \frac{e^{\lambda z/2}}{(z-\eta_i)^{t+1} z^{N-t-1}(1-z)}$, for $i = 1, 2$, with $\eta_i \triangleq \overline{\gamma}/(\theta_i + \overline{\gamma})$. As $g_i(z)$, for $i = 1, 2$, may contain a pole of order $(N - t - 1)$ at $z = 0$ (for $N > t + 1$) and a pole of order $(t + 1)$ at $z = \eta_i$ (see Fig. A.1), in order to evaluate the contour integral in (A-2), we need the residues of $g_i(z)$ at these poles. Thus, two cases arise as follows.

Case I: $N > t + 1$

In this case, the function $g_i(z)$, $i = 1, 2$, contains a $(t + 1)$-th ordered pole at $z = \eta_i$ and a $(N - t - 1)$-th ordered pole at $z = 0$.

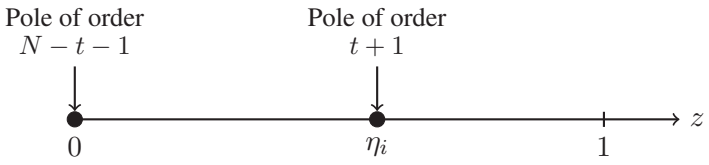

Fig. A.1. Possible poles of $g_i(z)$, $i = 1, 2$, in the z-plane.

Case II: $N \leq t+1$

For this case, $g_i(z)$, $i = 1, 2$, does not have any pole at $z = 0$, and only the pole at $z = \eta_i$ contributes to the contour integral.

The two cases thus lead to $\overline{P}_{md}^{\text{asy}}$ of the form

$$\overline{P}_{md}^{\text{asy}} = \begin{cases} 1 - a\Gamma(t+1)e^{-\frac{\lambda}{2}} \sum_{i=1}^{2} \text{Res}[g_i(z); \eta_i, t+1] & \\ \qquad +\text{Res}[g_i(z); 0, N-t-1], & \text{for } N > t+1 \\ 1 - a\Gamma(t+1)e^{-\frac{\lambda}{2}} \sum_{i=1}^{2} \text{Res}[g_i(z); \eta_i, t+1], & \text{for } N \leq t+1 \end{cases} \tag{A-3}$$

where the notation $\text{Res}[g(z); z_0, p]$ denotes the residue of the function $g(z)$ at pole $z = z_0$ of order p. This residue is defined as [138]

$$\text{Res}[g(z); z_0, p] \triangleq \frac{1}{(p-1)!} \frac{d^{p-1}}{dz^{p-1}} [g(z)(z - z_0)^p] \Big|_{z=z_0}. \tag{A-4}$$

The residue $\text{Res}(g_i; \eta_i, t+1)$, $i = 1, 2$, can thus be expressed in closed-form as (see Appendix A.2)

$$\text{Res}[g_i(z); \eta_i, t+1] = \frac{1}{(\theta_i + \overline{\gamma})^{t+1} t!} \sum_{k=0}^{t} \binom{t}{k} \psi_{\eta_i}^{(k)} \phi_{\eta_i}^{(t-k)}, \tag{A-5}$$

where $\psi_{\eta_i}^{(k)}$ is the k-th order derivative of $\psi(z) \triangleq 1/(z^{N-t-1})$ with respect to z, and $\phi_{\eta_i}^{(t-k)}$ is the $(t-k)$-th order derivative of $\phi(z) \triangleq e^{\lambda z/2}/(1-z)$ with respect to z, both evaluated at $z = \eta_i$, which are given by

$$\psi_{\eta_i}^{(k)} = \frac{(-1)^k}{\eta_i^{N-t-1+k}} \prod_{j=1}^{k} (N - t + j - 2), \tag{A-6}$$

$$\phi_{\eta_i}^{(t-k)} = e^{\frac{\lambda}{2}\eta_i} \sum_{\nu=0}^{n} \frac{(\lambda/2)^{n-\nu}}{(1-\eta_i)^{\nu+1}} \frac{n!}{(n-\nu)!}. \tag{A-7}$$

By following the steps similar to those used in deriving Res$[g_i(z); \eta_i, t+1]$, the residue term Res$[g_i(z); 0, N-t-1]$, $i = 1, 2$, can be obtained to be (details omitted for the sake of brevity)

$$\text{Res}(g_i; 0, N-t-1) = \frac{1}{(\theta_i + \overline{\gamma})^{t+1}(N-t-2)!} \sum_{k=0}^{N-t-2} \binom{N-t-2}{k} \chi_0^{(k)} \phi_0^{(N-t-k-2)}, \tag{A-8}$$

where $\chi_0^{(k)}$ is the k-th order derivative of $\chi(z) \triangleq 1/(z-\eta_i)^{t+1}$ with respect to z, evaluated at $z = 0$ and can be derived to be

$$\chi_0^{(k)} = \frac{(-1)^{-(t+1)}}{\eta_i^{t+k+1}} \prod_{j=1}^{k} (t+j), \tag{A-9}$$

and $\phi_0^{(N-t-k-2)}$ is the same as $\phi_{\eta_i}^{(t-k)}$ with $(t-k)$ and η_i replaced by $(N-t-k-2)$ and 0, respectively. Then, using (A-5)-(A-9) in (A-3) results in (3.16).

A.2 Derivation of (A-5)

By applying the definition of the residue given in (A-4), Res$[g_i(z); \eta_i, t+1]$, $i = 1, 2$, can be expressed as

$$\text{Res}[g_i(z); \eta_i, t+1] = \frac{1}{(\theta_i + \overline{\gamma})^{t+1} t!} \frac{d^t}{dz^t} [\psi(z)\phi(z)] \Big|_{z=\eta_i}. \tag{A-10}$$

Then, utilizing the general Leibniz rule for finding the t-th order derivative of a product [26, eq. (3.3.8)] on the right-hand side of (A-10), followed by evaluating the resulting expression at $z = \eta_i$ gives

$$\frac{d^t}{dz^t} [\psi(z)\phi(z)] \Big|_{z=\eta_i} = \sum_{k=0}^{t} \binom{t}{k} \psi_{\eta_i}^{(k)} \phi_{\eta_i}^{(t-k)}. \tag{A-11}$$

Thus, substituting (A-11) into (A-10) yields (A-5). The coefficients $\psi_{\eta_i}^{(k)}$ of (A-11) can be derived by mathematical induction to be as in (A-6). For deriving $\phi_{\eta_i}^{(t-k)}$, the Leibniz rule can be re-applied after expressing $\phi(z)$ as a product of the terms $e^{\lambda z/2}$ and $1/(1-z)$ and then, following some algebraic manipulations, to yield (A-7).

A.3 Derivation of $\overline{A'}_{\text{asy}}$ (3.35)

By substituting (3.6) into (3.34), the average CAUC over $f^{\text{app}}(\beta)$ can be expressed as

$$\overline{A'}_{\text{asy}} = 1 - a\sum_{k=0}^{N-1}\frac{\overline{\gamma}^k}{2^k k!}\mathcal{I}_1 + a\sum_{k=1-N}^{N-1}\frac{\Gamma(N+k)}{2^{N+k}\Gamma(N)}\mathcal{I}_2, \tag{A-12}$$

where $\mathcal{I}_1$ is defined as

$$\mathcal{I}_1 \triangleq \sum_{i=1}^{2}\int_0^\infty \beta^{t+k}e^{-(\theta_i+\frac{\overline{\gamma}}{2})\beta}d\beta = \sum_{i=1}^{2}\frac{\Gamma(t+k+1)}{(\theta_i+\overline{\gamma}/2)^{t+k+1}}, \tag{A-13}$$

where the definition of Gamma function $\Gamma(\cdot)$ is used to solve the integral, and $\mathcal{I}_2$ is defined as

$$\mathcal{I}_2 \triangleq \sum_{i=1}^{2}\int_0^\infty \beta^t {}_1\tilde{F}_1\left(N+k; k+1; \frac{\overline{\gamma}}{2}\beta\right)e^{-(\theta_i+\overline{\gamma})\beta}d\beta = \sum_{i=1}^{2}\mathcal{I}_{2,i}. \tag{A-14}$$

To solve the integral $\mathcal{I}_{2,i}$, $i = 1, 2$, in (A-14), we proceed as follows. Given the generalized hypergeometric function ${}_pF_q(a_1, ..., a_p; b_1, ..., b_q; z)$, the corresponding regularized hypergeometric function is given by [139] (with the abuse of notation) as

$$\begin{aligned} {}_p\tilde{F}_q(a_1, ..., a_p; b_1, ..., b_q; z) &= \frac{{}_pF_q(a_1, ..., a_p; b_1, ..., b_q; z)}{\Gamma(b_1)...\Gamma(b_q)} \\ &= \sum_{v=0}^{\infty}\frac{\prod_{j=1}^{p}(a_j)_v\, z^v}{v!\prod_{j=1}^{q}\Gamma(v+b_j)}, \end{aligned} \tag{A-15}$$

where $(a_j)_v = \Gamma(a_j+v)/\Gamma(a_j)$ is the Pochhammer's symbol. Then, using (A-15) with $p = q = 1$ and substituting the resulting series expression into $\mathcal{I}_{2,i}$, we get $\mathcal{I}_{2,i} = {}_2\tilde{F}_1\big(t+1, k+N; k+1; \frac{\overline{\gamma}}{2(\theta_i+\overline{\gamma})}\big)/(\overline{\gamma}+\theta_i)^{t+1}$, where the definition of Gamma function $\Gamma(\cdot)$ is applied to solve the resulting integral followed by the use of (A-15) for $p = 2$, $q = 1$. Thus, substituting $\mathcal{I}_{2,i}$ into (A-14) gives

$$\mathcal{I}_2 = \sum_{i=1}^{2}\frac{1}{(\overline{\gamma}+\theta_i)^{t+1}}{}_2\tilde{F}_1\left(t+1, k+N; k+1; \frac{\overline{\gamma}}{2(\theta_i+\overline{\gamma})}\right). \tag{A-16}$$

Then, substituting (A-13) and (A-16) into (A-12) yields $\overline{A'}_{\text{asy}}$ (3.35).

Appendix B

Gamma and CLT approximations for Chapter 4

B.1 Derivation of P_d and P_f for Gamma approximation

If we assume the decision variable T_p to be Gamma distributed, the detection probability ($P_{d,\text{Gam}}$) and false alarm probability ($P_{f,\text{Gam}}$) can be derived by matching the first two moments of $T_p|H_1$ and $T_p|H_0$, respectively, to those of the Gamma random variable, thus yielding

$$\begin{aligned} P_{d,\text{Gam}} &= 1 - \frac{\mathcal{G}(\lambda/\theta_1, k_1)}{\Gamma(k_1)}, \\ P_{f,\text{Gam}} &= 1 - \frac{\mathcal{G}(\lambda/\theta_0, k_0)}{\Gamma(k_0)}, \end{aligned} \tag{B-1}$$

where the parameters can be derived to be

$$\begin{aligned} k_0 &= \frac{N\Gamma^2(p/2+1)}{\Gamma(p+1) - \Gamma^2(p/2+1)}, \\ \theta_0 &= \frac{\Gamma(p+1) - \Gamma^2(p/2+1)]}{N\Gamma(p/2+1)}, \text{ and} \\ k_1 &= k_0, \\ \theta_1 &= (1+\gamma)^{p/2}\theta_0. \end{aligned} \tag{B-2}$$

B.2 Derivation of P_d and P_f for CLT approximation

If number of samples is very large ($N \gg 1$), the CLT may be invoked such that T_p is Gaussian distributed with mean $\mu_0 = \Gamma(p/2+1)$ and variance $\sigma_0^2 = \frac{\Gamma(p+1)-\Gamma^2(p/2+1)}{N}$ under H_0, or with mean $\mu_1 = (1+\gamma)^{p/2}\mu_0$ and variance $\sigma_1^2 = (1+\gamma)^p\sigma_0^2$ under H_1. It is straightforward to show that the CDF of T_p under both hypotheses can be expressed in terms of the Gaussian-Q function $Q(x) = (1/\sqrt{2\pi})\int_x^\infty e^{-t^2/2}dt$. Then, the detection and false alarm probabilities utilizing the CLT approximation can be easily expressed as

$$\begin{aligned} P_{d,\text{CLT}} &= Q\left(\frac{\lambda-\mu_1}{\sigma_1}\right), \\ P_{f,\text{CLT}} &= Q\left(\frac{\lambda-\mu_0}{\sigma_0}\right). \end{aligned} \tag{B-3}$$

Appendix C

Derivations for Chapter 5

C.1 Derivation of (5.11)

We have $y_i|H_0 \sim \mathcal{CN}(0, \sigma_w^2)$, and $y_i|H_1 \sim \mathcal{CN}(0, \sigma_w^2(1+\gamma))$. Thus, $|y_i|^2$ normalized with respect to σ_w^2 under hypothesis H_j, $|y_i|^2/\sigma_w^2\,|H_j$, is exponentially distributed with parameter A_j, $j = 0, 1$. Since the samples are i.i.d., the mean of $T_p|H_j$, denoted M_j, can be expressed as (after interchanging the order of integration and summation)

$$M_j = \frac{1}{N}\sum_{i=1}^{N}\int_0^\infty x^{p/2}e^{-A_j x}dx = \Gamma(p/2+1)/A_j^{p/2}.$$

Similarly, the variance of $T_p|H_j$, denoted by σ_j^2, can be obtained to be

$$\sigma_j^2 = \frac{\Gamma(p+1) - \Gamma^2\big(p/2+1\big)}{NA_j^p}.$$

Then, use of the transformation (5.2), matching the corresponding means and variances, and solving for θ and ψ_j yields (5.11).